Applications of Machine Learning for Modelling of Ice Flexural Strength

By

©Robert Burton B.Eng

A Thesis submitted to the
School of Graduate Studies
In partial fulfillment of the requirements for the degree of

Masters of Engineering
Faculty of Engineering and Applied Science
Memorial University

May 2024
St. John's, Newfoundland and Labrador, Canada

This page left blank intentionally

Abstract

The design of marine vessels and structures operating in regions where ice is present, must consider the loads transferred to the structure upon impact with an ice feature. The flexural strength of ice is an important material property and can have significant impact on the loads transferred to a structure. Flexural strength is generally considered to be dependent on the size or scale of the sample (often reported as beam volume), ice temperature and brine volume (in the case of sea ice), however the influence of temperature and beam volume have been debated in the literature. Conventionally flexural strength was often modelled as a constant (i.e. average strength), or was modelled as a single parameter or dual parameter (sea ice only) empirical relationship. Employing an extensive database of flexural strength measurements, with over 2000 freshwater and 2800 sea ice measurements, machine learning (ML) algorithms were utilized to define a relationship between these ice parameters and the measured flexural strength. The implementation of ML algorithms was able to highlight a link between freshwater flexural strength and ice temperature, a relationship often ignored or not perceivable in existing models. When considering sea ice, the use of ML algorithms were able to highlight a dependence of flexural strength on scale, brine volume and temperature. These findings have the potential to impact the design of ice strengthened structures, and highlights the importance of accurately recording these parameters when performing tests in the either the field or laboratory.

Key Words

Sea Ice, Freshwater Ice, Flexural Strength, Machine Learning, Level Ice Loads

Acknowledgements

I would like to thank Dr. Rocky Taylor and Dr. Renat Yulmetov for their continued support and guidance throughout the program. Their feedback and expert advise in the fields of ice mechanics and machine learning were indispensable.

I am thankful to Mohamed Aly for his efforts in digitizing the flexural strength database. This database was instrumental in the successful completion of this work.

Funding for this work from Innovate NL, the Natural Sciences and Engineering Research Council (NSERC) of Canada, and Hibernia Management and Development Company Ltd. (HMDC) are gratefully acknowledged. Additional thanks are extended to Memorial University's School of Graduate Students for their financial support throughout the program.

A special thank-you to my parents, Everett and Irene Burton, who have wholeheartedly supported and encouraged me from day one, and for encouraging my inquisitive nature as a child.

Finally, I would like to express my gratitude towards to my beautiful wife Brianne, and our lovely children Zoey and Annelise for their loving support and encouragement. Your unwavering support and confidence during the many long days and nights made this possible.

Co-Authorship Acknowledgements

Part of the work presented in Chapter 5: *Freshwater Ice Analysis* was published in a paper entitled "Estimating Freshwater Level Ice Loads on Sloping Structures Using Machine Learning-Derived Flexural Strength", and was published and presented at the 26th IAHR International Symposium on Ice, see Burton et al. (2022).

Part of the work in Chapter 6: *Sea Ice Analysis* was published in a paper entitled "Estimating Level Sea Ice Loads on Sloping Structures Using Machine Learning-Derived Flexural Strength", and was published and presented at the 27th International Conference on Port and Ocean Engineering under Arctic Conditions (POAC 2023), see Burton et al. (2023).

The author of this thesis was primary author on both papers, with Dr. Rocky Taylor and Dr. Renat Yulmetov having co-authorship credits in both papers. Co-authors Dr. Rocky Taylor and Dr. Renat Yulmetov served in conceptualizing the research, securing funding, and providing guidance and support during data analysis and interpretation as well as reviewing and editing the manuscript. The primary author took on the primary role in research execution, compiling and analyzing data, leading the organization, synthesis and interpretation of results, as well as the preparation and revision of the manuscript.

Table of Contents

List of Figures

List of Tables

Nomenclature

α	Cone angle to the horizontal
$\bar{y}$	mean of the observed data
$\hat{y}_i$	predicted data
μ	Ice-cone coefficient of friction
ρ_i	Density of ice
ρ_w	Density of water
σ_f	Flexural strength
σ_m	Measured flexural strength
σ_p	Plotted or adjusted flexural strength
b	Beam breadth
c_n	Constant number n
E	Elastic Modulus of ice
F	Concentrated load
g	Acceleration due to gravity
h	Beam height
h_f	Ride-up height
h_{ice}	Ice thickness
L	Beam length
l_c	Elastic critical length
P	Ice property
S	Salinity
V	Beam volume
v	Poissions ratio for ice
V_1	Reference beam volume

v_b Brine volume

y_i observed data

Weakest Link Model

α Weibull shape parameter

β Weibull scale parameter

ΔV_i Volume of an individual element

γ Weibull location parameter

$\langle R \rangle$ Expected beam strength

$\phi(x)$ State of stress within a system as a function of location

$F_R(r)$ Failure probability of the beam

$F_T(r)$ Distribution function for each beam element

k Number of elements

$m(r)$ Weibull power-law material function

r Strength of an individual element

r_1 Weibull scale parameter

r_o Lower limit of strength

r_R Reference strength value

s Stress state at point x

v^* Reduced volume

v_o Volume of an individual element

Acronyms

AFDD Accumulated Freezing Degree Days

ANN Artificial Neural Network

ETR Extra Trees Regressor

GBR Gradient Boosted Trees Regressor

KNR k-Nearest Neighbour Regressor

LSR Least Squares Regression

ML Machine Learning

MLPR Multi-layer Perceptron Regressor

RMSE Root Mean Squared Error

SHAP SHapley Additive eXplanation Method

1 Introduction

1.1 Overview

The design of marine structures and vessels intended to operate in ice-prone waters must take into account the global and local loads resulting from impacts with an ice feature. In reference to level ice loads, the amount of force transferred to the structure is the lesser of the environmental driving forces (wind, waves, current, etc.) or the ice strength. Ice failure will generally occur in either compression or tension. Loading a sheet in tension is generally the result of buckling or bending the ice sheet, resulting from an eccentric loading scenario such as level ice impacting an inclined plane. The failure of ice in flexure is dependent upon the flexural strength of the ice. The flexural strength of ice is significantly lower than the compressive strength (Sanderson (1988), Timco and O'Brien (1994)) resulting in lower loads being transferred to the structure. Stationary structures such as bridge piers and offshore wind turbines as well as ice-breaking vessels will often take advantage of the lower flexural strength of ice by implementing sloping elements at the waterline to promote the failure of ice in flexure. As a result the flexural strength of ice holds significance in the engineering and design of offshore structures and vessels.

1.2 Purpose

The geophysical nature of ice leads to a material prone to the inclusion of natural flaws and impurities. The effects of the physical properties of the ice and how they affect the measured flexural strength of both freshwater ice and sea ice are of interest to scientists and engineers

alike. In the current work special attention is given to the effects of temperature, beam volume (i.e. scale effects) and brine volume (when considering sea ice) and their impact on the flexural strength of ice.

There are theoretical and empirical evidence that suggest these three ice properties should have an appreciable impact on the flexural strength of an ice sample. However, with respect to sea ice, only brine volume has garnered widespread acceptance as a governing factor in determining flexural strength (e.g. Weeks and Assur (1967), Dykins (1968), Weeks and Assur (1972), Tozawa and Taguchi (1986), Timco and O'Brien (1994) and Frederking and Sudom (2013)). The influence of scale effects is debated among researchers (e.g. Frederking and Sudom (2013), Lau et al. (2001), Williams and Parsons (1994), Maattanen (1975), Lavrov (1971), Blanchet et al. (1997), Timco and O'Brien (1994), Parsons et al. (1992) and Parsons and Lal (1991)), as is the influence of temperature (e.g. Weeks and Assur (1972), Maattanen (1975), Gow (1977), Lainey and Tinawi (1984) and Gow and Ueda (1989)) . When considering freshwater ice few models exist for estimating flexural strength, however, most available models are single parameter and limited to either temperature or scale dependence.

The main objective of this thesis is to investigate the influence of scale effects, brine volume (for sea ice only) and temperature on the flexural strength of ice through the application of Machine Learning (ML) algorithms. ML has been employed across many disciplines and fields of study with great success, from analysis of medical diagnostic imagery, facial recognition, natural language processing and recommender systems tailoring the advertisements seen by users online. ML has a lot to offer and is often perceived as a solution to every problem, however ML is not always the best tool for the job. The goal of this research has been to determine the applicability of ML to the field of ice mechanics, in particular the estimation of flexural strength. The scope of work for this research has been defined as:

- Review standard measurement methodologies employed during laboratory and in situ field testing.
- Conduct a review of previous studies related to the topics of ice mechanics and flexural strength
- Examine the effects of scale, brine volume and temperature on recorded flexural strength data
- Develop a machine learning model for flexural strength predictions applicable to freshwater ice and sea ice
- Compare the machine learning models to previous empirical models and discuss whether the application of machine learning can offer any improvements over the existing models
- Discuss the overall results of the research and provide recommendations for further research

1.3 Outline of thesis

A literature review was conducted investigating the influence of scale effects, brine volume and temperature on the flexural strength of ice, results of this review are presented in Chapter 2. In Chapter 3 a flexural strength database is introduced along with the preprocessing steps taken to ensure the quality of the data. An overview of ML and several common algorithms are introduced in Chapter 4. Chapter 5 contains a discussion on the analysis of flexural strength of freshwater ice as a function of scale and temperature. In Chapter 6, the focus shifts to sea ice and a discussion of the analysis of sea ice flexural strength as a function of scale, brine volume and temperature. A summary including a discussion of the main conclusions and future research considerations are presented in Chapter 7.

2 Literature Review

In the following sections a review of common ice failure methods will be presented with particular attention focusing on flexural failure and associated flexural strength. This will be followed by a brief review of simple beam theory and three of the most common methods to experimentally measure flexural strength of an ice beam. Finally a brief discussion on the physics of ice growth and the theoretical and experimental evidence supporting the relationship between ice properties (beam volume, brine volume and ice temperature) and flexural strength.

2.1 Ice Failure Methods

There are multiple mechanisms by which an ice sheet can fail upon interacting with a structure. In its simplest form the failure of an ice sheet can be reduced to failure resulting from loading the ice sheet in compression or tension. When level ice interacts with a structure, a compressive force is generated when the driving force (eg. wind, waves, tides etc.) is in the same plane as the resulting reactive force from the structure. In order for an ice sheet to experience a tensile load, a portion of the reactive force must be out of plane with the driving force resulting in an eccentric loading. An example of such a reactive force would be the horizontal and vertical forces generated when level ice impacts a sloped-walled structure. In this case the resulting vertical load puts the ice sheet in a state of flexure having tension in either the upper or lower fibres depending on direction of the slope.

According to Sanderson (1988) there are six ice failure mechanisms generally associated with compressive loading, which can be separated into global modes including creep, buckling,

radial and circumferential cracking, and local modes of spalling and crushing as shown in Figure 2.1. The failure mechanisms are generally dependent upon the indentation rate (U/D) and the aspect ratio (D/h), where U is the speed at which the incoming ice sheet and indenter are interacting, D is the width of the indenter (or structure) and h is the thickness of the ice sheet.

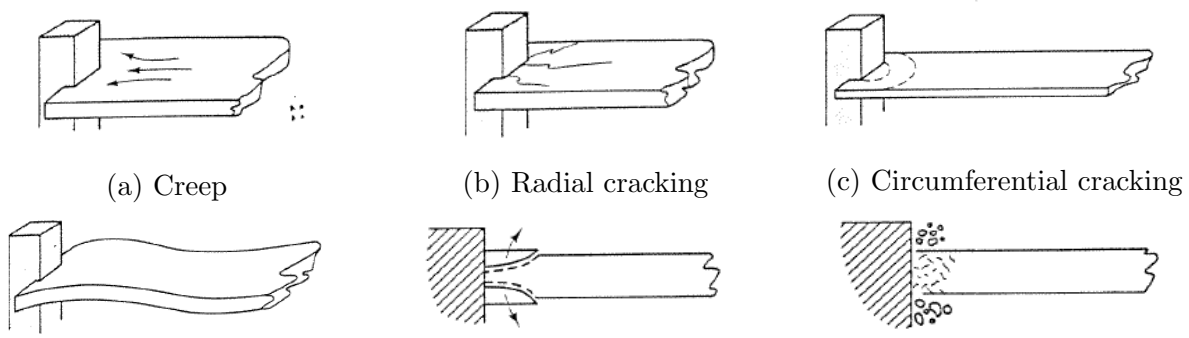

(a) Creep (b) Radial cracking (c) Circumferential cracking

(d) Buckling (e) Spalling (f) Crushing

Figure 2.1: Ice failure mechanism (Sanderson, 1988)

The failure of an ice sheet in pure creep, i.e. without cracking, requires very low indentation rates which, in nature, are generally only observed in glacial interactions. Sanderson (1988) states that regardless of the geometry or aspect ratio if the indentation rate is low enough the deformation will be entirely creep. In thin ice sheets elastic deformations in the form of buckling can be observed within an ice sheet and generally culminates in circumferential cracking. In addition to buckling the formation of circumferential cracks can also be the result of an eccentrically loaded ice sheet (Sanderson, 1988), such as the result of an interaction with a sloping surface. Radial cracking is described by Palmer et al. (1983) as "the growth of vertical cracks, directed radially from the contact region and running through the whole thickness". Ice too thick to buckle generally begins to experience compressive ice failure when interacting with a vertically walled structure. This compressive failure typically results in localized crushing generating fine-grained particles, or spalling as a result of crack propagation to the top and bottom surfaces of the ice sheet.

When an ice sheet is subjected to bending the fracture mechanics are altered, and failure of the sheet is generally due to tension in the extreme fibres. The flexural strength of ice is significantly lower than the compressive strength (Sanderson (1988), Timco and O'Brien (1994)) resulting in lower loads being transferred to the structure. While it may not make sense in every application, the use of sloping elements at the waterline should be considered for all structures operating in ice as a means to reduce global loads. For this reason accurate models of flexural strength are invaluable to the design and operation of offshore structures.

2.2 Flexural Strength

The accuracy and precision of modelled flexural strength are directly influenced by the quality of the input data, which is acquired via flexural strength measurements. Flexural strength is not a basic material property and cannot be measured directly in the same manner as compressive and tensile strength. Flexural strength is a derived strength based on the principles of simple beam theory and is governed by the testing method, ice beam dimensions, measured forces and location of beam failure.

2.2.1 Simple Beam Theory

The flexural strength of a beam is generally defined based one of three flexural strength tests: cantilever, 3-point bending or 4-point bending. Flexural strength of the beam is then derived based on simple beam theory using the maximum force measured during the test, beam dimensions and location of the load. The flexural strength derivations from simple beam theory using the cantilever, 3-point and 4-point bending tests are provided in Equation 2.1, 2.2 and 2.3 respectively.

$$\sigma_{f_{cant}} = \frac{6FL}{bh^2} \tag{2.1}$$

$$\sigma_{f_{3pt}} = \frac{3FL}{2bh^2} \tag{2.2}$$

$$\sigma_{f_{4pt}} = \frac{FL}{bh^2} \tag{2.3}$$

where: σ_f is the flexural strength, F is the maximum measured load, L is the length of the beam, b is the width of the beam and h is the height of the beam. These equations assume a neutral axis at the center of the beam, the load in 3-point bending is at the midpoint of the beam, and the loads in 4-point bending are $L/3$ from the supports as indicated in Figure 2.2

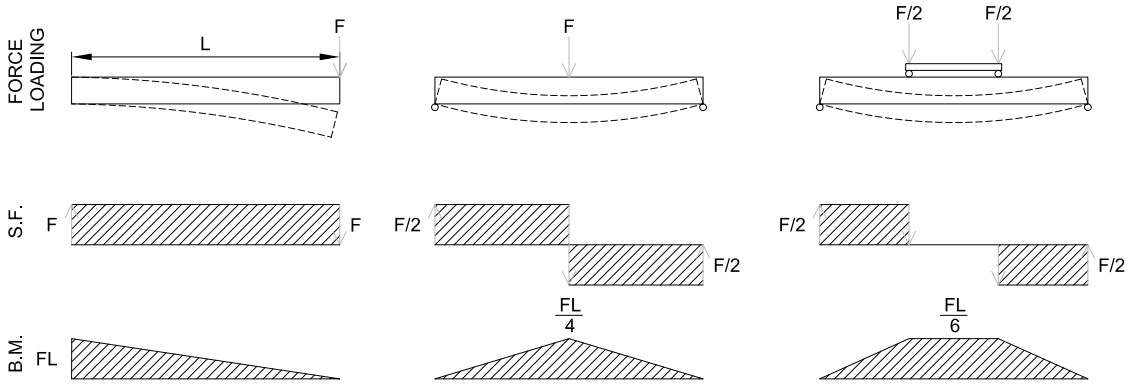

(a) Cantilever beam (b) 3-point bending (c) 4-point bending

Figure 2.2: Loading, shear and bending moment diagrams

2.2.2 Simple Beam Theory Assumptions

Simple beam theory has a number of underlining assumptions, five commonly accepted assumptions of simple beam theory are:

1. The cross-section maintains its shape and scale along the length of the beam
2. The cross-section of a beam remains plane after deformation
3. The cross-section remains normal to the deformed axis of the beam
4. The deformation is elastic and the material is both isotropic and homogeneous
5. The elastic moduli in tension and compression are equal

The primary issue with the beam theory assumptions when applied to ice is that of the material being isotropic and homogeneous. Firstly ice behaves different when loaded vertically versus horizontally as discussed by Schwarz and Weeks (1977) who also described ice as an anisotropic material with non-linear stress distributions across the depth. According to Schwarz (1975), when under flexure the neutral axis of an ice beam shifts from the centre towards the compressed fibres due to the differing elastic modulus in compression and tension. As for the homogeneity of ice, naturally occurring ice is prone to the inclusion of air and or brine pockets as well as other naturally occurring flaws and cracks. These natural inclusions can result in localized stress concentrations reducing the capacity of the ice.

For this reason, the flexural strength of ice is often referenced as a index strength (Schwarz and Weeks (1977), Timco and O'Brien (1994)), as the exact true flexural strength is not easily attained. While the use of simple beam theory for ice beam flexural strength evaluation may not be fully accurate, Schwarz (1975) concluded that the force-deflection curves indicate the stress-strain relationship is linear suggesting that simple beam theory is adequate for close approximations of flexural strength.

2.2.3 Physical Testing of Flexural Strength

There are three primary physical testing approaches as noted earlier: cantilever, three-point and four-point bending tests, these tests are either performed in situ or in laboratory type testing. The use of in situ tests are favoured, where possible, as they permit the ice to maintain a more natural temperature gradient through its depth, and in the case of sea ice they reduce the amount of brine lost when a sample is removed from the water. Laboratory testing on the other hand often permits more accurate control of the testing temperature and more sophisticated tools are generally available for sample preparation and testing.

2.2.3.1 Cantilever Beam Tests

The cantilever beam test is the easiest of the three tests to perform in situ and can be scaled up to accommodate larger beams with greater ease. A cantilever tests is conducted by first cutting a u-shaped channel in the ice leaving an ice beam supported on one end by the ice sheet, secondly a force is exerted at the free end of the beam and sequentially loaded until failure. The application of the load can be performed in either a push down or pull up direction depending on the test equipment.

A potential issue with cantilever beam tests is the presence of external stress concentrations at the root of the beam. The sharp corners left after cutting the beam free from the surrounding ice sheet have been suggested to result in stress concentrations, leading to a reduction in flexural strength capacity when compared to 3-point or 4-point bending. Using freshwater beams Gow et al. (1978) found that flexural strength for 3-point bending frequently exceeded the strength of cantilever beams cut from the same ice sheet by a factor of two. When considering sea ice Timco (1985) found there was no appreciable difference between the results from cantilever tests verses 3-point or 4-point bending. Sea ice behaviour

is more plastic in nature compared to freshwater (Schwarz and Weeks, 1977), and therefore this behaviour may help relieve these external stress concentration.

The issue of stress concentrations does not exist in the 3-point and 4-point bending tests, therefore these two tests should be the preferred method of flexural strength testing. However, the cantilever test has some advantages: firstly the ease of preparing and performing the tests in the field cannot be understated, secondly the beam remains immersed in water helping to maintain a more natural temperature gradient and brine volume content. It has been suggested that flexural strength measurements from cantilever beam tests could be adjusted using a correction factor to account for the presence of stress concentrations. Gow et al. (1988) and Gow and Ueda (1989) found that the inclusion of stress relief cuts by way of filleted corner at the root of the beam increased the flexural strength capacity by upwards of two times that of conventionally cut beams. Considering that conventionally cut cantilever beams were found to be upwards of 2 times lower than 3-point (or 4-point) bending tests with an average between 1.2 and 1.7 lower (Gow et al., 1978), the basis for a correction factor could be argued. Aly et al. (2019) found that measurements from 3-point and 4-point bending tests were just over 2 times higher than cantilever results. Similar results were also found by Wang et al. (2020) who suggested 1.8 as a correction factor. For the data in question a correction factor of 2 was applied to the cantilever strengths to account for the effects of stress concentrations.

2.2.3.2 3-point and 4-point Bending Tests

3-point and 4-point bending tests are often referred to as simple beam tests in reference to the manner in which the beams are supported. In simple beam tests, the ice beam is completely cut free from the surrounding ice sheet. The beam is then supported at each end and a load is then applied at the center of the beam (3-point) or at two locations which

are equidistant from the end supports (4-point) as presented in Figure 2.2, the load is then increased monotonically until failure.

One issue with the 3-point bending test is that failure generally occurs at the center of the beam at the point of highest bending moment (see Figure 2.2b). Therefore, potential exists for a weaker point to exist within the beam which simply was not loaded to failure. The 4-point bending tests attempt to correct this by separating the load application points and creating a region of constant moment within the beam (see Figure 2.2c), providing a wider window through which the beam can fail at its weakest point.

2.3 Ice Properties and Ice Mechanics

The strength of ice is dependent upon a number of key factors including the physical properties of the ice itself and the method employed to measure said strength. Timco and O'Brien (1994) found that the physical ice properties of ice temperature, grain structure, grain size and beam volume are contributing factors to the strength of both freshwater ice and sea ice. When considering sea ice the salinity or brine volume are also of importance. Experimental set-up and procedures can also impact the strength of ice including parameters such as loading direction, loading rate and test type (cantilever or simple beam).

The scope of work here was limited to investigating the impact of beam volume (or scale effect), temperature and brine volume on the flexural strength of freshwater ice and sea ice, all other parameters will be generalized as "other factors". However, before exploring these properties a quick review of some of the principles of ice formation will help in providing some necessary background information.

2.3.1 Physics of Ice Growth

An overview of many principles associated with ice growth are covered in Timco and Weeks, 2010 and will be discussed briefly in the following sections.

2.3.1.1 Formation of Brine Pockets

Timco and Weeks (2010) describes the ice lattice as being highly selective and not very receptive to impurities such as salts. During the formation of ice the growing ice sheet attempts to expel the salts present in sea water. As expected this expulsion process is not 100% efficient resulting in some salt being left behind in brine pockets. The amount of salt left behind is generally a function of the growth rate of the ice and the salinity of the originating sea water. Average salinity of first year ice is around 4-6 parts per thousand (ppt or ‰) compared to the average salinity of sea water being 32-35‰.

2.3.1.2 Grain Structures

There are multiple grain structures possible during the development of an ice sheet, the three most common structures according to Timco and Weeks (2010) are: granular, columnar and discontinuous columnar.

Granular ice generally forms as a result of wave action stirring up recently formed frazil ice. Due to this stirring action, the orientation of the grain structure is very random, resulting in an ice sheet having isotropic (or near isotropic) mechanical properties. The formation of brine pockets within granular ice generally forms between the ice crystals and not within the crystals themselves.

Columnar ice can form at the surface when conditions are calm or beneath an initial layer of granular ice which can help reduce the vertical motions of the water column. Within columnar ice the brine pockets are located within vertically orientated planes within the

ice crystals. These planes result in a reduction of ice to ice contact and result in a plane of weakness. Columnar ice has two varieties based on the horizontal orientation of the c-axis within the individual crystals: random or aligned. Random crystal orientation have no directional dependency within the horizontal plan, while aligned crystals have the c-axis all oriented in the same direction. The properties of "aligned" ice can vary significantly depending on if the ice is loaded parallel or perpendicular to the orientation of the crystals. The horizontal orientation of crystal c-axis are believed to reflect the mean current direction beneath the ice (Weeks and Gow, 1980).

2.3.2 Beam Volume - Scale Effects

The influence of beam volume on ice strength has been investigated by numerous researchers. Some researches have determined that ice strength declines with increasing beam volume (Frederking and Sudom (2013), Lau et al. (2001), Williams and Parsons (1994), Maattanen (1975) and Lavrov (1971)), while others believe there is no significant relationship (Blanchet et al. (1997), Timco and O'Brien (1994), Parsons et al. (1992), Parsons and Lal (1991)). Therefore, there is some debate as to the legitimacy of these scale-effects on flexural strength. In the following sections both theoretical and experimental evidence for scale effects will be discussed.

2.3.2.1 Scale-Effect Theory

Theoretically the concept that ice strength is inversely proportional to the volume of the sample can be explored through the weakest link model as described by Weibull (1951). Jordaan (2005) describes this weakest link model as a structure composed of a series of n elements, where the structure will fail if one of those elements fails. Lets assume the strength of each element is independent and identically distributed (iid) and follows the distribution function $F_T(t)$. Then if T_i is the strength of the ith element and the strength of the entire

structure is R, then $R = \min(T_1, T_2, T_3, ..., T_i, ..., T_n)$ and the failure probability of the entire structure $F_R(r)$ can be written as,

$$F_R(r) = 1 - [1 - F_T(r)]^n \tag{2.4}$$

This can also be expressed as,

$$F_R(r) = 1 - \exp\{n \ln[1 - F_T(r)]\} \tag{2.5}$$

If one considers an ice beam of volume V which is composed of n individual elements of volume v_0, then $V = nv_0$ (or $n = V/v_0$), and $F_R(r)$ can be written as,

$$F_R(r) = 1 - \exp\left\{\frac{V}{v_0} \ln[1 - F_T(r)]\right\} \tag{2.6}$$

A power-law material function, $m(r)$, was suggested by Weibull as a replacement for the expression $\{-\ln[1 - F_T(r)]\}$ and is expressed below,

$$m(r) = \left(\frac{r - r_0}{r_1}\right)^{\alpha} \tag{2.7}$$

where α and r_1 are the distribution shape and scale parameters respectively, and r_0 is the lower limit of the ice strength. Using this material function Equation 2.6 can be rewritten as,

$$F_R(r) = 1 - \exp\left\{-\frac{V}{v_0}\left(\frac{r - r_0}{r_1}\right)^{\alpha}\right\} \tag{2.8}$$

If one compares Equation 2.8 to that of the standard three-parameter Weibull distribution as shown here,

$$F_X(x) = 1 - \exp\left\{-\left(\frac{x-\gamma}{\beta}\right)^{\alpha}\right\} \tag{2.9}$$

it can be observed that both equations have the identical form, where

$$x \equiv r \tag{2.10}$$

$$\beta \equiv \left(\frac{v_0}{V}\right)^{1/\alpha} r_1 \tag{2.11}$$

$$\gamma \equiv r_0 \tag{2.12}$$

Generally, r_0 can be assumed as zero as this is a natural minimum for strength and therefore simplifying the failure probability to,

$$F_R(r) = 1 - \exp\left\{-\frac{V}{v_0}\left(\frac{r}{r_1}\right)^{\alpha}\right\} \tag{2.13}$$

2.3.2.1.1 Inhomogeneous Stress State and Reduced Volume Formulation

The failure probability defined in Equation 2.13 is based on a homogeneous stress state, however the stress level in an ice beam can vary significantly from element to element resulting in a inhomogeneous stress state. Weibull (1951) suggested that for a small volume, ΔV, around a given point (with a Cartesian coordinates of x) the stress state at each element could be considered homogeneous. Jordaan (2005) suggests that this elemental stress state ($\sigma(x_i)$) could then be represented by a single scaler, s, and can be expressed as,

$$s = r_R \, \phi(x) \tag{2.14}$$

where r_R is a reference value and $\phi(x)$ is the stress state within the structure as a function of position within the structure.

The strength of the ith element, T_i, can then be described by the distribution function,

$$F_T(s) = F_T[r\phi(x)] \tag{2.15}$$

The distribution function $F_T(s)$ is generally the same as used previously in Equation 2.6 ($F_T(t)$) where t is replaced by s and the deterministic stress variations across the structure are represented by ϕ. If the volume of the structure is considered to be segmented into k small elements ΔV_m , $m = 1, 2, ...k$ than Equation 2.6 can be rewritten as,

$$F_R(r) = 1 - \exp\left[\frac{1}{v_0}\sum_{i=1}^{k}\left(\Delta V_i \ln\{1 - F_T[r\phi(x)]\}\right)\right] \tag{2.16}$$

The summation can be replaced with an integral resulting in,

$$F_R(r) = 1 - \exp\left\{\frac{1}{v_0}\int_V \ln\left\{1 - F_T[r\phi(x_i)]\right\} \mathrm{d}v\right\} \tag{2.17}$$

rewriting the material function from earlier as,

$$m(r) = \left(\frac{r\phi(x_i) - r_0}{r_1}\right)^{\alpha} \tag{2.18}$$

the failure probability can be expressed as,

$$F_R(r) = 1 - \exp\left\{-\frac{1}{v_0}\int_V \left(\frac{r\phi(x_i) - r_0}{r_1}\right)^{\alpha} \mathrm{d}v\right\} \tag{2.19}$$

if we assume that $r_0 = 0$, further simplification can be made to the failure probability such that,

$$F_R(r) = 1 - \exp\left\{-\frac{1}{v_0}\left(\frac{r}{r_1}\right)^{\alpha}\int_V \phi^{\alpha}(x_i)\,\mathrm{d}v\right\} \tag{2.20}$$

Here the integral defines a "reduced volume" which can be represented as,

$$v^* = \int_V \phi^{\alpha}(x_i)\,\mathrm{d}v \tag{2.21}$$

substituting the "reduced volume" into the failure probability the distribution can be written as,

$$F_R(r) = 1 - \exp\left[-\frac{v^*}{v_0}\left(\frac{r}{r_1}\right)^{\alpha}\right] \tag{2.22}$$

Making a comparison between this distribution and the one defined in Equation 2.13, one can observed that the two equations are identical, if the reduced volume, v^*, replaces the volume of the body, V, from the homogeneous stress.

The mean strength of an ice beam can be obtained from Weibull theory, where the mean of Equation 2.13 is,

$$\langle R\rangle = r_o + r_1\left(\frac{V}{v_0}\right)^{-1/\alpha}\Gamma\left(1 + \frac{1}{\alpha}\right) \tag{2.23}$$

Comparing the strengths of two beams, represented by V_A and V_B, results in,

$$\frac{\langle R\rangle_1}{\langle R\rangle_2} = \frac{r_o + r_1\left(\frac{V_A}{v_0}\right)^{-1/\alpha}\Gamma\left(1+\frac{1}{\alpha}\right)}{r_o + r_1\left(\frac{V_B}{v_0}\right)^{-1/\alpha}\Gamma\left(1+\frac{1}{\alpha}\right)} \tag{2.24}$$

then,

$$\frac{\langle R\rangle_1}{\langle R\rangle_2} = \left(\frac{V_B}{V_A}\right)^{1/\alpha} \tag{2.25}$$

From this relationship it can be observed that the average strength, $\langle R\rangle$, of an ice beam is inversely proportional the volume raised to some power.

2.3.2.2 Past Work on Scale Effect

One of the pioneering investigators into the effect of beam geometry on flexural strength was Lavrov, who determined that flexural strength decreases with increasing beam width (Lavrov, 1971).

Maattanen (1975) performed a series of tests in which the width of the beam was varied. Maattanen theorized that as beam width increases from a "narrow" beam to a "wide" beam the stress field transitions from one to two-dimensional, therefore in accordance with fracture mechanics the failure of defects between ice crystals would increase. Maattanen did not note any significant links between beam length and flexural strength.

Gow and Ueda (1989) did not find any significant change in flexural strength when increasing the size of the test beams, and Parsons and Lal (1991) found the relationship between flexural strength and beam size to be inconclusive.

Parsons et al. (1992) conducted a size-effect study on simply supported beams under 3-point loading. Expected flexural strength values ($\langle R\rangle$) are derived based on Equation 2.23 repeated below.

$$\langle R \rangle = r_o + r_1 \left(\frac{V}{v_0}\right)^{-1/\alpha} \Gamma\left(1 + \frac{1}{\alpha}\right) \qquad \text{(2.23 revisited)}$$

where it can be seen that volume dependencies on strength are governed by the Weibull Modulus (α). The author states that based on the experimental data the value of α (based on a maximum-likelihood fit of the three parameter Weibull distribution) should fall between 4.3 and 7.7 for sea ice and 5.8 and 7.3 for freshwater ice. An exponential regression of the mean strength (σ) versus volume (V) results in $\sigma \propto V^{1/12}$ or $\alpha \approx 12$ for sea ice and an $\alpha \gg 12$ for freshwater ice. This indicates that scale effect trends are present in both sea ice and freshwater ice, albeit lower than would be implied by the variability in ice flexural strength measurements.

Timco and O'Brien (1994), see Section 2.3.3, performed an extensive review of measured freshwater and sea ice flexural strengths for the purpose of creating a correlation between the properties of ice and flexural strength. The authors found that on average there was a difference between flexural strengths of large and small scale beams, however this difference could be attributed to the reduction in brine volume observed in the small scale beams. This theory of brine volume causing the reduction in strength was also discussed in Timco (1985), where the author performed a review of the flexural behaviour of ice, both freshwater and sea ice, for the purpose of defining the properties of modelled ice.

Williams and Parsons (1994) performed a review on a flexural strength database containing 1771 sea ice and 650 freshwater ice data points from three-point, four-point and cantilever beam tests. The purpose of their review was to perform an empirical study of the dependence of flexural strength on the five primary physical parameters of ice (or testing method) including: brine volume, sample size, grain diameter, temperature and strain rate. When investigating the flexural strength of freshwater ice, the data were limited to tests involving 3-point and 4-point bending only. As discussed in Section 2.2.3.1 flexural strengths of fresh-

water cantilever tests can be significantly impacted by the presence of stress concentrations at the root of the beam, for this reason the authors choose to eliminate cantilever tests from their analysis.

Using correlation analyses the authors were able to determine which parameters have the strongest interrelationships to flexural strength. For sea ice, brine volume was determined to have the strongest correlation followed by beam volume. The authors developed a two-parameter exponential model on brine volume and beam volume as seen below:

$$\sigma_f = 1760 \exp\left(-5.395\sqrt{v_b}\right) \left(\frac{V}{V_1}\right)^{-0.0507} \tag{2.26}$$

where V is beam volume and V_1 is 0.01 m^3 based the standard volume of their test samples (also referred to as a reference volume). For freshwater they found the flexural strength model to be:

$$\sigma_f = 1629 \left(\frac{V}{V_1}\right)^{-0.084} \tag{2.27}$$

Williams and Parsons (1994) compared the model results for freshwater ice (Equation 2.27) with measured results in Figure 2.3. In an effort to present the influence of beam volume without the effects of brine volume (v_b), sea ice flexural strengths were adjusted according to:

$$\sigma_p = \sigma_m \left(5.395 \left(v_b - \sqrt{0.03}\right)\right) \tag{2.28}$$

where σ_p is the plotted (or adjusted) strength and σ_m is the measured strength. Modelled strengths (Equation 2.26) were then compared to adjusted strengths as shown in Figure 2.4.

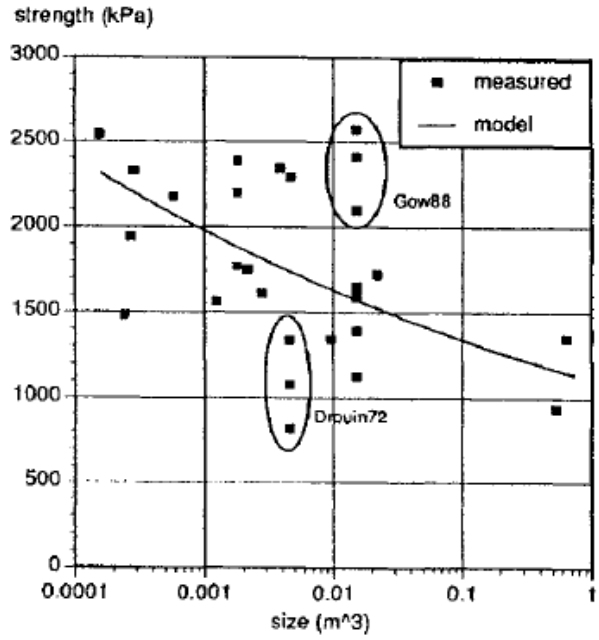

Figure 2.3: Measured and model strength of simple freshwater beams versus beam size (Williams and Parsons, 1994)

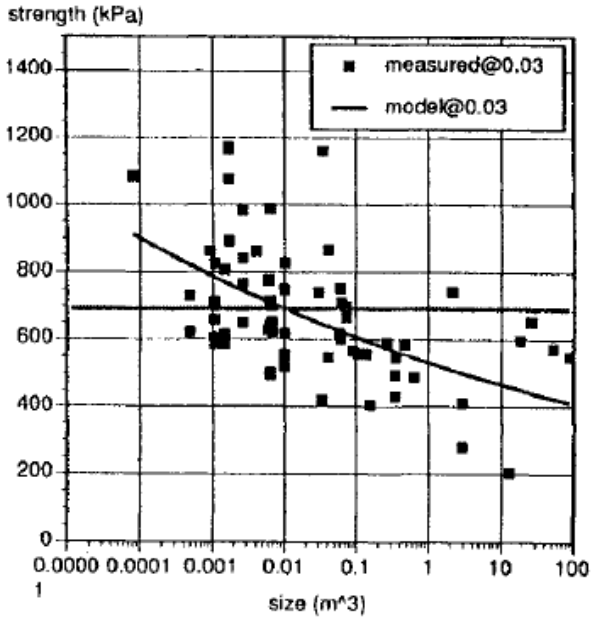

Figure 2.4: Measured and model strength of sea ice ice beams near $v_b = 0.03$ versus beam size (Williams and Parsons, 1994)

Lau et al. (2001) performed a series of flexural tests on small saline ice beams and appended their data to that of Williams and Parsons (1994). Their results were in-line with Williams and Parsons and demonstrated a clear scale effect trend in both freshwater ice and sea ice. Additionally they performed correlation analysis on Williams and Parsons (Equation 2.26) and Timco and O'Brien (1994) (Equation 2.34) and found that Williams and Parsons and Timco and O'Brien under predicted flexural strength by about 11% and 38% respectively, and indicated that the inclusion of the size parameter in Williams and Parsons was the reason for their model experiencing lower error.

Frederking and Sudom (2013) performed a review on the measured flexural strength of multi-year ice from a series of beam tests and ship ramming trials. They observed a decrease in flexural strength as beam volume increased, or in the case of multi-year flows, as the thickness of the flow increased.

Based on the Weibull weakest-link theory, scale effect trends are expected to be present in ice samples. Tozawa and Taguchi (1986) performed a series of 3-point bending tests on freshwater ice specimens of varying size to evaluate the Weibull theory. Their work consisted of more than 100 3-point bending tests with the results presented in Figure 2.5. The expected mean strengths for the medium and small specimen sizes were shown to align very well with the estimated mean strengths from the Weibull model, giving validity the Weibull theory and demonstrating a clear trend towards lower strengths with increasing beam size.

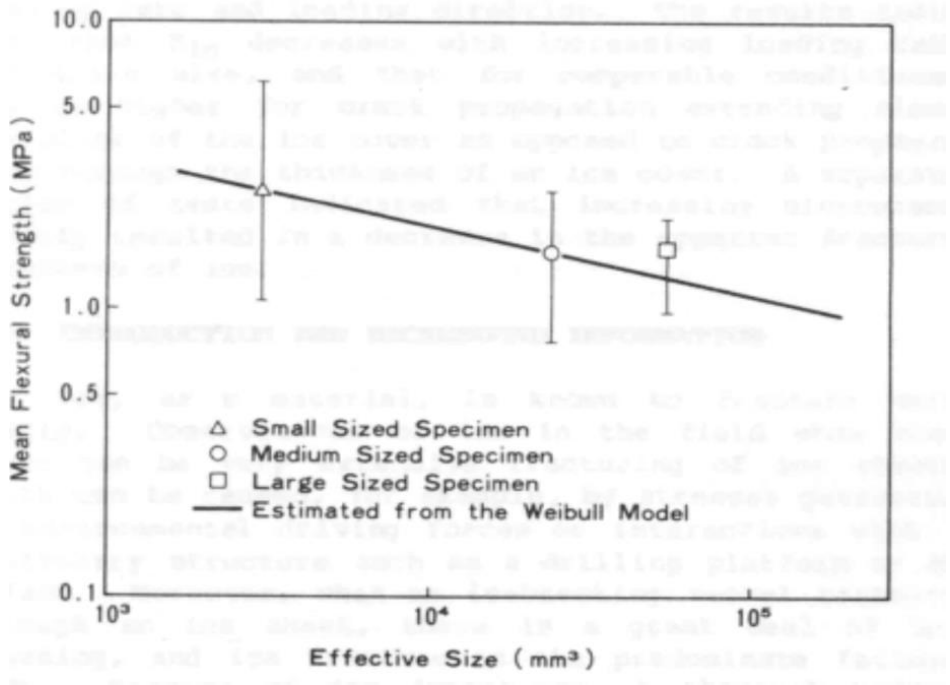

Figure 2.5: Flexural strength vs effective size (Tozawa and Taguchi, 1986)

Aly et al. (2019) assembled a comprehensive flexural strength database containing 2073 freshwater ice and 2843 sea ice flexural strength measurements. The authors performed a regression analysis on the database and developed flexural strength models for both freshwater ice (see Equation 2.29) and sea ice (see Equation 2.30). As demonstrated in the flexural strength models, the authors found that beam volume plays a significant role in the flexural strength of both freshwater ice and sea ice.

$$\sigma_f = 840 \left(\frac{V}{V_1} \right)^{-0.13} \tag{2.29}$$

$$\sigma_f = 1324 \left(\frac{V}{V_1} \right)^{-0.054} \exp(-4.969\sqrt{v_b}) \tag{2.30}$$

Buil et al. (2022) performed an analysis of flexural strength tests for both freshwater and saline ice beams using an explainable ML approach. Their database was based on 608 freshwater and 281 saline ice tests, however, this represents the number of tests prior to data filtering, the final database size was not provided. In this work the authors determined the influence of the various model features on the ML model predictions using the SHapley Additive eXplanation Method (SHAP) and MDI methods. From the SHAP analysis they determined that beam volume was ranked 4$^{\text{th}}$ behind temperature, test type (cantilever or three-point bending) and beam length to depth ratio. In their analysis a conclusive trend between beam volume and flexural strength was not observed, and while in general large beams resulted in lower loads too much variability existed to make any conclusive statements based on the database they considered.

2.3.3 Brine Volume

The influence of brine volume on ice strength has been investigated by a number of authors and it is generally well accepted that ice strength (compressive or flexural) is inversely proportional to brine volume (Weeks and Assur (1967), Dykins (1968), Weeks and Assur (1972), Tozawa and Taguchi (1986), Timco and O'Brien (1994), Frederking and Sudom (2013)). The following sections contain a brief discussion on the formation of brine within an ice sheet as well as some past work relating brine volume to flexural strength.

2.3.3.1 Brine Expulsion

As discussed in Section 2.3.1.1 the entrapment of brine within an ice sample is related to the growth rate, as growth rate increases the amount of trapped brine increases (Cox and Weeks, 1988). The expulsion of brine from an ice sheet is a time and temperature dependent process (Cox and Weeks, 1988). Firstly the temperature dependency, as temperatures decrease water within previously expelled brine is subject to freezing. Once again salts are expelled from the ice lattice, and as the newly forming ice occupies approximately 10% more volume than the water from which it formed, the remaining brine becomes compressed assisting in the drainage of brine from the sheet. Brine will also drain from the ice under gravity, the rate of gravity drainage is related to the temperature and porosity of the ice.

2.3.3.2 Past Work on Brine Volume

The presence of brine and solid salts within an ice sample are quantified using either brine volume or salinity. Brine volume can be expressed as a function of temperature and salinity as defined by Frankenstein and Garner (1967), see Equation 2.31.

$$v_b = S\left(\frac{49.185}{T} + 0.532\right) \tag{2.31}$$

Brine volume is generally randomly distributed throughout an ice sample in what are commonly referred to as brine pockets. The presence of these brine pockets can be considered flaws in the ice sample, therefore as the quantity or size of these pockets increase, the probability that one of those flaws will result in a stress concentration sufficient to cause failure of the sample increases. Weeks and Assur (1967) further suggested that it is logical for ice strength to decrease with increasing brine volume due to a reduction in the amount of solid ice.

The relationship between strength and brine volume has been represented by the following expression as presented in Schwarz and Weeks (1977) and Weeks and Ackley (1986), where σ_0 and a are constants.

$$\sigma = \sigma_0 \left(1 - a\sqrt{v_b}\right) \tag{2.32}$$

Cox and Weeks (1988), in a discussion on the properties of first year ice, performed a least-squares regression on a database from Vaudrey (1977) and found a relationship between brine volume and strength as shown below,

$$\sigma_f = 0.959 - 0.0608\sqrt{v_b} \qquad \text{[MPa]} \tag{2.33}$$

Timco and O'Brien (1994) performed an extensive review of measured freshwater and sea ice flexural strengths for the purpose of creating a correlation between the properties of ice and flexural strength. In their review nearly 3000 measured flexural strength data points were analysed including 1556 for freshwater and 939 for sea ice. The author found that on average there was a difference between flexural strengths of large and small scale beams, however this difference could be attributed to the reduction in brine volume observed in the small scale beams. This theory of brine volume causing the reduction in strength was also discussed in Timco (1985), where the author performed a review of the flexural behaviour of ice, both freshwater and sea ice, for the purpose of defining the properties of modelled ice. Here the author also found that on average the strength values were lower in the large beam samples, and concluded this was likely a cause of the increased brine volume within the larger beams. Brine volume levels in the beams were thought to be an artifact of the general timing and location of the testing; larger samples are generally prepared in the late fall or early spring resulting in warmer ice temperatures, while small beam tests often performed

at colder temperatures and under conditions in which brine drainage is more likely to have occurred. The authors noted that the scatter in flexural strength generally decreased as brine volume increased, suggesting that ice with low brine volume is less ductile. From this work Timco and O'Brien (1994) developed a flexural strength model based only on brine volume, as shown below.

$$\sigma_f = 1760 \exp\left(-5.88\sqrt{v_b}\right) \qquad \text{[kPa]} \tag{2.34}$$

Timco and O'Brien (1994) noted that strength should be a function of the total porosity of the sample taking into account brine volume in addition to air volume (entrapped air bubbles), however the total porosity requires an accurate measurement of the ice density, and unfortunately this is not frequently reported in the literature and therefore not included in their model. Frederking and Sudom (2013) noted that Equation 2.34 over predicted the flexural strength of multi-year ice, concluding that the inclusion of air porosity should also be considered in determining flexural strength.

Further study on brine volume was performed by Aly et al. (2019) who also found that flexural strength of sea ice is inversely proportional to brine volume. Regression analysis on their database consisting of more than 2800 sea ice test results (see Section 2.3.2.2 for more details) resulted in the relationship presented below in Equation 2.35, this relationship is very similar to Timco and O'Brien (1994) presented earlier.

$$\sigma_f = 1730 \exp(-4.89\sqrt{v_b}) \qquad \text{[kPa]} \tag{2.35}$$

According to Buil et al. (2022) the influence of brine volume was ranked 5$^{\text{th}}$ behind temperature, test type (cantilever or three-point bending), beam length to depth ratio and

beam volume. Inspite of the low ranking, their analysis did observe a relationship between decreasing flexural strength with increasing brine volume.

Timco and O'Brien (1994) noted that sea ice flexural strength can vary throughout a typical "winter" as shown in Figure 2.6. Flexural strength is low in early season corresponding to ice that is thinner with higher salinity and temperatures that are still relatively warm. Strength begins to increase throughout the winter as the ice builds thickness and temperatures decrease. Brine volume generally decreases as the season progresses due to brine drainage which is a function of both time and temperature (Cox and Weeks, 1988). At the end of the ice season when temperatures begin to increase and the ice begins to deteriorate the flexural strength begins to drop off rapidly.

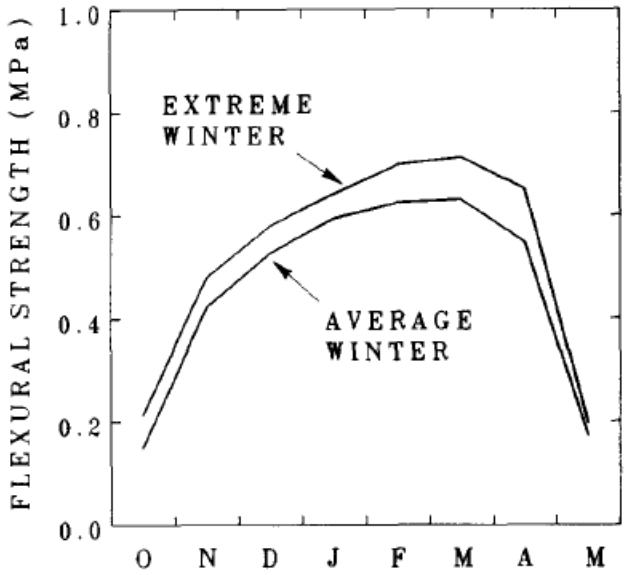

Figure 2.6: Flexural strength versus the time of year (from October (O) to May (M)) for Beaufort Sea ice sheets for both an average and an extreme winter (Timco and O'Brien, 1994).

Timco and Weeks (2010) emphasized that the relationship in Equation 2.34 is not valid for the whole season, but limited to cold ice still in the growth process. As temperatures increase in the spring and the ice warms and begins to decay, the internal brine pockets

begin to migrate and interconnect, culminating in the drainage of brine from the ice. As a result this ice has a very high porosity concentration in spite of a lower brine volume.

Considering the formation of brine pockets within an ice sheet and the process of brine drainage, salinity of an ice sheet will be dependent on the depth within the sheet, and can even vary across small samples (Timco and O'Brien, 1994). The ability to accurately portray the salinity profile in a model of flexural strength would add a lot of complexity to the model, therefore average salinity is a much more reasonable input. According to Timco and Frederking (1990) the average salinity within an ice sheet can be approximated according to the thickness (h_{ice}) of the sheet as,

$$\begin{aligned} S &= 13.4 - 17.4h_{ice} \qquad \text{for: } h_{ice} < 0.34\text{m} \\ S &= 8.0 - 1.62h_{ice} \qquad \text{for: } h_{ice} \geq 0.34\text{m} \end{aligned} \tag{2.36}$$

2.3.4 Temperature

A number of authors have investigated the effects of temperature on the flexural strength of ice. The general consensus is the flexural strength of sea ice decreases as ice temperatures increase (Timco and O'Brien (1994), Saeki et al. (1978), Lainey and Tinawi (1981), Butkovich (1959) and Dykins (1971)). When concerning freshwater ice, Timco and O'Brien (1994) found no strong connection between temperature and flexural strength. When discussing flexural strength of sea ice Timco and O'Brien (1994) noted the effect of temperature has two primary components: firstly the impact on the ice lattice itself and secondly in the impact of temperature on distribution of brine volume.

2.3.4.1 Impact on Brine Volume

As discussed in Sections 2.3.1.1 and 2.3.3.1, the temperature of the ice sheet has a direct influence on the brine volume content within the sheet. As temperatures decrease more brine is expelled from within the sheet, therefore strength of the ice should increase with decreasing temperatures. Frederking and Sudom (2013) found that in multi-year ice flows flexural strength was highest in floes with colder temperatures.

As discussed in Section 2.3.3.2 the seasonal variability observed in flexural strength can be correlated to the temperature, with strength increasing with increasing ice thickness and decreasing temperatures.

As discussed earlier, Timco (1985) found that strength values for smaller beams were generally higher than those for larger beams. They contributed the strength reduction to two factors: an increase in brine within the large beams and a colder ice temperature during the small beams tests. The reduction of brine volume within the small samples is likely the combination of both the temperature variation and the increased potential for brine drainage when removing the samples from the parent ice sheet.

2.3.4.2 Past work on Temperature

The relationship between increasing ice flexural strength with decreasing temperatures has been documented by a number of researchers. Tests performed on sea ice by Butkovich (1959) (see Figure 2.7), Dykins (1971) (see Figure 2.8), Saeki et al. (1978) (see Figure 2.9) and Lainey and Tinawi (1981) (see Figure 2.10) all indicated an inverse relationship between temperature and flexural strength.

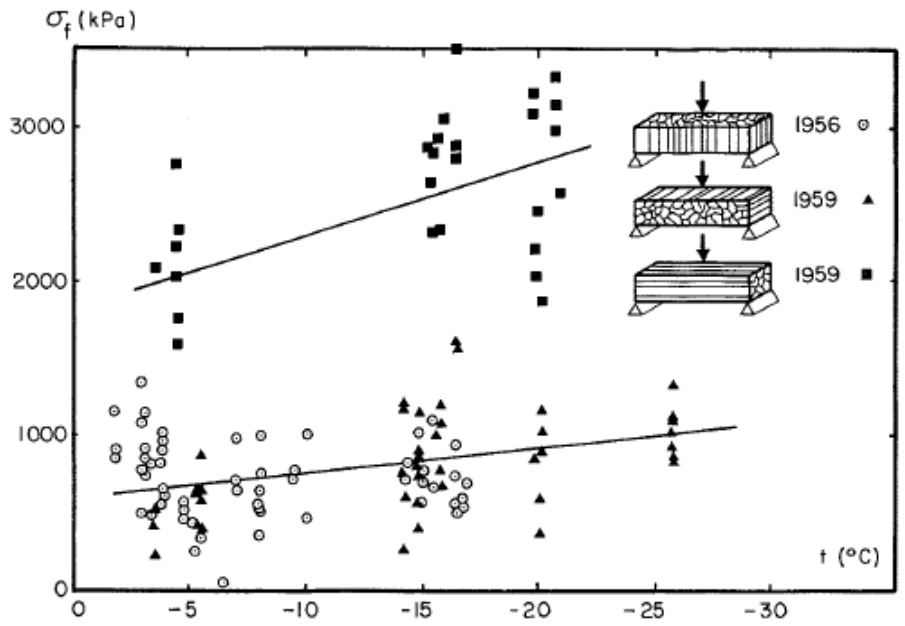

Figure 2.7: Flexural strength vs temperature (Butkovich, 1959,Butkovich, 1956)

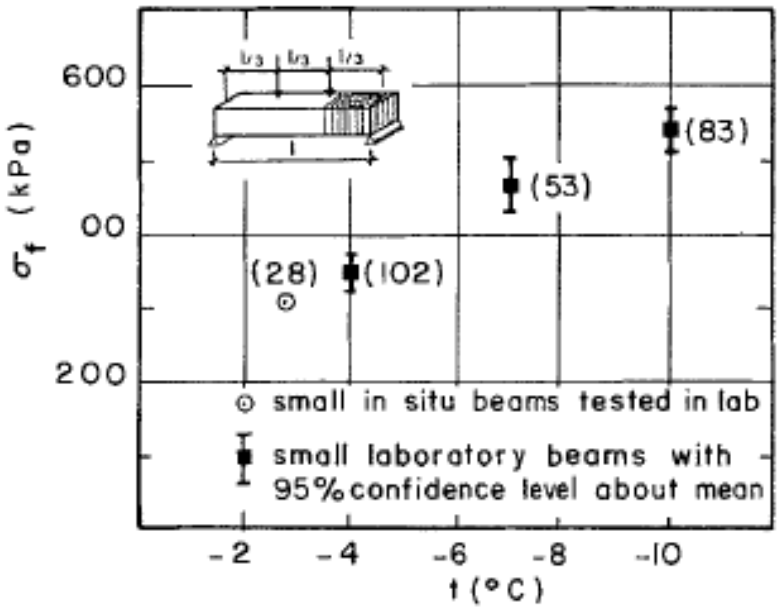

Figure 2.8: Flexural strength vs temperature (Dykins, 1971)

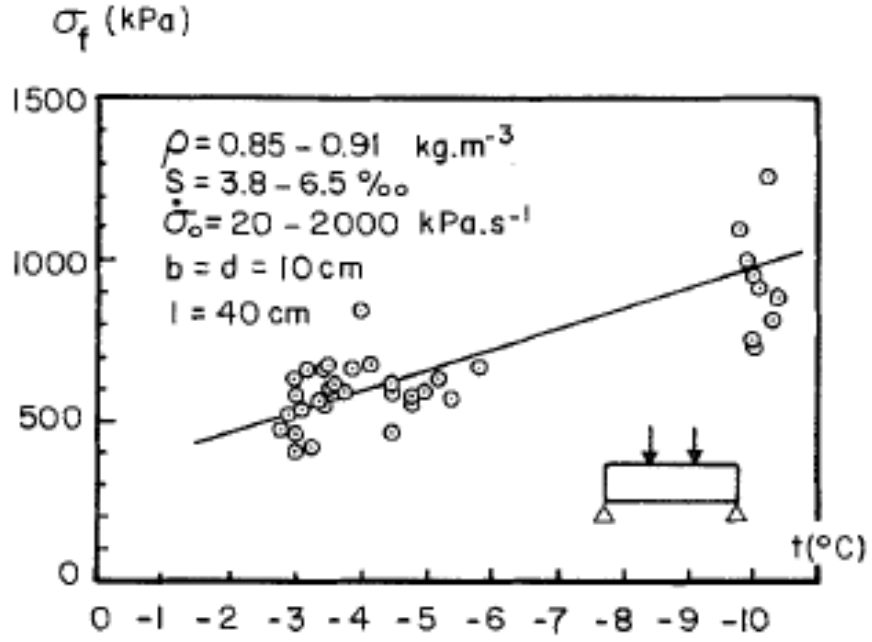

Figure 2.9: Flexural strength vs temperature (Saeki et al., 1978)

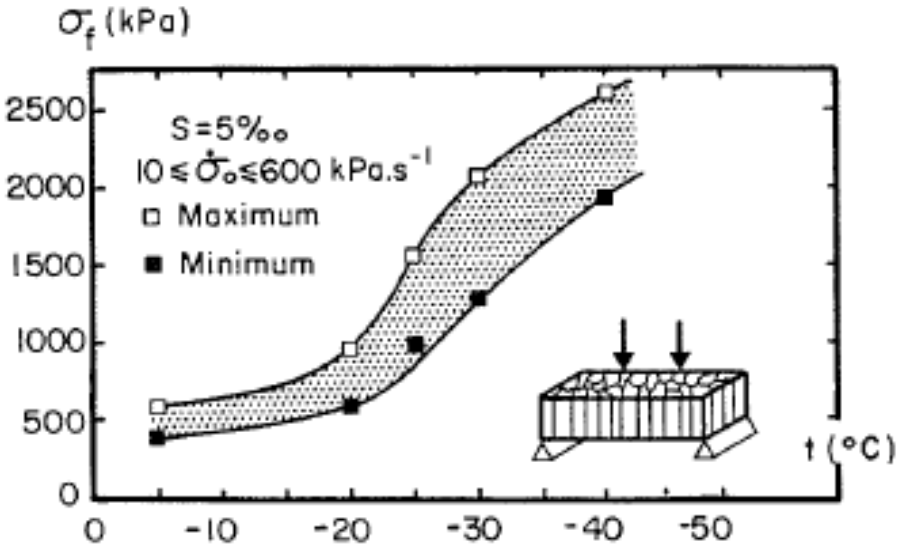

Figure 2.10: Flexural strength vs temperature (Lainey and Tinawi, 1981)

Weeks and Assur (1972) determined that the flexural strength of both freshwater ice and sea ice increased with decreasing temperature. Maattanen (1975) and Gow (1977) found that

not only does the current ice temperature play a role in flexural strength but the temperature history during ice formation is also of significance. This aligns with the discussion of brine expulsion with temperature as discussed earlier (Section 2.3.3.1).

Gow et al. (1978) noted an appreciable dependence between flexural strength and temperature for large lake ice beams. Gow and Ueda (1989) performed a series of test of freshwater ice beams, and found that for beams with a temperature gradient between the top and bottom fibres there was little dependence of flexural strength on temperature. However, if these beams were allowed to reach constant temperature, i.e. being isothermal, there was a significant increase in flexural strength as beam temperature decreased.

Lainey and Tinawi (1984) found that flexural strength of sea ice increased with decreasing temperature, but noted that temperature appears to have much less significance in freshwater ice. Lainey and Tinawi also noted that substantial increases in strength were found for temperatures below -23°C. Timco and O'Brien (1994) found that strength decreased significantly above -4.5°C and also observed a much higher degree of scatter. They contributed these low strengths to be a result of "candling", which refers to melting along the grain boundaries as a result of solar radiation. This "candling" can result in extremely low strengths even when the ice still has considerable thickness.

Williams and Parsons (1994) performed correlation analysis between flexural strength and the ice properties of brine volume, sample size, temperature, grain size and strain rate. The strongest correlations were with brine volume and sample size (respectively), however temperature and the others were also found to be of significance.

Saeki et al. (1978), Blanchet et al. (1997) and Ji et al. (2011) analysed flexural strength data on sea ice. The relationship between temperature and flexural strength according to Saeki et al., Blanchet et al. and Ji et al. are provided in Equations 2.37, 2.38 and 2.39 respectively.

$$\sigma_f = 3.4 - 0.64T \qquad [\text{kg/cm}^2] \tag{2.37}$$

$$\sigma_f = 0.5836 - 1.413T \qquad [\text{MPa}] \tag{2.38}$$

$$\sigma_f = 0.35 - 0.09T \qquad [\text{MPa}] \tag{2.39}$$

These equations are summarized in Figure 2.11, and it can be seen that the Blanchet et al. results in values significantly higher than the other two models, leading one to believe that perhaps a typesetting error is present in the model. However, without any references to cross validate the model and due to the significant offset in the Blanchet et al. model, this model will not be used in any analysis in this work.

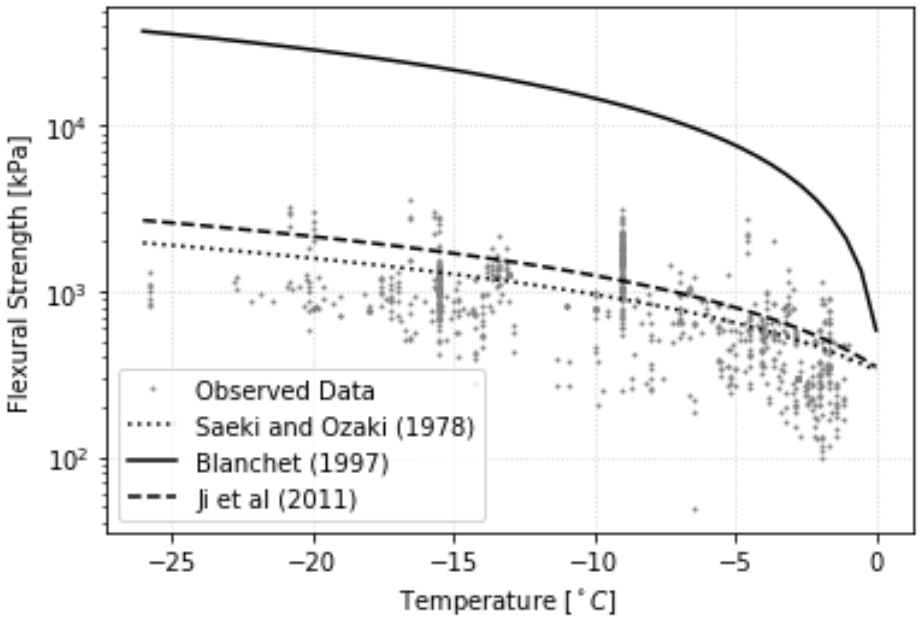

Figure 2.11: Flexural strength as a function of temperature

According to Buil et al. (2022) temperature is the primary ice feature impacting flexural strength. Additionally, the authors determine that flexural strength decreased as ice temperatures increased.

2.4 Summary

In Section 2.1, an overview of ice failure methods were presented, followed by a review of ice flexural strength testing methods in Section 2.2, the three most common methods being cantilever, three-point and four-point bending. Each method has associated advantages and disadvantages. Cantilever tests are the easiest of the three to perform in the field, more readily adaptable to various beam sizes and better at preserving the temperature and salinity profiles of the beam. Three-point and four-point bending tests eliminate the influence of stress concentrations observed at the root of cantilever beams. Four-point bending produces a zone of constant moment and zero shear between the two loading points, increasing the likelihood of the beam failing at its weakest point and not the point of highest load as is generally the case in three-point bending. While four-point bending may offer slightly better quality results, the limited availability of flexural strength data solely from four-point bending requires results from all test methods to be considered.

In Section 2.3 a review of ice properties and their effect on ice flexural strength were presented, along with an overview of the fundamental approach to scale effect in materials. Based on theory and observed data, there is a general consensus that flexural strength has an inverse relationship with brine volume, beam volume and temperature.

The influence of brine volume on the flexural strength of ice has been investigated by a number of authors and it is generally well accepted that ice strength is inversely proportional to brine volume (Weeks and Assur (1967), Dykins (1968), Weeks and Assur (1972), Tozawa and Taguchi (1986), Timco and O'Brien (1994) and Frederking and Sudom (2013)).

The presence, or at least the significance, of scale effect trends in both sea ice and freshwater ice has been debated in the literature. The results from physical testing by a number of authors were either inconclusive or showed scale effect to be insignificant (Gow and Ueda (1989), Timco and O'Brien (1994) and Parsons et al. (1992)). As presented earlier, there is theoretical evidence to suggest scale-effect should be present, this theory has been validated by several researchers who have found that the presence of scale effects trends in ice are of significance (e.g. Tozawa and Taguchi (1986), Williams and Parsons (1994) and Lau et al. (2001)) and should be considered when modelling flexural strength.

Like beam volume, the effects of temperature are debated in the literature, and have varying results depending on whether the discussion is on freshwater ice or sea ice. Weeks and Assur (1972), Maattanen (1975) and Gow (1977) found a link between decreasing flexural strength with increasing temperatures. Several authors found that only a weak link between flexural strength and temperature exists for freshwater ice including Lainey and Tinawi (1984) and Gow and Ueda (1989), while Buil et al. (2022) found that temperature was the key feature in predicting flexural strength.

Using an extensive database of flexural strength measurements, an updated investigation into the effects of ice properties such as beam volume, brine volume and temperature on flexural strength are investigated for both Freshwater Ice (Chapter 5) and Sea Ice (Chapter 6).

3 Flexural Strength Database

The accuracy and validity of a ML model is governed by the data upon which the model are trained. In the following sections, the freshwater ice and sea ice flexural strength database will be presented including details on the preprocessing steps required before model training could begin.

3.1 Data Source

The primary source of data for this work were acquired from a database compiled by Aly et al. (2019) based on an archive of technical publications reporting on freshwater ice and sea ice beam tests. Additional data from a series of field programs conducted between 2010-2018 (Karulina et al., 2019), were appended to the Aly et al. database. The database is quite extensive, with 4100 freshwater ice and over 2700 sea ice data points.

The amount of data presented within a technical publication can vary significant from one publication to the next. The core test parameters of interest to the database are the volume of the test beam, measured strength, ice type (freshwater or sea ice), the type of test (cantilever, three-point or four-point bending), brine volume, ice temperature, salinity and location of the test(field or laboratory). In many cases one or more of these core parameters were not presented in a given publication, resulting in the need for data preprocessing.

3.2 Data Preprocessing

Prior to any model development the database was subjected to two forms of preprocessing; filtering and data adjustment.

3.2.1 Data Filtering

The database was inspected and filtered to remove any unnecessary or unusable data, the following steps were taken when filtering the database:

Step 1: Freshwater Ice vs Sea Ice: Separate models were developed for freshwater ice and sea ice, therefore, it was necessary to split the database according to the type of ice tested. Subsequent steps were performed on both the freshwater ice and sea ice subsets.

Step 2: Null Values: The ML algorithms do not perform well when the features (input data) contain null values, therefore entries with null values were removed from database.

Step 3: Field vs Laboratory Testing: For this work, the strength of naturally occurring ice is the primary interest, and for the current database this refers to tests which have been performed in the field. Laboratory test are generally conducted on ice samples which are grown in the laboratory under strict controlled conditions. Great care is generally taken to ensure these samples are grown to minimize the inclusion of flaws such as cracks and air pockets, and samples with such flaws are often not chosen for testing. Naturally occurring ice on the other hand, is prone to the inclusion of many flaws, including cracks, debris/air pocket inclusions, layer separation due to freeze thaw cycles and many more. The strength of naturally occurring ice samples is generally lower than that of the laboratory grown samples.

With each filtering step the number of data entries in the database decreased. The results of the above data filtering reduced the freshwater ice and sea ice databases to 641 and 803 entries respectively, details on the number of remaining entries after each filtering step are provided in Table 3.1. The 641 entries in the freshwater database detail the work of seven researchers (or research groups) as listed in Table 3.2. The 803 entries in the sea ice database detail the work of 14 researchers (or research groups) as listed described in Table 3.3. Flexural strength as a function beam volume for the resultant freshwater ice and sea ice database can be seen in Figures 3.1 and 3.2, additional plots of sea ice flexural strength as a function of brine volume and temperature are provided in Figures 3.3 and 3.4.

Table 3.1: Number of entries resulting after each preprocessing step

	Step 1 (Ice Type)	**Step 2** (Null Values)	**Step 3** (Location)
Freshwater Ice	4100	4076	641
Sea Ice	2755	1171	803

Table 3.2: Journal papers for freshwater ice analysis

Primary Author	**Title**
Frankenstein (1959)	*Strength data on lake ice*
Lavrov (1971)	*Deformation and strength of ice*
Gow and Langston (1975)	*Flexural Strength of Lake Ice in Relation to Its Growth Structure and Thermal History.*
Gow et al. (1978)	*Flexural strength of ice on temperate lakes: comparative tests of large cantilever and simply supported beams*
Frederking and Timco (1983)	*On measuring flexural properties of ice using cantilever beams*
Frederking and Sudom (2013)	*Review of flexural strength of multi-year ice*
Karulina et al. (2019)	*Full-scale flexural strength of sea ice and freshwater ice in Spitsbergen Fjords and North-West Barents Sea*

Table 3.3: Journal papers for sea ice analysis

Author	**Title**
Butkovich (1956)	*Strength studies of sea ice*
Butkovich (1959)	*On the mechanical properties of sea ice, Thule, Greenland, 1957*
Frankenstein and Garner (1970)	*Dynamic young's modulus and flexural strength of sea ice*
Williams et al. (1991)	*Full-scale ice breaker trials CCGS Sir John Franklin Indian Arm/Little Burnt Bay 1991*
Williams et al. (1992)	*Ice and snow measurements in support of the operational evaluation of the Nathaniel B. Palmer in the Antarctic winter environment*
Williams, Crocker, et al. (1993)	*Northumberland Strait ice properties measurements*
Williams, Kirby, et al. (1993)	*Strength and Fracture Toughness of First-Year Arctic Sea Ice*
Saeki et al. (1981)	*Experimental study on flexural strength and elastic modulus of sea ice*
Dykins (1968)	*Tensile and flexural properties of saline ice*
Blanchet et al. (1997)	*Mechanical properties of first-year sea ice at Tarsiut Island*
Christensen (1986)	*Sea ice strength measurements from the inner Danish Waters in early 1985*
Kujala et al. (1990)	*Results from in situ four point bending tests with Baltic Sea ice*
Frederking and Sudom (2013)	*Review of flexural strength of multi-year ice*
Karulina et al. (2019)	*Full-scale flexural strength of sea ice and freshwater ice in Spitsbergen Fjords and North-West Barents Sea*

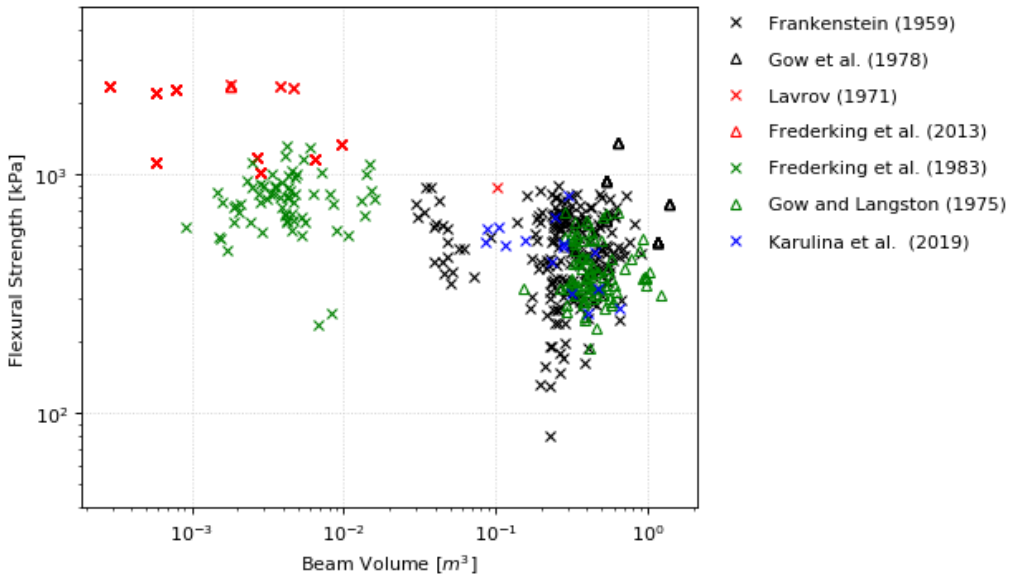

Figure 3.1: Resultant freshwater ice database: Flexural strength as a function of beam volume

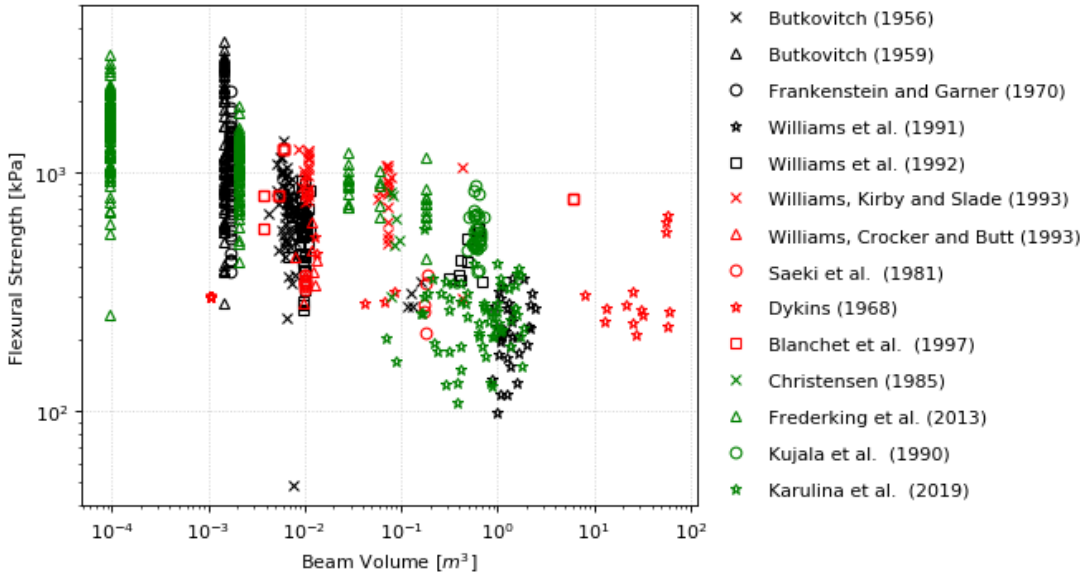

Figure 3.2: Resultant sea ice database: Flexural strength as a function of beam volume

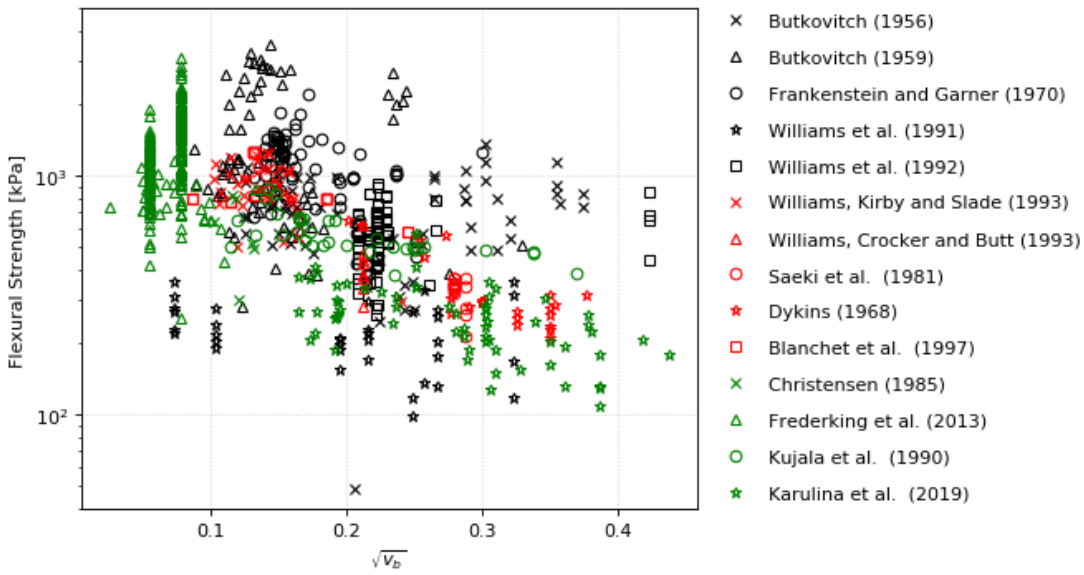

Figure 3.3: Resultant sea ice database: Flexural strength as a function of the square root of brine volume fraction

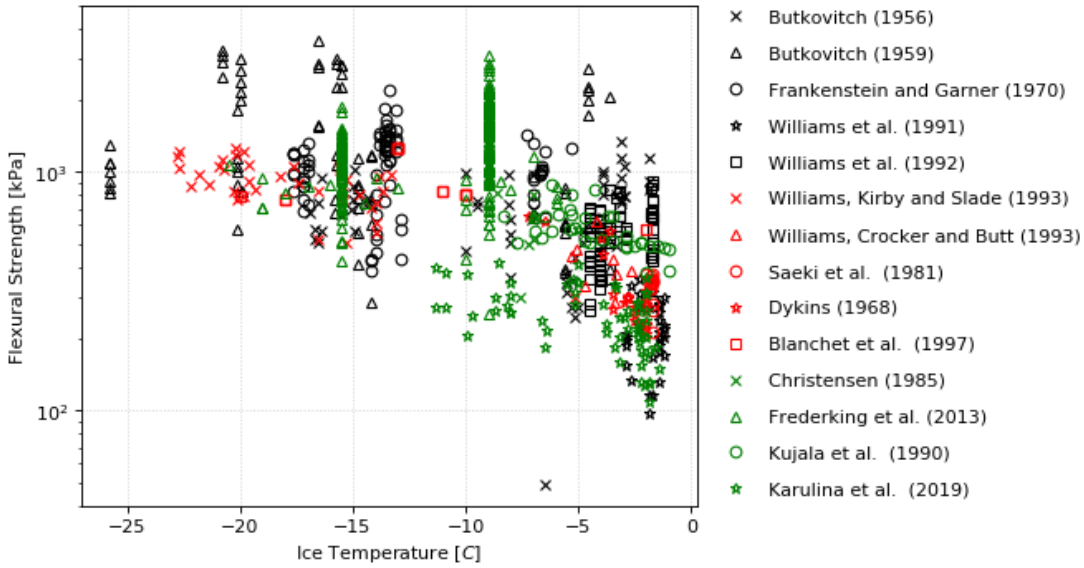

Figure 3.4: Resultant sea ice database: Flexural strength as a function of ice temperature

A high degree of variability in the flexural strength of both freshwater and sea ice samples can be observed in Figures 3.1, 3.2, 3.3 and 3.4. A portion of this variability is likely due to natural variations that can be observed within a given ice sheet, however the effect of

variations in test mechanics and ice sample properties from test to test are also a factor. For instance parameters such loading rate, loading direction, ice density, total porosity and grain size are not always publicized along with the flexural strength results, however, each of these parameters can have an impact on the resultant flexural strengths.

3.2.2 Data Adjustment: Cantilevered Tests

As discussed in Section 2.2.3.1, the presence of stress concentrations at the root of cantilever beams can result in a significant reduction in the flexural strength of the beam. The influence of stress concentrations was found to be more prevalent in freshwater beams when compared to sea ice beams. In the freshwater database approximately 80% of all field measurements were performed using the cantilever beam test, therefore there is significant motivation to keep the cantilever beam tests as part of the analysis. To permit the use of cantilever beam measurements a correction factor must be applied to adjust the recorded strengths. The use of a correction factor has been discussed in Section 2.2.3.1 where Aly et al. (2019) suggested a factor of 2, which is in line with the results presented by Gow et al. (1978). To verify these correction factors a comparison between cantilever and simple beam measurements was performed. A Least Squares Regression (LSR) line was fit to the natural log of flexural strength and beam volume for both cantilever and simple beam tests as shown in Figure 3.5, the resultant equations are shown in Equation 3.1 (cantilever tests) and Equation 3.2 (simple beam tests). From the figure and LSR equations, it is evident that the trend lines for both the cantilever and simple beam measurements have nearly identical slopes (equivalent at the hundredths place), and taking the ratio of these two equations results in simple beam strengths being approximately 2 times higher than the cantilever beam strengths. Therefore, in following with Aly et al. (2019) and Gow et al. (1978) in addition to the comparison performed here, a correction factor of 2.0 was applied to the cantilevered strength values for the analysis conducted in this work.

$$\sigma_{f\,\text{Cantilever}} = 399\frac{V}{V_1}^{-0.13} \tag{3.1}$$

$$\sigma_{f\,\text{Simple Beam}} = 828\frac{V}{V_1}^{-0.13} \tag{3.2}$$

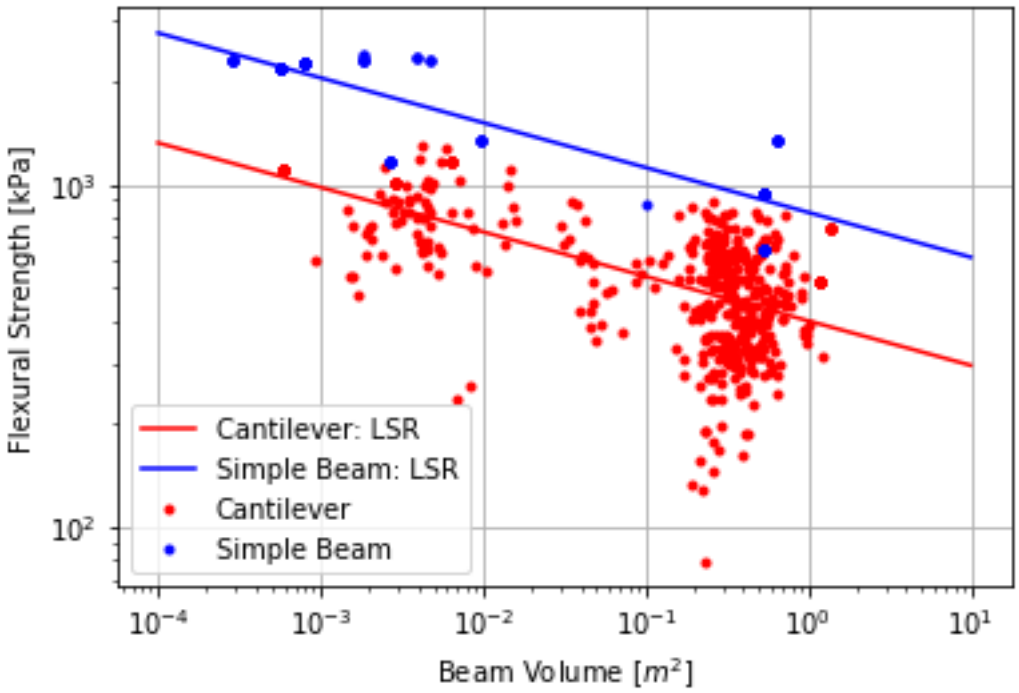

Figure 3.5: Freshwater flexural strength vs beam volume: Cantilever vs simple beam

3.3 Summary

The flexural strength database contained a total of 4100 freshwater and 2755 sea ice flexural strength measurements. Removing null values and omitting laboratory tests the number of measurements were reduced to 641 and 803 for freshwater and sea ice respectively. The developement of ML and empirical models presented in the following sections are based on these 641 freshwater and 803 sea ice flexural strength measurements.

4 Machine Learning

Machine Learning (ML) is best described as the field of study that gives computers the ability to learn without being explicitly programmed. This definition is generally attributed to Arthur Samuel (1959) one of the pioneers in ML. The following sections will present some background on general model development, selected machine learning algorithms as well as some general information surrounding the practical use of machine learning libraries.

4.1 Background

The implementation of ML in this work was performed using a Python based ML library developed by Scikit Learn (Scikit-learn, 2021). This library contains an extensive compilation of learning algorithms in addition to tools for data analysis and quality control of the input data.

The input dataset, including the independent and dependent variables, are partitioned to form two sets of data, a training set and a test set. The formation of these datasets involve the random selection of a data entry from the input dataset which is then randomly placed in either the training set or test set. The training set is generally larger than the test set and is often comprised of 70% of the input dataset. As the name implies, the model is trained on, or learns based on, the training set while the test set is used to evaluate or test the model on new or unseen data.

The range of values within these model features must also be considered, as some ML algorithms are sensitive to large variations within the features. In particular algorithms which

exploit distances or similarities between data points are susceptible to errors as a result of high feature variance. To avoid one feature creating a bias within the model, a common practice is to perform feature scaling via normalization or standardization. In the current work there are three main features of interest, beam volume with values ranging from 9.3×10^{-6} m^2 to $60m^2$, brine volume ranging from 0 to 370 ppt and temperature ranging from -55°C to 0°C. In this work the data were standardized, in which each feature is rescaled to have a mean of 0 and a variance of one.

Each ML algorithm contains a set number of input parameters, generally referred to as hyperparameters, which are used to control how the model reacts with the training data. The proper selection of these hyperparameters are paramount in the optimization of the model.

4.2 Algorithms

The work presented here will focus on four supervised learning regression algorithms including: multi-layer perceptron, gradient boosted trees, extra trees and k-nearest neighbours. A brief introduction to each of these algorithms is provided in the following sections. As the goal of this research was in the application of ML algorithms and not in the development or advancement of these algorithms, the review will focus primary on the basic approach of the algorithm with an attempt to highlight the advantages and disadvantages of each algorithm. For further details on the individual algorithms there are numerous options available in the technical literature, such as Belyadi and Haghighat (2021), Zhou (2021) and Scikit-learn (2021).

4.2.1 Multi-layer Perceptron Regression

The Multi-layer Perceptron Regressor (MLPR) is categorized as an Artificial Neural Network (ANN), and the basic components of the algorithm include neurons (or nodes), an input layers, a hidden layer(s) and an output layer. The number of nodes in each layer and the number of hidden layers are amendable according to the needs of the model being developed. There is no communication between nodes within a given layer, however adjacent layers are fully interconnected, as demonstrated in Figure 4.1. Each node to node link is associated with a weight (e.g. w_{11}), input values are then passed along these links and multiplied by the associated weight. Each node receives the weighted sum from the nodes in the previous layer which is subjected to an activation function and passed on to the next layer. This forward passing of information culminates with the output layer receiving the final weighted sums which are subsequently subjected to the activation function concluding as the model response. A regularization parameter is generally employed to help improve the generalization of the model and reduce overfitting.

Training a MLPR model involves the forward passing or propagation of information as discussed above and the back propagation of information. On the first pass the weights of the links are estimated, at the end of a pass a comparison is made between the predicted output and the expected output and the weights are then automatically adjusted for each layer. This adjustment of weights, referred to as back propagation, is performed by a process referred to as "gradient decent" which attempts to minimize the error within the function. The number of iterations is generally defined by the user, and with each iteration the error (expected vs predicted) should decrease.

For the MLPR there are numerous hyperparameters which require tuning to arrive at an optimized model. The tuning of these hyperparameters can be aided through the use of built-in functions within the ML library. Hyperparameters requiring specific attention are:

- the number of hidden layers,
- the weight optimization solver,
- the number of iterations through the network,
- the strength of the regularization parameter (α), and
- the activation function.

The MLPR does have a few disadvantages which must be considered prior to use. Firstly, the inclusion of hidden layers results in a non-convex loss function and therefore multiple local minimum can exist. The primary means for limiting the effects of a non-convex loss function is in the selection of the regularization parameter (α). The MLPR is also sensitive to the variance within the input data, therefore feature scaling is necessary to ensure no single feature is disproportionately represented.

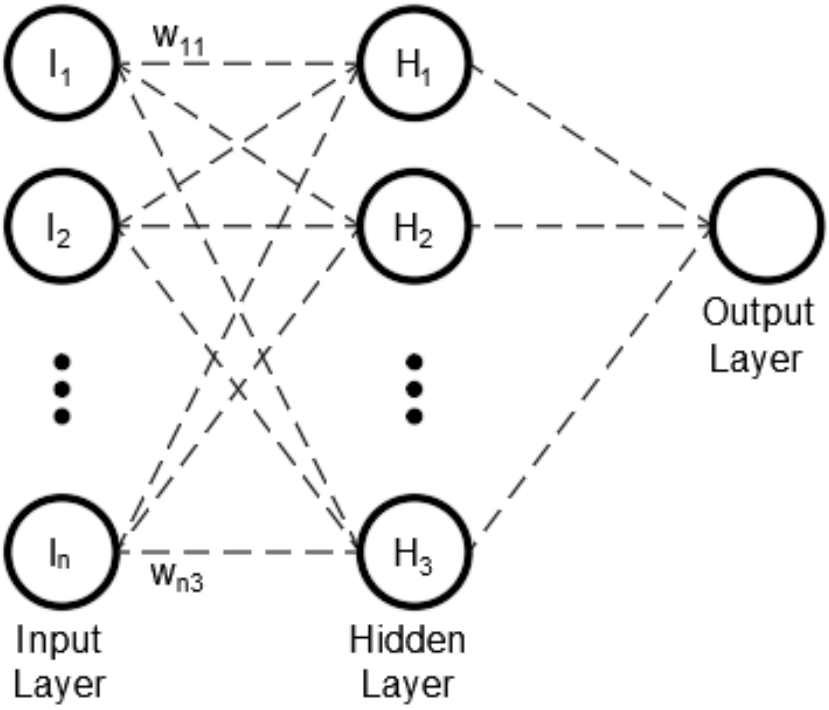

Figure 4.1: An example MLPR layer structure

4.2.2 Decision Trees

Decision trees are non-parametric supervised learning algorithms which can be applicable to both classification and regression problems. In general, decision trees are relative simple in concept and can often be presented visually, such as in Figure 4.2. Unlike some algorithms decision trees are not sensitive to the variance within the data and therefore do not require feature scaling. Decision trees have the potential to become overly complex resulting in models which overfit the data, this issue can often be mitigated through the careful selection of the hyperparameters. Due to the nature of the decision tree process, the predicted outcomes are not smooth and continuous but piecewise approximations and as a result decision trees do not perform well when attempting to extrapolate beyond the limits of the training data. When extrapolating, decision trees will base predictions on the nearest leaf nodes to the query point, and with each query calling on the same leaf nodes extrapolation results in constant predictions.

Decision trees can also be unstable, where small changes to the input data can generate vastly different tree structures affecting model predictions. One means by which to reduce this sensitivity is to implement the use of ensemble modelling. Two decision tree ensemble models, Extra Trees Regressor (ETR) and Gradient Boosted Trees Regressor (GBR), were employed in this study and a brief discussion of each are contained in the following sections.

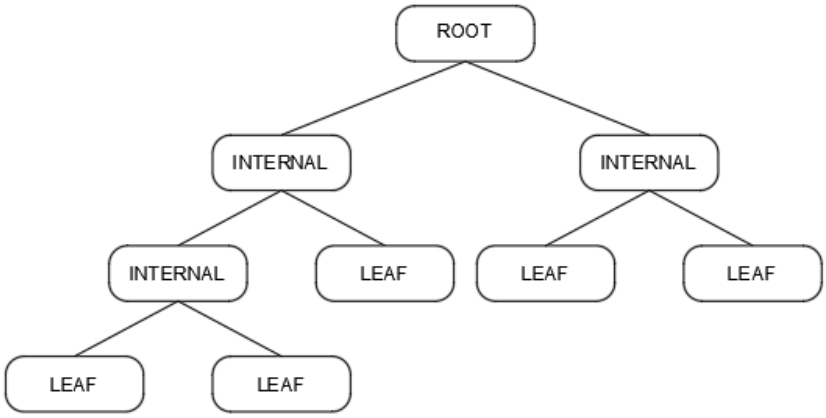

Figure 4.2: A simple decision tree

4.2.2.1 Extra Trees Regression

The ETR is an ensemble method in which n number of trees are generated from various sub-samples of the training data (Scikit-learn, 2021). The decision of splitting is performed using a random subset of features, the threshold for these features are drawn at random and the best of these random thresholds is selected as the splitting rule.

The ETR algorithm accepts a number hyperparameters which require tuning to arrive at an optimized model, three hyperparameters requiring specific attention are:

- the number of estimators (or trees) in the ensemble,
- the maximum depth of the tree, and
- the minimum number of samples required at any given leaf

The *max depth* parameter controls the number of splits within each tree, the *number of estimators* determines the number of trees and the *minimum samples per leaf* sets the minimum number of samples in each branch of the tree.

Individual decision trees have been found to exhibit high variance and generally over fit the data. However, the randomness associated with ETR has been found to reduce this variance

resulting in a model which is less prone to overfitting. Another benefit of the randomness is that ETR models have improved computational cost when compared to other decision tree models such as Random Forest. The issues surrounding decision trees and data extrapolation are still present when using ETR

4.2.2.2 Gradient Boosted Trees Regression

GBR, like ETR is an ensemble method in which n number of trees are generated and used in the predictions, however GBR differs in how the trees are generated and combined. As described in Belyadi and Haghighat (2021) GBR builds an ensemble model by sequentially training on many smaller simpler models referred to as weak learners. With the assembly of each weak learner the error rate (difference between predicted and observed) can be generated and used to determine the gradient, which is essentially the partial derivative of the loss function. Using the gradient, modifications to the model parameters can be estimated to reduce the error in the next round.

There are multiple hyperparameters required for successful operation of the GBR algorighm, a few of the hyperparameters requiring specific attention are:

- the *learning rate*, which controls the contribution of each tree,
- the *maximum depth* of the individual trees,
- the *number of features* considered when determining the best split,
- the *minimum samples per leaf*, and
- the *number of estimators* or boosting stages to be performed

The application of GBR, like ETR, can help to lower the variance observed within a model and reduce a models tendency towards overfitting. Like ETR, the issues surrounding data extrapolation are still present when using GBR.

4.2.3 k-Nearest Neighbours Regression

k-Nearest Neighbour Regressor (KNR) is a common yet simple supervised learning method that can be employed for both classification and regression. Predictions for a query point are generated based on the k-nearest training samples or neighbours. Predictions in regression applications are generally made by averaging these k neighbours. These neighbours can be weighted by distance such that the closer a neighbour is to the query point the higher the weight, or each neighbour can be assigned a uniform weighting. An example of a KNR model is presented in Figure 4.3, showing two query points and their associated five nearest neighbour data points.

For KNR there are numerous hyperparameters which require tuning to arrive at an optimized model, three hyperparameters requiring specific attention are:

- the number of neighbours,
- the method of weighting, and
- the algorithm used to compute the nearest neighbours

KNR models are very intuitive and easy to follow, and like decision trees are not sensitive to the variations in the features and therefore do not require feature scaling. However, KNR tend to decrease in efficiency for large datasets or for datasets with a large number of features. Also KNR does not perform well when attempting to predict beyond the range of the training data, as all new predictions will based on the same subset of neighbours.

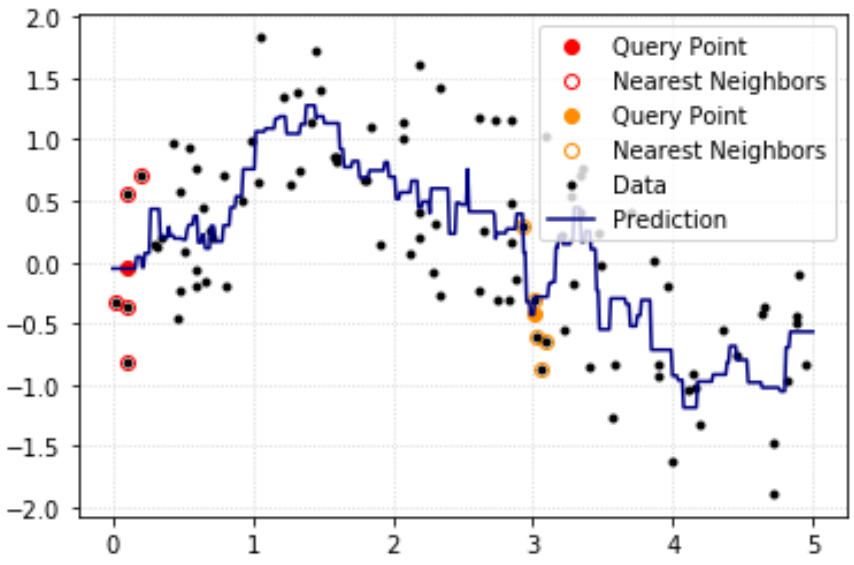

Figure 4.3: Example KNR model

4.3 Ensemble Modelling

As discussed in Section 4.2.2 where multiple decision trees were combined to form the ensemble models of ETR and GBR, a similar application of ensemble modelling can be employed to improve upon the characteristics of an individual models (MLPR, ETR, GBR and KNR). In the current work a total of six ensemble models were developed consisting of model pairs generated from the original four individual models.

4.4 Model Evaluation and Selection

During evaluation and comparison between the various ML regression algorithms, a number of evaluation metrics may be used including:

- Root Mean Squared Error (RMSE),
- Coefficient of determination,

- Expected physical behaviour,
- Generalization and overfitting behaviour

4.4.1 Root Mean Square Error

RMSE is the standard deviation of the residuals, and provides a measure of the prediction error of a regression model. The RMSE is calculated according to Equation 4.1 where n, y_i and $\hat{y}_i$ are the number of data points, the observed data, and the predicted data respectively.

$$RMSE = \sqrt{\frac{\sum_{i=1}^{n}(y_i - \hat{y}_i)^2}{n}} \tag{4.1}$$

4.4.2 Coefficient of Determination

Coefficient of Determination, often denoted as R^2, is a measure of how much of the variability in the dependant variable can be predicted from the independent variable(s). The calculation of R^2 is defined in Equation 4.2, where y, $\hat{y}$ and $\bar{y}$ represent the observed data, predicted data and mean of the observed data respectively.

$$\begin{aligned} SSR &= \sum_{i=1}^{n}(\hat{y}_i - \bar{y})^2 \\ SSE &= \sum_{i=1}^{n}(y_i - \hat{y})^2 \\ SST &= \sum_{i=1}^{n}(y_i - \bar{y})^2 \\ R^2 &= \frac{SSR}{SST} = 1 - \frac{SSE}{SST} \end{aligned} \tag{4.2}$$

The calculation of R^2 is generally based on the assumption that the data are linear, normally distributed, independent and have constant varaince. It could be argued that the data used in this analysis do not strictly comply with all these assumptions. However, the R^2 coefficent still has utility in assessing the predicted outcomes of the models.

4.4.3 Expected Physical Behaviour

The expected behaviour of ice based on theoretical and empirical evidence is also considered during model evaluation. As discussed in Section 2.3 the models are expected to present a trend towards lower flexural strength with increasing beam volume, brine volume and temperatures. Models which demonstrate these expected physical behaviour will be given a higher ranking.

4.4.4 Generalization and Overfitting

When tuning a model it is important to balance the accuracy of the model with the ability to generalize to the underlining trends within the data. In most instances a ML model can be tuned such that it produces a very high accuracy to the training data, simply by "memorizing" the expected result. This is referred to as overfitting, an example of which can be seen in Figure 4.4. An overfitted model does not generalize well and will have low statistical accuracy on data not previously seen. An underfitting model on the other hand suffers from both poor generalization and low statistical accuracy on both observed and new data. The goal is to tune the model as to obtain a balanced predictive behaviour as shown in Figure 4.4. An appropriately balanced model will generalize well to the underlining data trends in addition to providing accurate predictions on new data. As shown in Figure 4.4 the balanced model may have lower accuracy metrics, however it offers a better representation of the underlining trends in the data. For this reason, it is important to consider the simplicity

of the model and how well it can generalize to the underling data trends in addition to the statistical accuracy metrics of the model.

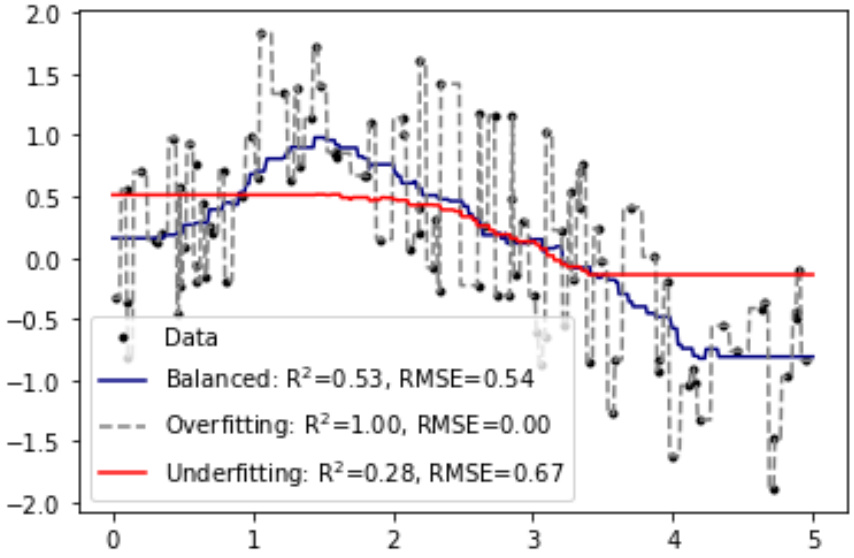

Figure 4.4: Example of overfitting, underfitting and balanced models

5 Freshwater Ice Analysis

In the following sections an investigation of freshwater ice flexural strength is presented, with a discussion on traditional and machine learning methods. A portion of the work in this Chapter was published in a paper entitled "Estimating Freshwater Level Ice Loads on Sloping Structures Using Machine Learning-Derived Flexural Strength," and was presented at the 26th IAHR International Symposium on Ice, see Burton et al. (2022). Co-authors Dr. Rocky Taylor and Dr. Renat Yulmetov served in conceptualizing the research, securing funding, and providing guidance and support during data analysis and interpretation as well as reviewing and editing the manuscript. The author took on the primary role in research execution, compiling and analyzing data, leading the organization, synthesis and interpretation of results, as well as preparation and revision of the manuscript.

5.1 Traditional Methods: Non-linear Regression

Non-linear models can serve as a robust means for estimating the flexural strength of freshwater ice. Single parameter polynomial regression models are often employed due to their linearity when plotting in a log-log scale. One such model is represented by the equation:

$$\sigma_f = C \times \left(\frac{V}{V_1}\right)^x \tag{5.1}$$

where σ_f is the flexural strength of ice, C and x are constants, V is the volume of the beam and V_1 is a reference volume. This single parameter polynomial model, simply referred to

as a linear model for the remainder of this work, was employed by Williams and Parsons (1994) (see Equation 5.2), Aly et al. (2019) (see Equation 5.3) and Burton et al. (2022) (see Equation 5.4). A modification to the filtering methods since the publication of Burton et al. (2022) and a subsequent regression analysis on the observed data resulted in the same equation as defined in Aly et al. The reference volume, V_1, generally refers to the standard volume of the ice samples used within a given test set-up, and for Williams and Parsons (1994) this volume was $0.01m^3$. For Aly et al. (2019) and Burton et al. (2022) the models referenced multiple tests of varying volume and therefore a reference volume was $1.0m^3$ was chosen. A graphical comparison of these models is provided in Figure 5.1, with Aly et al. (2019) and Burton et al. (2022) having nearly identical trendlines.

$$\sigma_f = 1629 \cdot \frac{V}{V_1}^{-0.084} \tag{5.2}$$

$$\sigma_f = 840 \cdot V^{-0.13} \tag{5.3}$$

$$\sigma_f = 847 \cdot V^{-0.13} \tag{5.4}$$

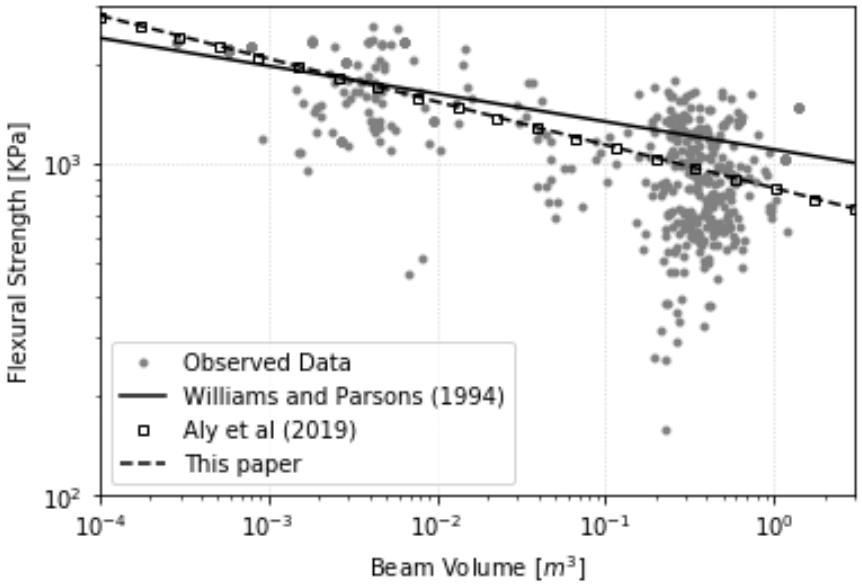

Figure 5.1: Non-linear model comparison

5.2 Machine Learning

In this work, ML regression algorithms were developed and applied to predict the flexural strength of freshwater ice. Four machine learning models were developed based on the MLPR, ETR, GBR and KNR algorithms. All models were generated and tuned using a Python machine learning library developed by Scikit-learn (2021). These models were compared and contrasted looking at model bias, accuracy and generalization as well as their ability to extrapolate and predict strengths for values outside of the training data. The application of ensemble modeling was also investigated, in which two or more models were blended, attempting to overcome their individual weaknesses by building upon their combined strengths.

5.2.1 Observed and Simulated Data

There are two primary datasets used during model development, observed data and simulated data. Observed data refers to the data as originally presented within the flexural strength database (see Chapter 3) and forms the basis for the training and testing of the models. The variability within the observed data can make it difficult to observe the underling data trends and as a result simulated data were generated to elucidate these data trends. Simulated datasets are composed of monotonically increasing beam volumes ranging from 0.0001m^3 to 50m^3, with each dataset being assigned a constant temperature. Several temperatures are investigated in this work including -1, -5, -10 and -25°C.

5.2.2 Independent Models

The following sections discuss the implementation of the four ML algorithms discussed earlier and the process by which the model hyperparameters are determined. The general process for tuning the model to the data began with the default hyperparameters, followed by hyperparameters selected using Scikit-Learn's parameter grid search optimization tool, and finally a manual tuning of the hyperparameters. ML model predictions for each algorithm are presented using observed and simulated data (T = -5°C) and compared against the empirical model presented by Aly et al. (2019) (see Equation 5.3).

When tuning the models careful consideration is given to both the statistical accuracy metrics and the generalization of the model. As noted earlier, when plotting model predictions using the observed data a higher degree of variability in the predictions is expected in comparison to the simulated data. The simulated data provides feedback on the generalization of the model, with less variability than is present in the observed data. However, careful observation of the model predictions using the observed data help to distinguish between variability within the model and the potential overfitting of the model. A careful balance of monitoring

the statistical accuracy metrics alongside the generalization of the model are performed throughout the tuning process.

5.2.2.1 Multilayer Perceptron Regressor

As discussed in Section 4.2.1 the MLPR algorithm has a number of hyperparameters which require tuning to achieve an optimized model. Four of most influential hyperparameters were found to be the strength of the L2 regularization term or *learning rate* (default = 0.001), the size and number of the hidden layers or *hidden layer size* (default = 100), the *activation function* (default = "relu") and the *solver* (default = "adam") used to optimize the weight of each node to node link.

MLPR output with default hyperparameters is show in Figure 5.2, and presents a reasonably good starting point for the optimization of the model. The generalization of the model is acceptable, however the abrupt turning point in the trend lines at approximately 0.5m^2 is undesirable requiring further tuning.

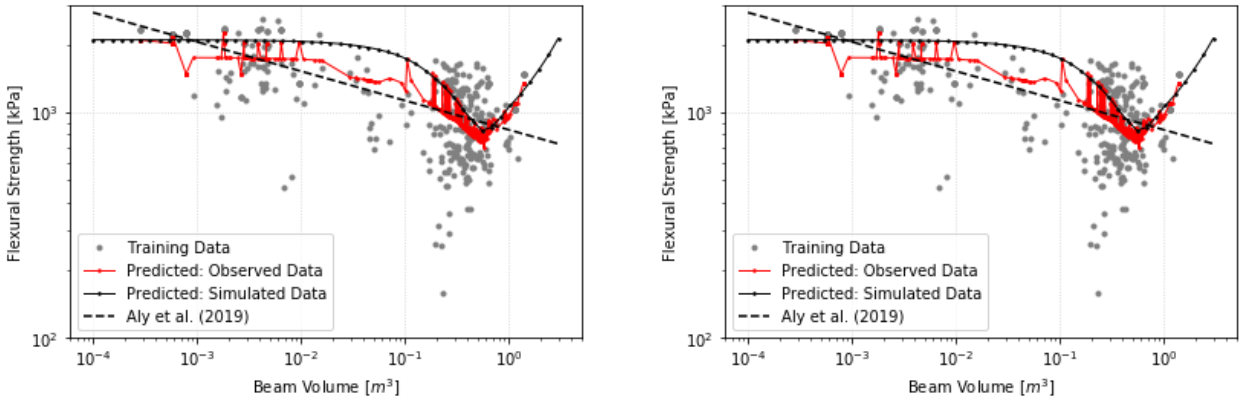

(a) Training data (b) Test data

Figure 5.2: MLPR: Default parameters

Using the optimization tool a new set of hyperparameters were established, with the *hidden layer size* changing to (5,5), the *activation function* set to "tanh" and the *solver* was switched

to “adam”. MLPR output using this new model is presented in in Figure 5.3 however, it is obvious that the newly established hyperparameters have resulted in the model overfitting the data and further tuning is required.

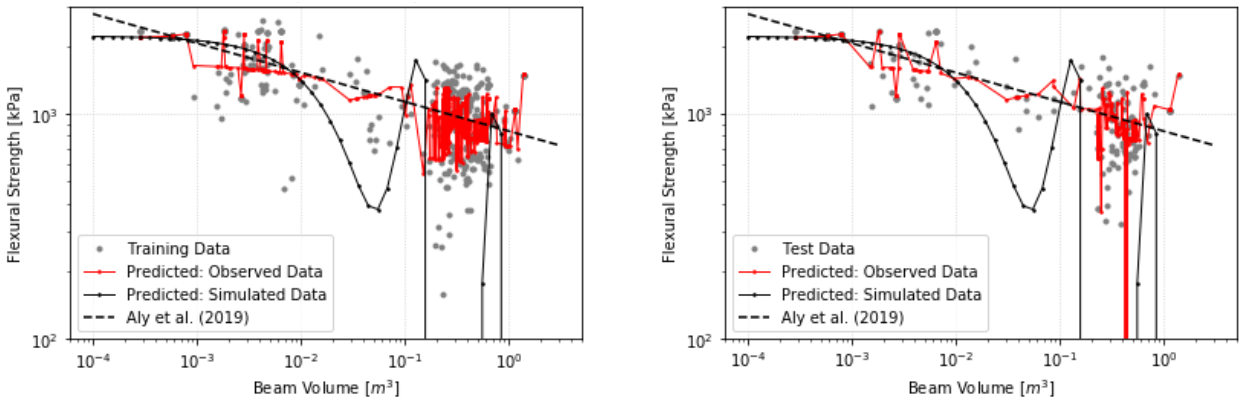

(a) Training data

(b) Test data

Figure 5.3: MLPR: Grid search selected parameters

With the grid search optimizer not performing as desired, a manual tuning of the hyperparameters was required, and the default parameters were selected as the starting point. Throughout the manual tuning process both the “relu” and “tanh” activation functions were compared. Two hyperparameters were adjusted during the manual tuning processing. Firstly the *learning rate* term was incrementally increased from the default value (0.001) with the optimal value found to be around 13. As the *hidden layer size* was incrementally decreased from the default value the overall model accuracy improved along with the model fit to the data, a value of 10 was ultimately chosen for the *hidden layer size*. During the manual tuning process the overall model accuracy as well as the fit of the model to the observed and simulated datasets were used as indicators when adjusting the hyperparameters. Results from the manually tuned model are provided in Figure 5.4 for both the training and test data sets. A summary of the MLPR hyperparameter selections are provided in Table 5.1.

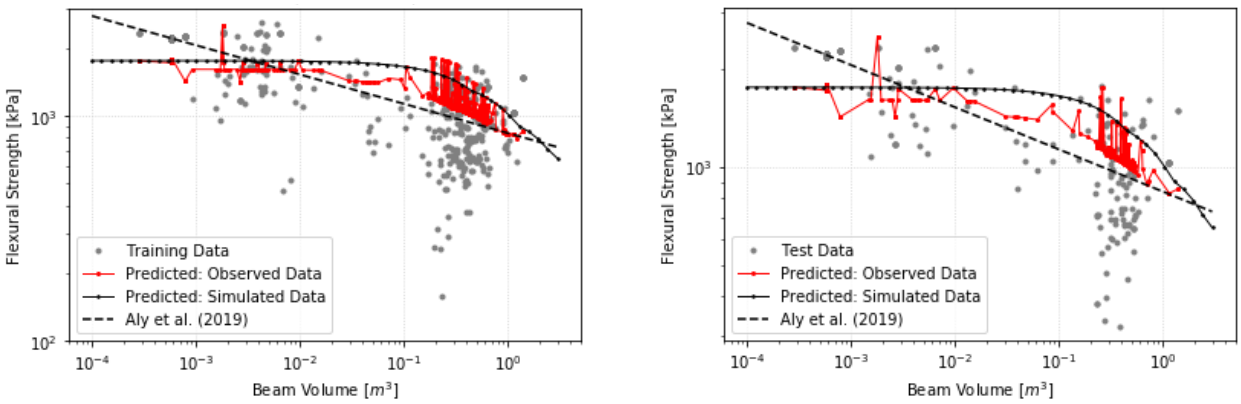

(a) Training data

(b) Test data

Figure 5.4: MLPR: Manually tuned hyperparameters

Table 5.1: MLPR: Hyperparameter summary

Hyperparameter	**Default**	**Grid Search**	**Manual**
Size of hidden layer	100	(5,5)	10
alpha	0.001	0.001	13
Activation function	"relu"	"tanh"	"relu"
Solver	"adam"	"lbfgs"	"adam"

5.2.2.2 Extra Trees Regressor

As discussed in Section 4.2.2.1 the ETR algorithm has a number of hyperparameters which require tuning to achieve an optimized model. Three of most influential hyperparameters were found to be the *maximum depth* (default = "none"), *number of trees* (default = 100) and *minimum samples per leaf* (default = 2).

ETR output with default hyperparameters is shown in Figure 5.5. The *maximum depth* default of "none" provides an unlimited number of splits in the tree. From Figure 5.5 it is clear that the model is very complex and is overfitting to the data. The parameter optimization tools were employed and the optimal *number of trees*, *maximum depth* and

minimum samples per leaf were determined to be 50, 11 and 2 respectively. The result of the ETR model based on these optimization parameters is shown in Figure 5.6.

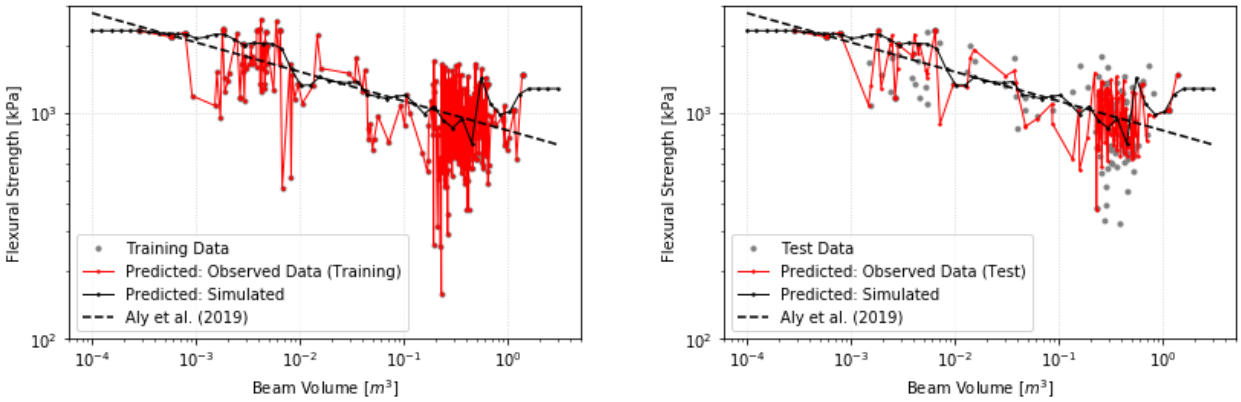

(a) Training data (b) Test data

Figure 5.5: ETR: Default parameters

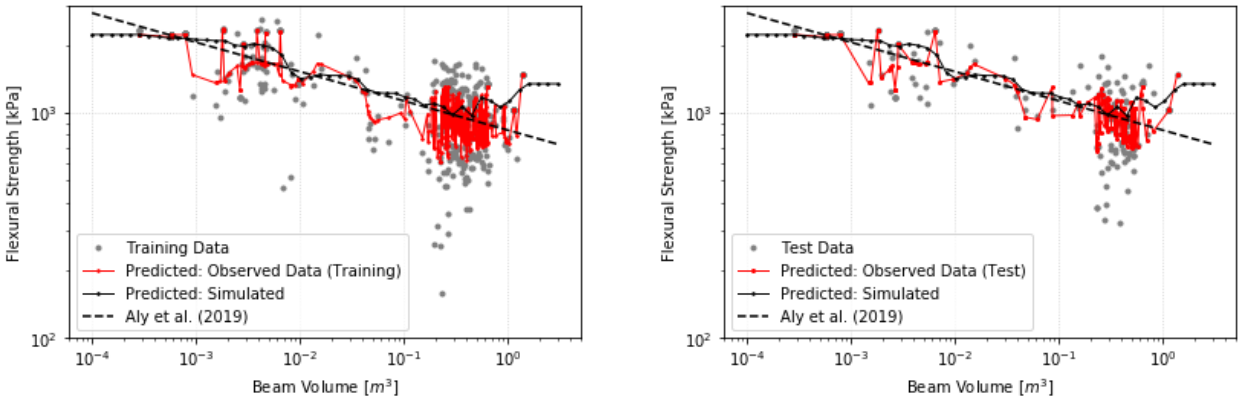

(a) Training data (b) Test data

Figure 5.6: ETR: Grid search selected parameters

The parameters defined by the optimization tool greatly reduced the overfitting observed in the default model however, the model is still showing signs of overfitting in particular for beam volumes exceeding $0.2m^2$. As discussed in Section 5.2.3 some of the variability seen for beam volumes exceeding $0.2m^2$ can be explained by the ice temperature. Further tweaking of the parameters was considered worthwhile in an effort to improve the fit of

the model. Various combinations of parameters were tested, in the end the selection of *number of estimators* was increased to 100, *max depth* was decreased to 8 and the *minimum samples per leaf* was increased to 5, the results of the ETR model using these modified hyperparameters are shown in Figure 5.7. These modification were successful in improving the overfitting of the data, and while some overfitting is still present in beam volumes greater than $0.2m^2$, a reduction in variance within this region has been observed. A summary of the ETR hyperparameter selections are provided in Table 5.2.

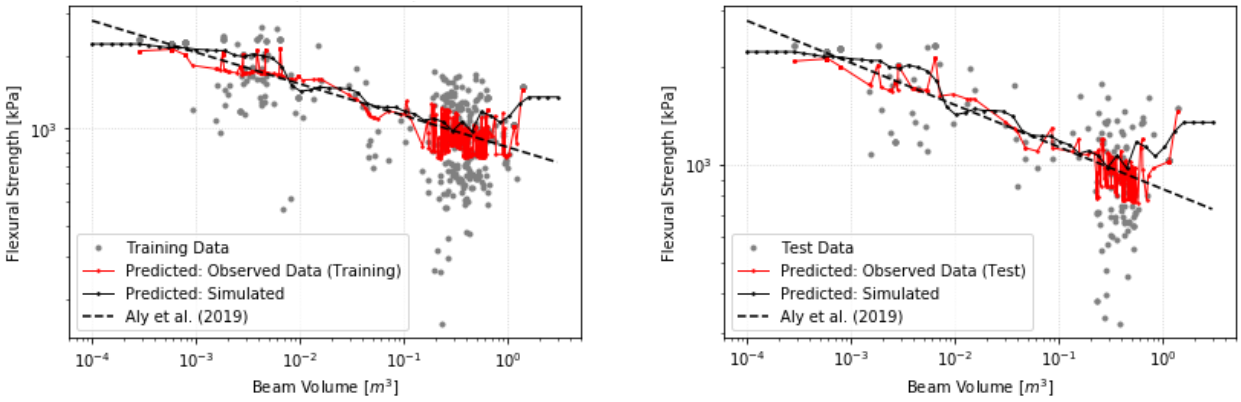

(a) Training data

(b) Test data

Figure 5.7: ETR: Manually tuned parameters

Table 5.2: ETR: Hyperparameter summary

Hyperparameter	**Default**	**Grid Search**	**Manual**
Maximum Depth	"none"	11	8
Number of Estimators	100	50	100
Minimum samples per leaf	2	2	5

5.2.2.3 Gradient Boosted Trees

As discussed in Section 4.2.2.2, the GBR algorithm has a number of hyperparameters which require tuning to achieve an optimized model. Four of most influential hyperparameters

were found to be the *maximum depth* (default = 3), *number of estimators* (default = 100), *minimum samples per leaf* (default = 1) and *learning rate* (default = 0.01).

GBR output with default hyperparameters is show in Figure 5.8, from which it is clearly evident that the model is overfitting the data. The parameter optimization tools were employed resulting in an optimal hyperparameters settings with *number of estimators* equal to 200, *learning rate* equal to 0.02, *minimum samples per leaf* is 3 and *max depth* equal to 4, as shown in Figure 5.9.

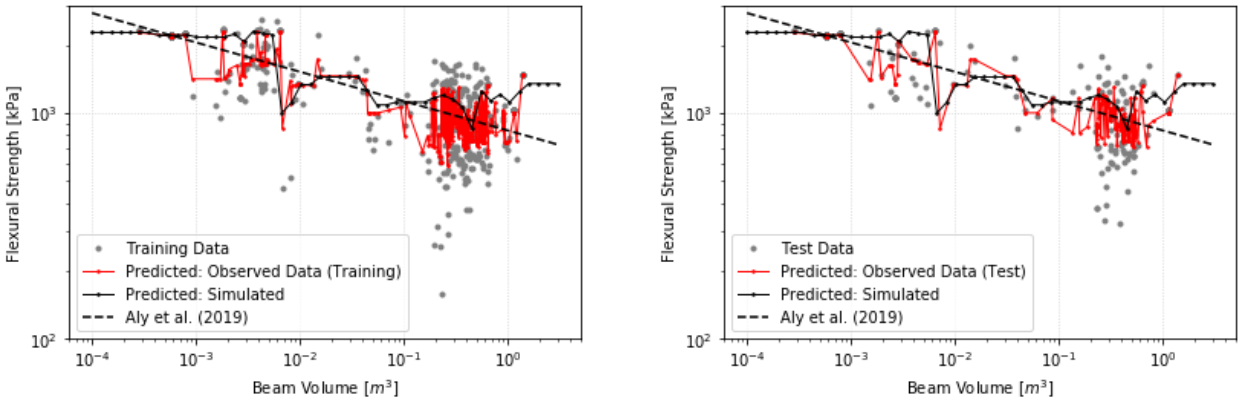

(a) GBT: Training data (b) GBT: Test data

Figure 5.8: GBT: Default parameters

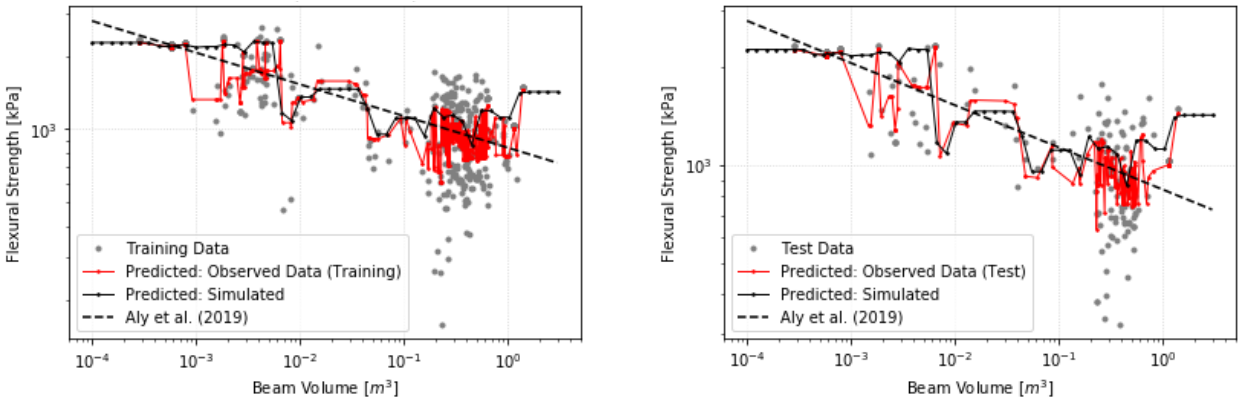

(a) GBT: Training data (b) GBT: Test data

Figure 5.9: GBT: Grid search selected hyperparameters

After optimization the GBR is still overfitting and not generalizing to the overall trend. This is particularly true for beam volumes exceeding $0.2m^2$. Manual tuning of the GBR hyperparameters was attempted, decreasing the *learning rate* and *maximum depth* to 0.01 and 2 respectively and increasing the *minimum samples per leaf* to 15. Results from manual tuning are provided in Figure 5.10 where overfitting has been decreased and while the overall general trend has improved, the trendlines are less continuous resulting in a more descretized output. A summary of the GBR hyperparameter selections are provided in Table 5.3.

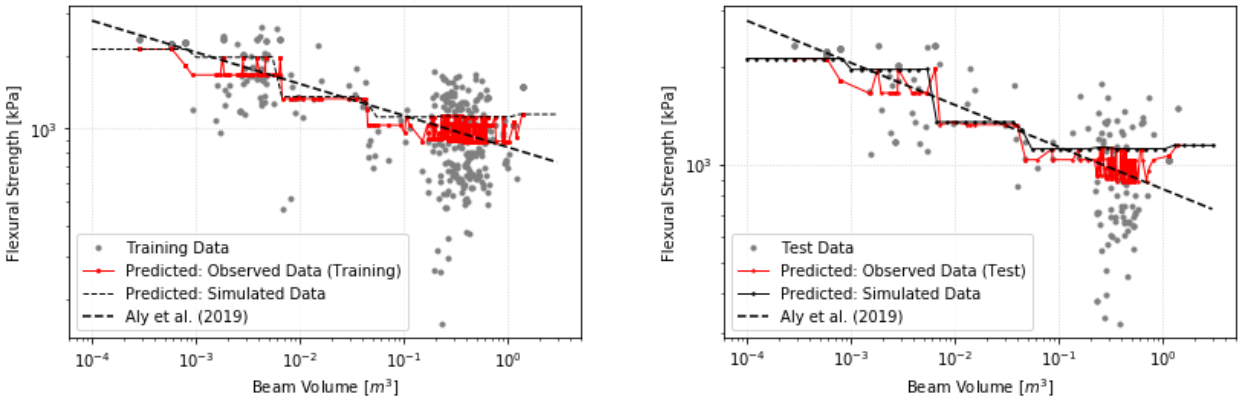

(a) GBT: Training data

(b) GBT: Test data

Figure 5.10: GBT: Manually tuned hyperparameters

Table 5.3: GBR: Hyperparameter summary

Hyperparameter	**Default**	**Grid Search**	**Manual**
Maximum Depth	3	4	2
Number of Estimators	100	200	200
Minimum samples per leaf	1	3	15
Learning rate	0.01	0.02	0.01

5.2.2.4 k-nearest Neighbours

As discussed in Section 4.2.3, the KNR algorithm is the simplest of the ML algorithms introduced in this work, and has only 3 hyperparameters which require tuning to achieve an

optimized model including *number of neighbours* (default = 5), *weighting method* (default = "uniform") and the *algorithm* used to compute the nearest neighbor (default = "auto").

KNR output with default hyperparameters is show in Figure 5.11, and presents a model which is overfitting the data. The parameter optimization tools were employed resulting in the *number of neighbours* increasing to 20 and the *weighting method* changing to "distance". The results of these alterations to the hyperparameters are shown in Figure 5.12 and show an increase in the overfitting of the model.

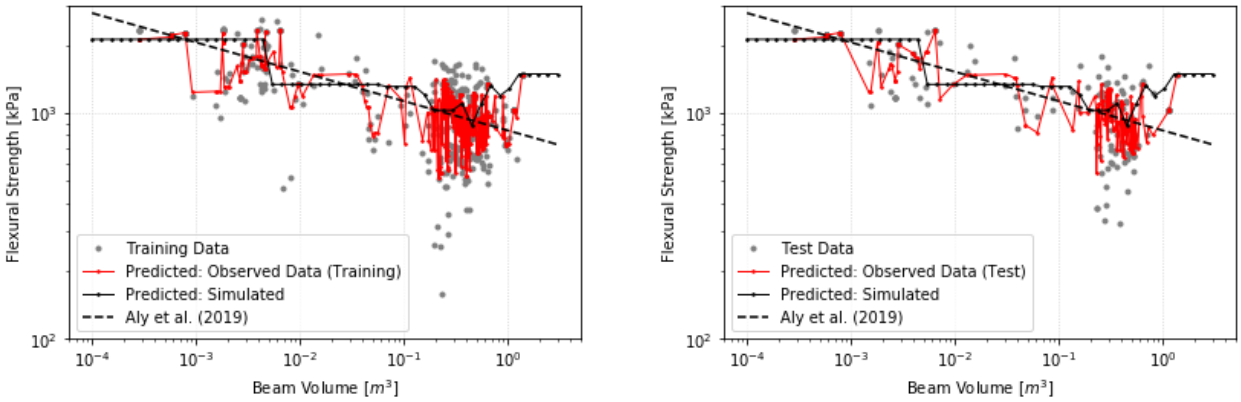

(a) KNR: Training data

(b) KNR: Test data

Figure 5.11: KNR: Default parameters

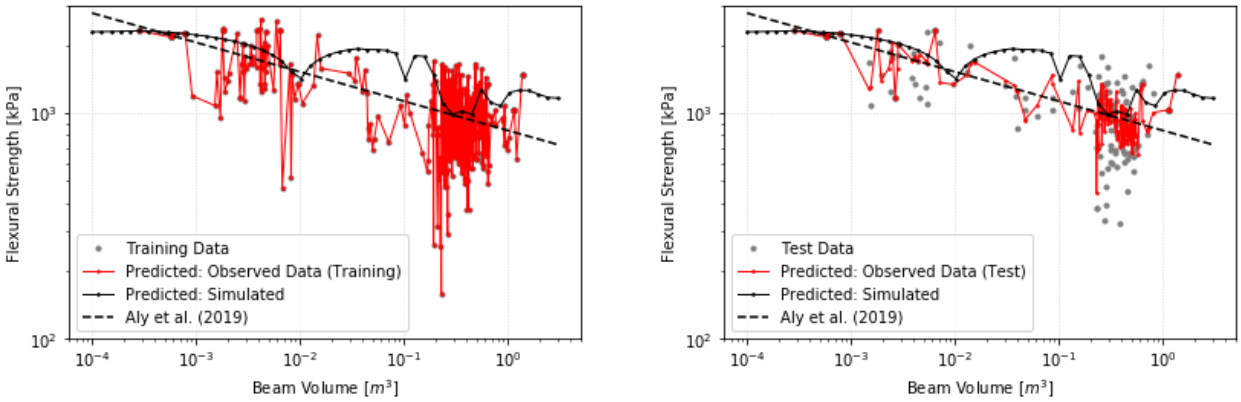

(a) KNR: Training data

(b) KNR: Test data

Figure 5.12: KNR: Grid search selected hyperparameters

The effect of the optimization tool on the KNR model was counter productive and overfitting of the data is more prevalent, therefore it was necessary to tune the model manually. The *weighting method* was returned to "uniform" and overfitting decreased significantly. Further attempts to decrease overfitting by increasing the *number of neighbours* were unsuccessful, therefore the *number of neighbours* was kept constant at 20. Results of the manual tuning are provided in Figure 5.13. A summary of the KNR hyperparameter selections are provided in Table 5.4.

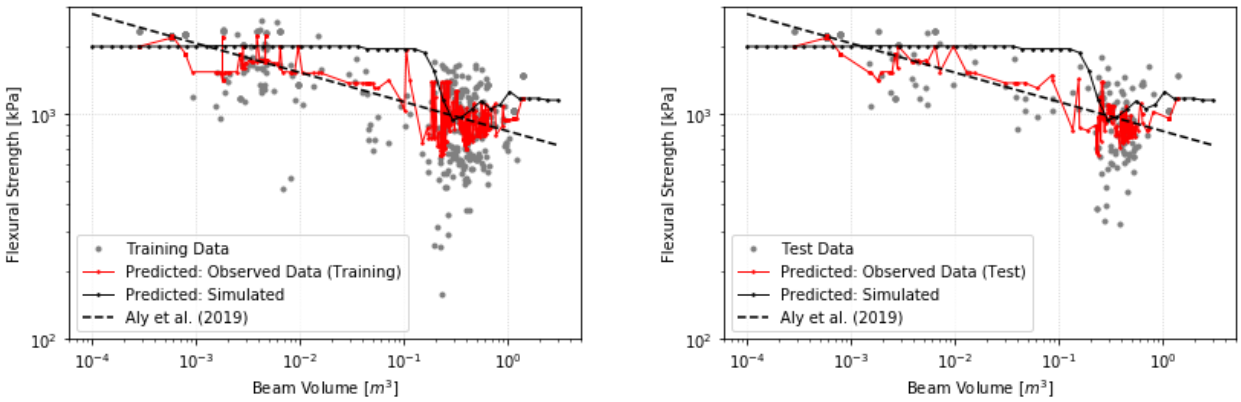

(a) KNR: Training data

(b) KNR: Test data

Figure 5.13: KNR: Manually tuned hyperparameters

Table 5.4: KNR: Hyperparameter summary

Hyperparameter	**Default**	**Grid Search**	**Manual**
Number of Neighbours	5	20	20
Weighting Method	"uniform"	"distance"	"uniform"
Algorithm	"auto"	"auto"	"auto"

5.2.3 Temperature Effects

The effect of temperature on the flexural strength of freshwater ice is expected to follow an inverse relationship, where strength increases as temperature decreases. Within the database there are large variations in ice strength across the whole range of recorded ice temperatures.

As a result, Aly et al. (2019) concluded that temperature does not have a significant effect on the flexural strength of freshwater ice.

To investigate the effect of temperature within the ML models, the model outputs were divided into two groups according to temperature. The first group contained all data points with recorded temperatures greater than or equal to -2.5°C, while group 2 contained all data points less than -2.5°C. The results are presented in Figures 5.14, 5.15, 5.16, and 5.17 for the MLPR, ETR, GBR and KNR models respectively. The effects of temperature are most clearly observed for beam volumes exceeding $0.1m^3$, where a separation between the temperature groups is apparent. While there is overlap between the groups, the colder temperature group clearly demonstrates higher flexural strength. Therefore, temperature variations within the observed data are expected to account for the majority of the scatter observed in the model predictions.

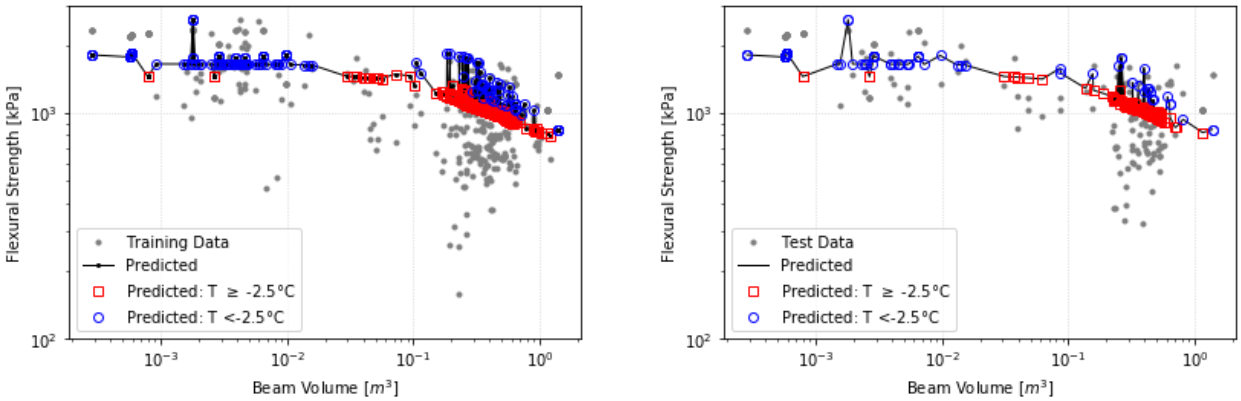

(a) MPR: Training data

(b) MPR: Test data

Figure 5.14: MPR: Temperature effects

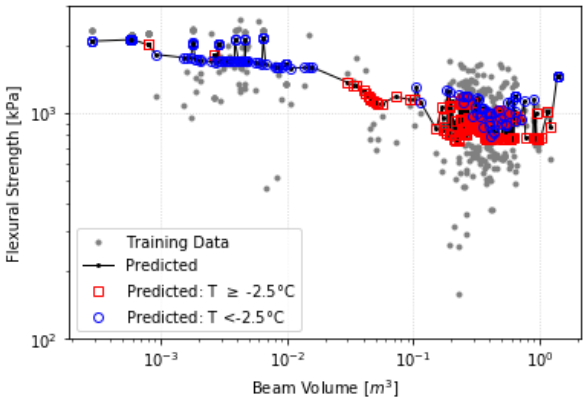

(a) ETR: Training data

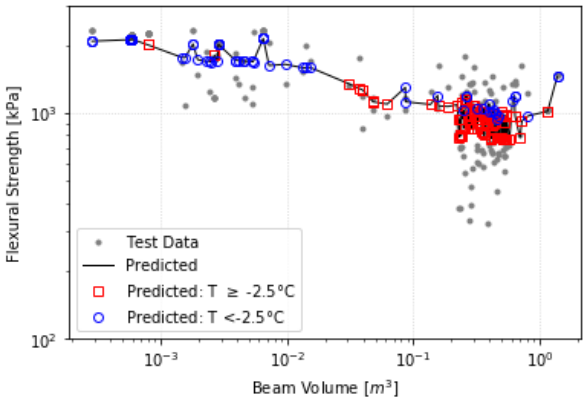

(b) ETR: Test data

Figure 5.15: ETR: Temperature effects

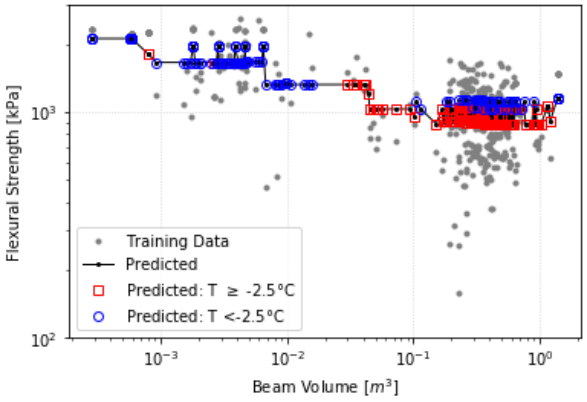

(a) GBR: Training data

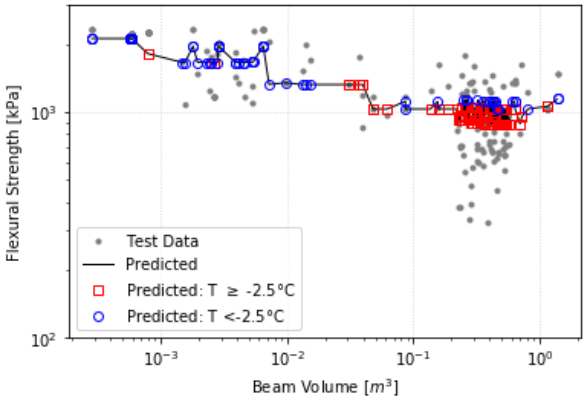

(b) GBR: Test data

Figure 5.16: GBR: Temperature effects

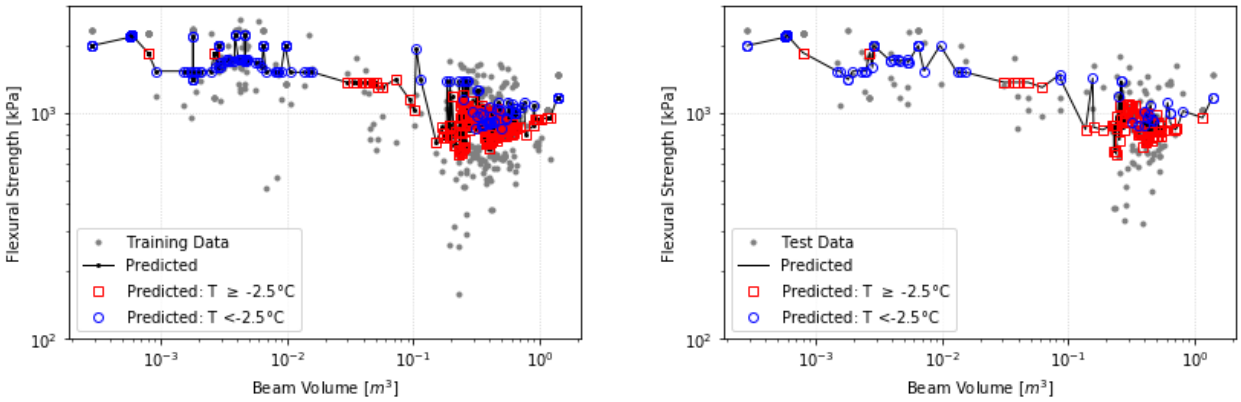

(a) KNR: Training data

(b) KNR: Test data

Figure 5.17: KNR: Temperature effects

In addition to observed data, the models were run using simulated datasets as discussed previously. The four machine learning models were run using simulated data sets with ice temperatures of -1, -5 and -10°C, and the results are presented in Figure 5.18 below. It is clear from these results that all four models demonstrate a temperature dependency within the model. The magnitude of this dependency varies from model to model, however it is clear that ice temperature should be a feature in the modelling of freshwater ice flexural strength.

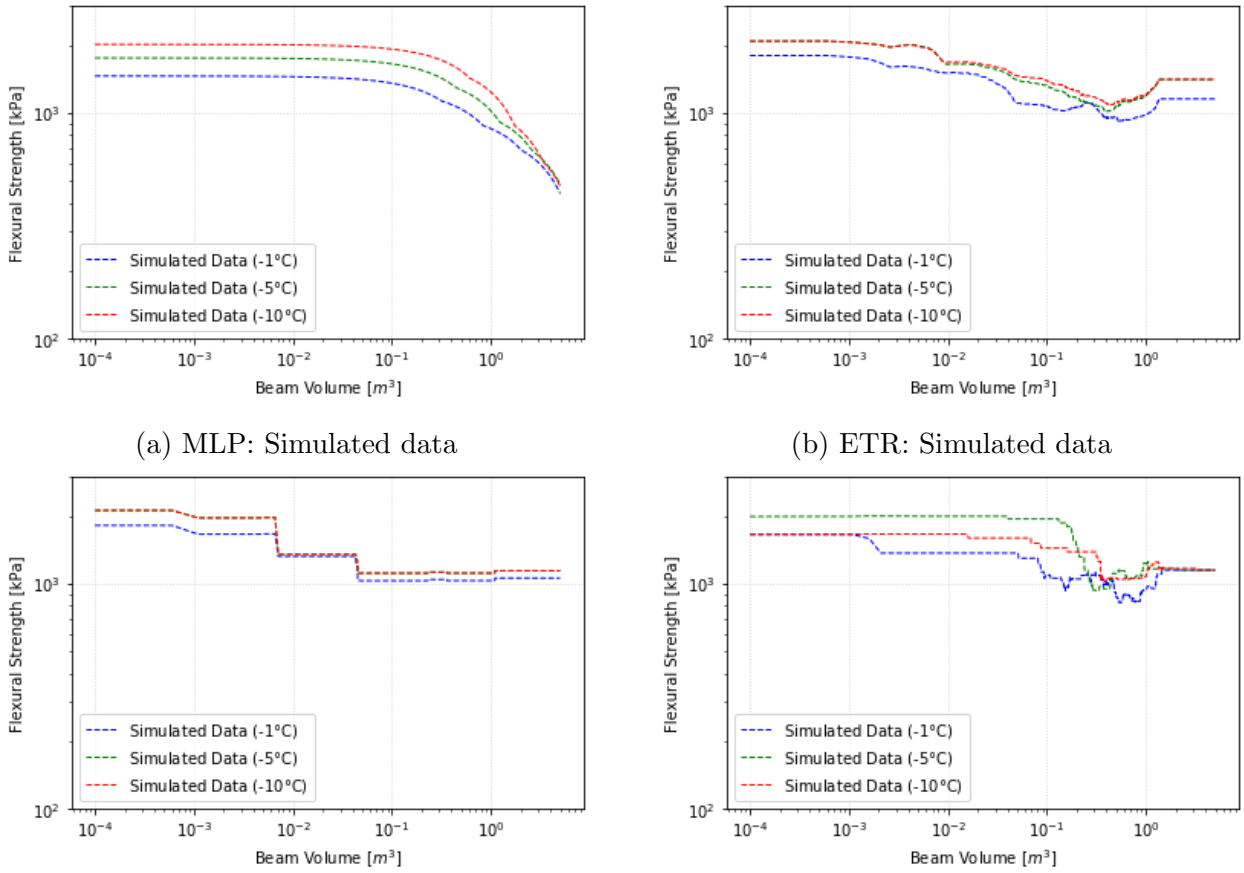

(a) MLP: Simulated data

(b) ETR: Simulated data

(c) GBR: Simulated data

(d) KNR: Simulated data

Figure 5.18: Temperature effects (simulated data)

5.2.4 Ensemble Models

The use of models employing a single algorithm can result in accurate predictions, however models employing multiple algorithms often outperform their single counterparts. An averaging ensemble method was employed to average the efforts of two single algorithms. Averaging ensembles help to balance out the individual weakness (e.g. variance and bias) of the independent models. In this work the four independent models were combined to form six two pair ensemble models, Figure 5.19 presents the ensemble predictions based on the observed database, and Figure 5.20 presents the ensemble models results using the sim-

ulated datasets. Further discussion on the ensemble models will be presented in the next section.

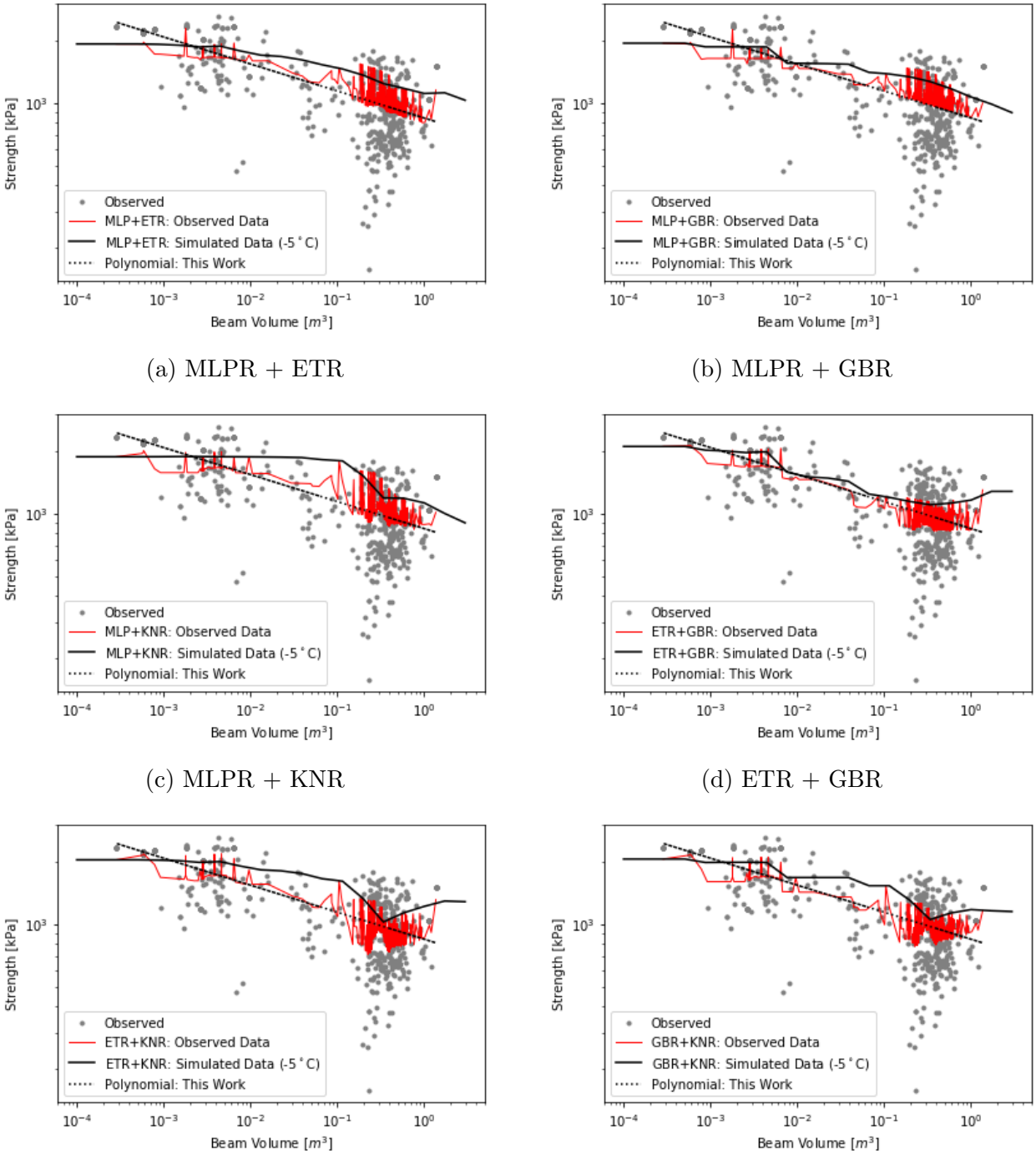

(a) MLPR + ETR

(b) MLPR + GBR

(c) MLPR + KNR

(d) ETR + GBR

(e) ETR + KNR

(f) GBR + KNR

Figure 5.19: Ensemble models: Observed data

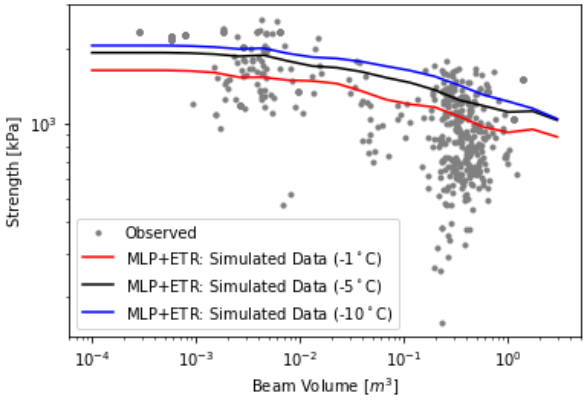

(a) MLPR + ETR

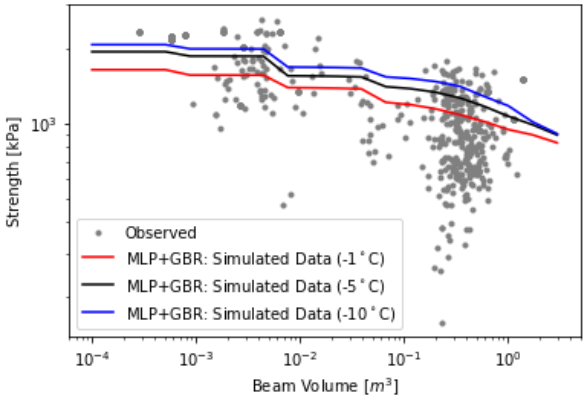

(b) MLPR + GBR

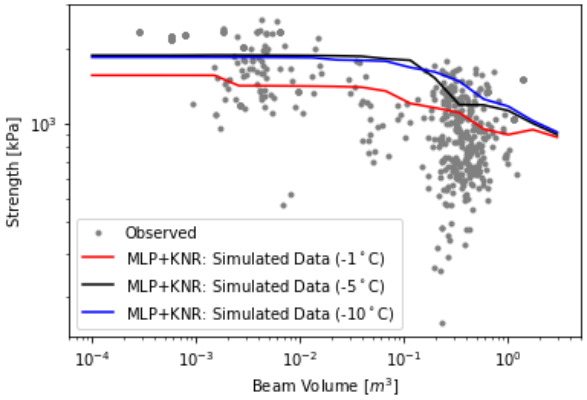

(c) MLPR + KNR

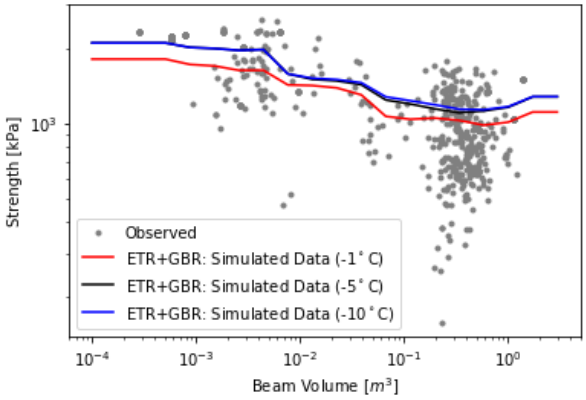

(d) ETR + GBR

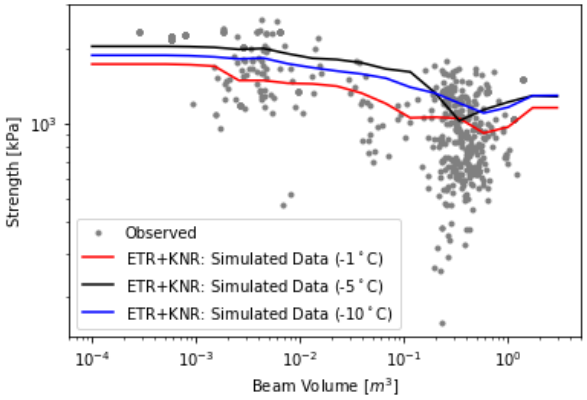

(e) ETR + KNR

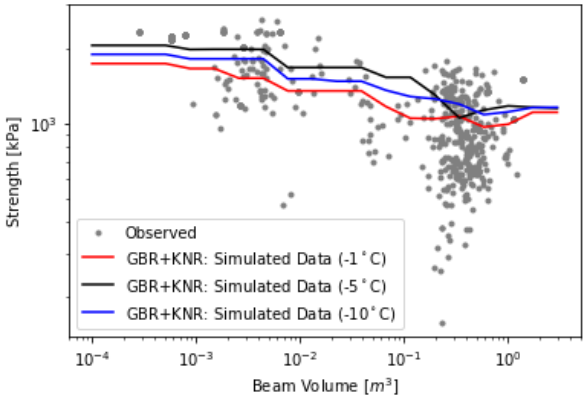

(f) GBR + KNR

Figure 5.20: Ensemble models: Simulated data

5.2.5 Observed vs Predicted

A comparison between observed and predicted values was conducted to further observe the performance of the individual and ensemble ML models, the results are presented in Figures 5.21 and 5.22. A summary of each model (individual and ensemble) was generated by categorizing the data according to the error between predicted and observed values, based on Equation 5.5. Errors greater than +10% were categorized as overpredicted, errors less than -10% are under-predicted while the remainder are considered approximately equivalent. A summary of all ten models showing the percentage of predicted data in each category is provided in Table 5.5.

$$err = \frac{Predicted - Observed}{Observed} \tag{5.5}$$

Table 5.5: Percent error: Observed vs predicted (test data)

Model	**Over**	**Under**	**Approx**
MLPR	41	47	12
ETR	29	25	46
GBR	32	29	39
KNR	32	32	36
MLPR + ETR	37	47	16
MLPR + GBR	38	42	20
MLPR + KNR	37	40	23
ETR + GBR	31	27.	42
ETR + KNR	30	30	40
GBR + KNR	33	30	37

Comparing the observed vs predicted plots and summary tables, the difference between the ML models is generally not significant. The scatter present in each of the individual plots is to be expected when compared to the variability present in the observed data. In general the individual ML models have a slight tendency towards an overprediction of flexural strength, while the ensemble models are more prone to an under-prediction. The scatter within the

individual models is similar with the exception of the GBR model, which appears to discretize the data into distinct bands. This descretization of data is less prevalent in the ensemble models where the GBR model is employed.

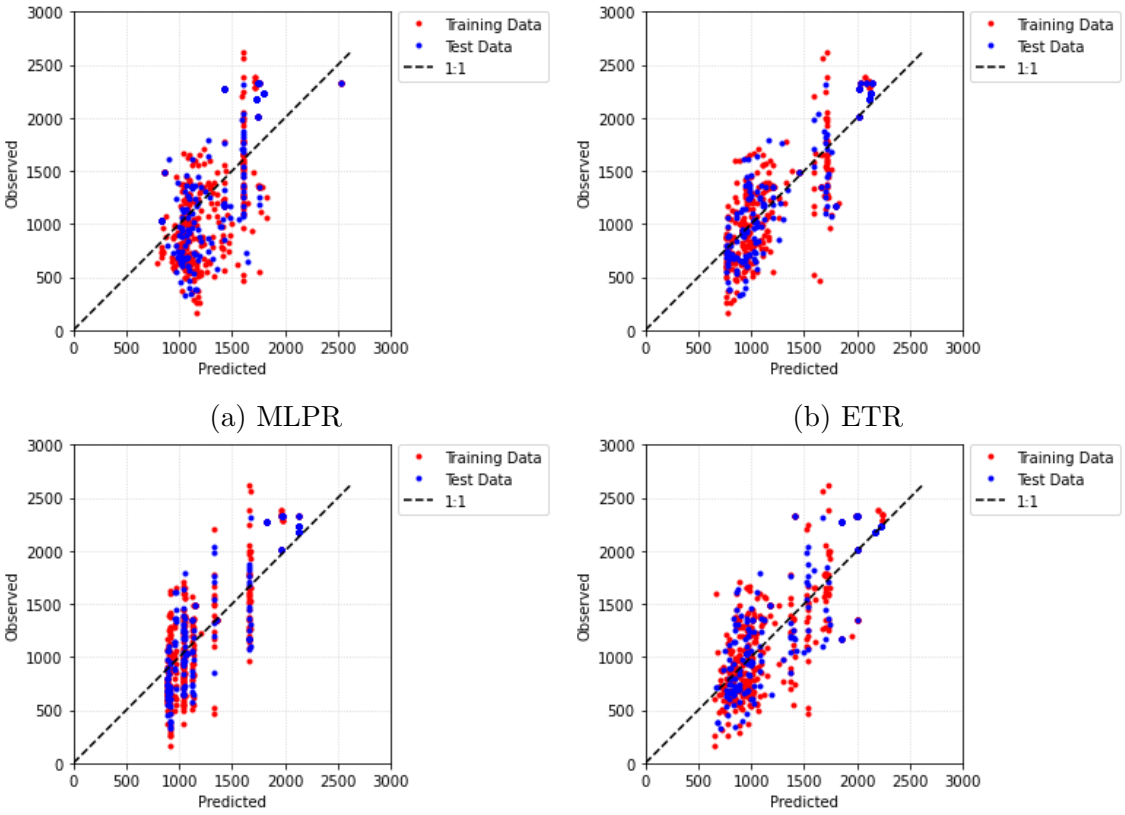

(a) MLPR

(b) ETR

(c) GBR

(d) KNR

Figure 5.21: ML: Observed vs predicted

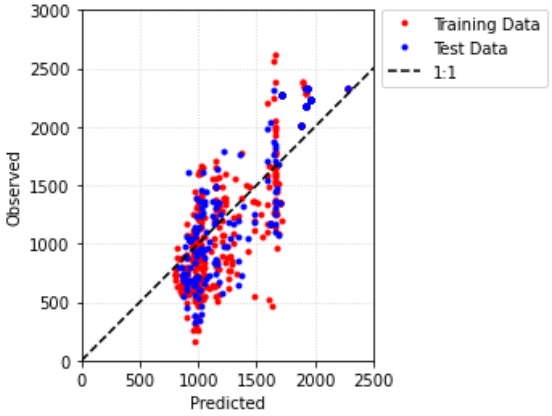

(a) MLPR + ETR

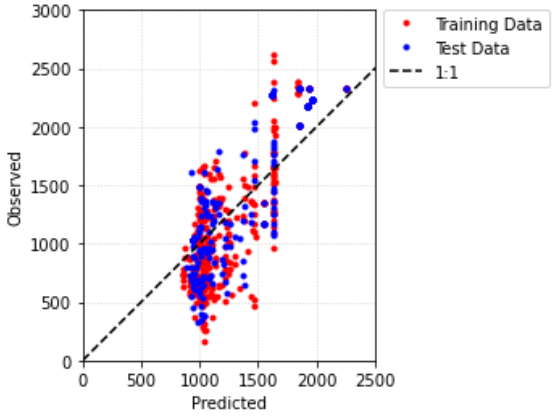

(b) MLPR + GBR

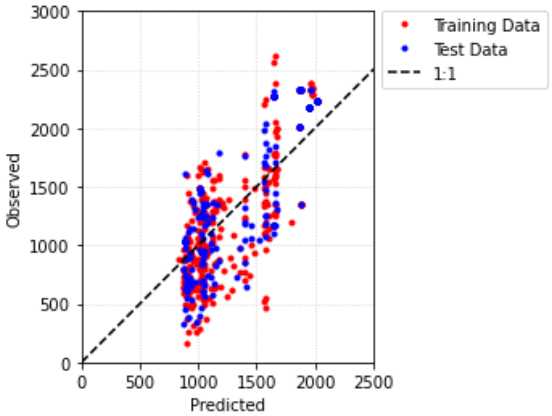

(c) MLPR + KNR

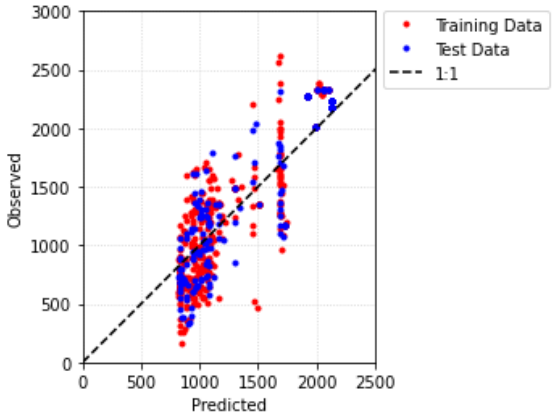

(d) ETR + GBR

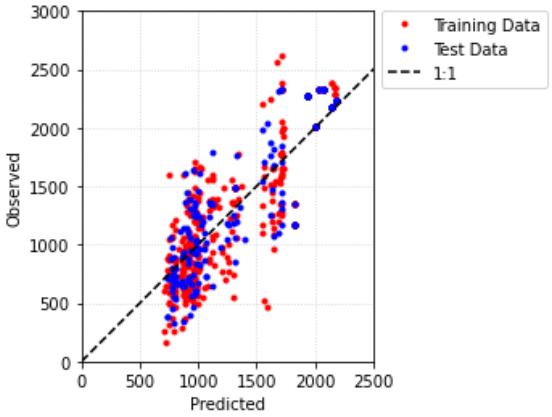

(e) ETR + KNR

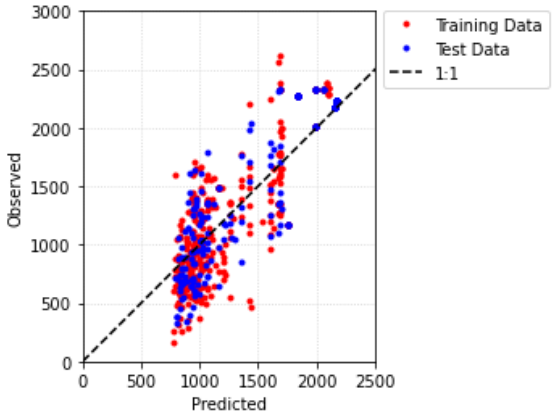

(f) GBR + KNR

Figure 5.22: ML: Observed vs predicted (ensemble)

5.2.6 Model Comparison

The trendlines presented by each of the four individual ML models are in general agreement with the expected relationship trends discussed in Section 2.3. Employing the simulated datasets these relationships trends are presented in Figure 5.23 for flexural strength as a function of beam volume. The statistical accuracy metrics of R^2 and RMSE for each of the four models are presented in Table 5.6. Based on these statistical metrics, the MLPR and ETR models are the weakest and strongest models respectively. And while KNR and GBR both outperform MLPR with respect to statistical metrics, these models are not well suited to data extrapolation and their respective trendlines are less favorable compared to MLPR.

Table 5.6: Comparisons of independent models

Model	R^2 **Train**	R^2 **Test**	**RMSE Train**	**RMSE Test**
MLPR	0.522	0.519	0.430	0.432
ETR	0.809	0.819	0.271	0.265
GBR	0.777	0.774	0.294	0.296
KNR	0.750	0.752	0.311	0.310

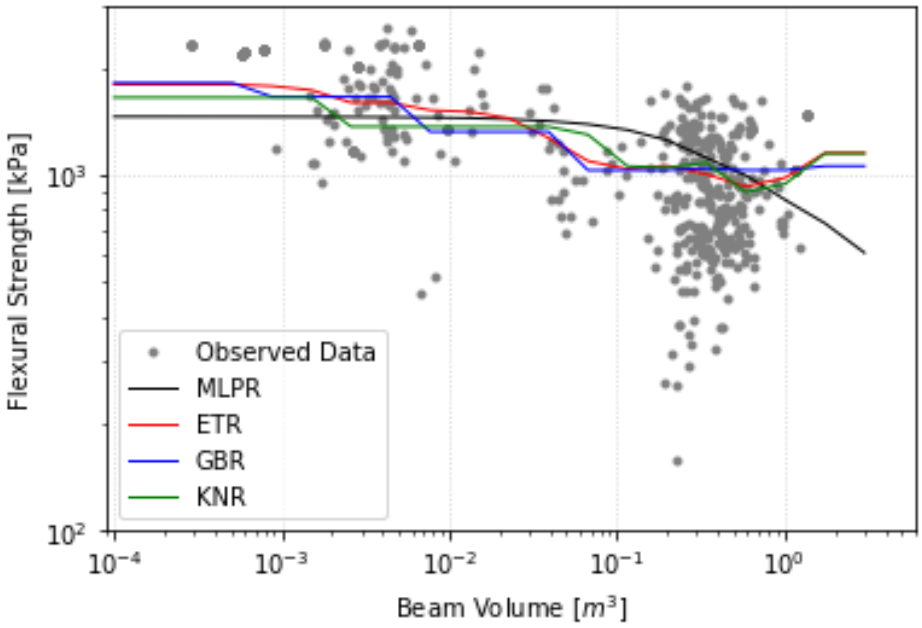

Figure 5.23: Comparison of independent models (freshwater)

All six ensemble models produced trendlines in general agreement with the expected trends discussed in Section 2.3. Ensemble model trendlines are presented in Figure 5.24, and statistical accuracy metrics are provided in Table 5.7.

The ability of an ensemble model to handle data extrapolation in an effective and expected manner is important in model selection. As discussed in Chapter 4.2, the internal processes of the ETR, GBR and KNR algorithms result in less than favorable extrapolated results. In short, when extrapolating these three algorithms tend to base their predictions on the same estimators resulting in constant predictions for extrapolation. The MLPR algorithm is more adaptable to extrapolation than the other three making it the ideal companion when exploring ensemble modelling. Reviewing the model statistics, observed trendlines and extrapolation characteristics, the most favourable model is the "MLPR + ETR" ensemble.

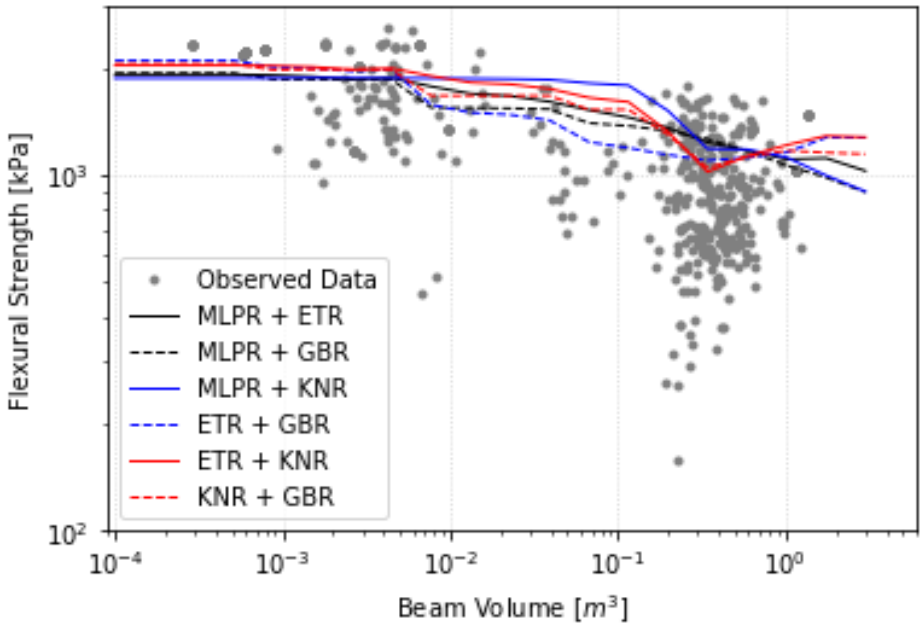

Figure 5.24: Comparison of ensemble models (freshwater)

Table 5.7: Comparisons of ensemble models

Ensemble	R^2 **Train**	R^2 **Test**	**RMSE Train**	**RMSE Test**
MLPR + ETR	0.718	0.724	0.33	0.327
MLPR + GBR	0.691	0.69	0.345	0.347
MLPR + KNR	0.698	0.698	0.342	0.343
ETR + GBR	0.800	0.803	0.278	0.276
ETR + KNR	0.790	0.796	0.285	0.281
GBR + KNR	0.780	0.777	0.292	0.294

5.3 Level Ice Loads

Considering the presence of temperature dependencies in the ML flexural strength models, the potential effects of temperature on structural loads and annual exceedance probabilities

are of interest. The MLPR+ETR machine learning model was subjected to a probabilistic design load calculation and compared with conventional approaches for a wind turbine installation in Lake Erie, including linear and constant strength models. Level ice load calculations are governed by the structure geometry and the level ice thickness to which the structure is exposed. Structural geometry of the wind turbine consists of a 60 degree downward breaking cone with a mean waterline diameter of 8m, as described in Croasdale et al. (2019). The level ice thickness (h_{ice}) is estimated based on the Accumulated Freezing Degree Days (AFDD) as discussed by Daly (2016) and presented in Equation 5.6. The calculation of ice loads were then generated based upon the methodology discussed in Brown et al. (2001).

$$h_{ice} = \alpha\sqrt{AFDD_n - AFDD_o} \tag{5.6}$$

In Equation 5.6, $AFDD_n$ is the number of AFDD recorded during the winter up to day n, $AFDD_o$ is the number of AFDD recorded before ice is first present, and α is a coefficient which can vary depending on the geographical location. For the Lake Erie region, the coefficient α and $AFDD_o$ were determined by Daly (2016) to be 2.39 and 43.4 respectively. The AFDD were sampled from a Weibull distribution based on Daly (2016), and ice beam volumes were estimated as $7h_{ice}^3$ based on recommendations by Schwarz et al. (1981).

Annual level ice loads were estimated using the constant, linear, and ML ensemble flexural strength models, and then ranked to produce an annual probability of exceedance for each model, as shown in Figure 5.25. For the constant flexural strength model a flexural strength value of 538 kPa was chosen based on Karulina et al. (2019). The linear model was based on the Aly et al. (2019) model (see Equation 5.3) using simulated ice thicknesses. The ML ensemble model used both simulated ice thicknesses and a constant temperature of -5°C to estimate flexural strength. The constant strength model produces the lowest global loads while the highest loads are predicted by the ML ensemble model.

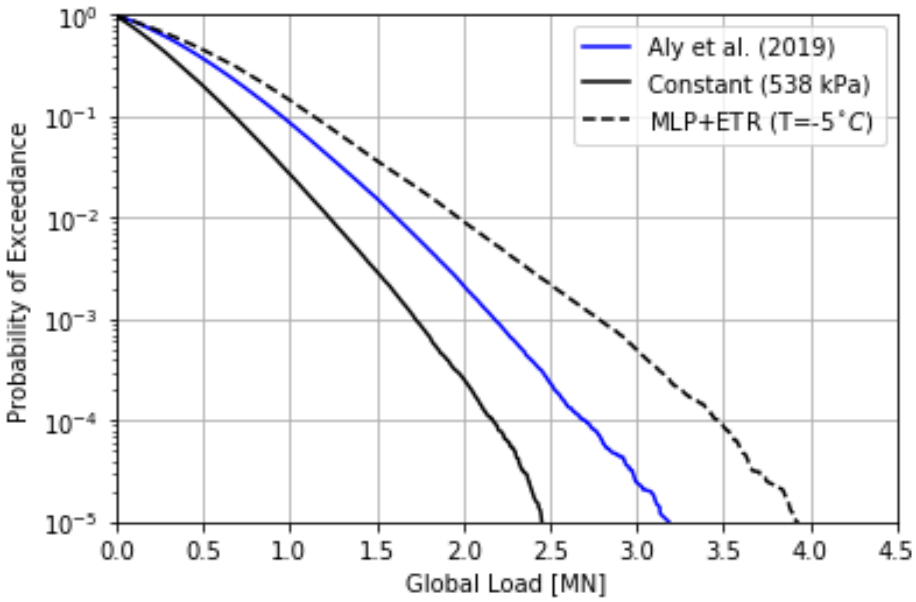

Figure 5.25: Level ice loads for various models

The MLPR+ETR ensemble model was also run for ice temperatures of -1°C and -10°C to determine the effect of temperature on global loads, the results are shown in Figure 5.26. The global loads for a 50-year return period for the linear model and the three MLPR+ETR models from Figure 5.26 are presented in Table 5.8. The ML and linear model are generally comparable at -1°C with the ensemble model being an average of 6% higher than the linear model. Separation between the linear and ML models increases as temperature decreases.

It can be observed from Figure 5.26, that for the same probability of exceedance the level ice loads decreases as temperatures increase. This trend is not unexpected as it mirrors the behaviour of decreasing flexural strength with increasing ice temperatures as presented earlier. For the scenario presented here, the MLPR+ETR model shows an approximate 18% decrease in global loads when ice temperatures increase from -10°C to -1°C. This is a very interesting trend as many regions are experiencing a rise in average annual temperatures as a result of climate change. Rising temperatures combined with the flexural strength

temperature dependencies discussed here, could result in reductions to global ice loads for future freshwater structures.

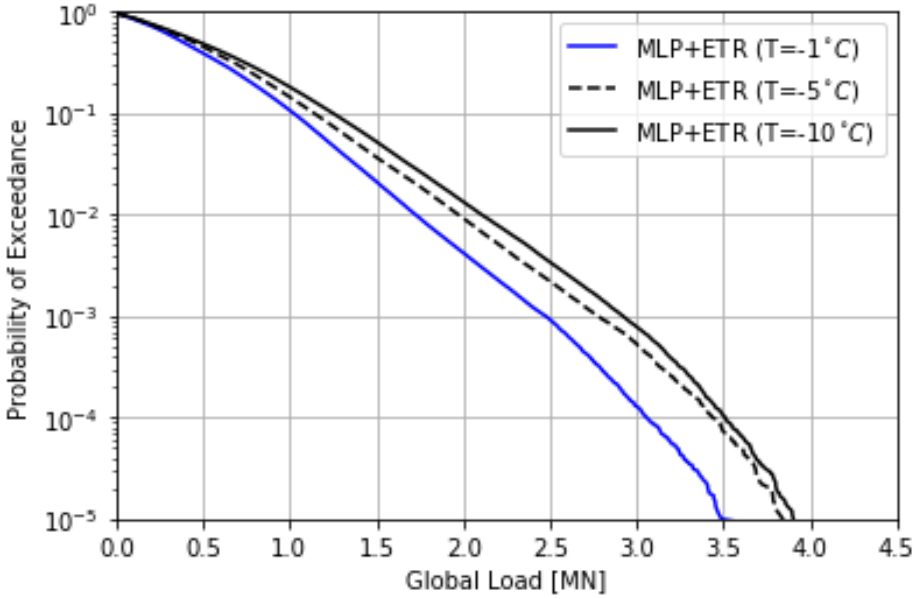

Figure 5.26: Level ice loads for ML model with various temperatures

Table 5.8: 50-year return period

Model	**Global Load [MN]**	**Percent Increase over Linear Model**
Linear	1.43	-
MLPR+ETR (-1°C)	1.52	6.3%
MLPR+ETR (-5°C)	1.73	21.0%
MLPR+ETR (-10°C)	1.84	29.4%

5.4 Summary

Freshwater flexural strength was found to have a dependence on both beam volume and temperature. The relationship between flexural strength and beam volume has been documented by several researchers and has also been demonstrated here in using the traditional methods as well as the ML models. The ML models have shown a significant decrease in

strength with increasing beam volume, with the largest reductions being present in beams greater than 0.1m^3.

Most researchers have ignored the effects of temperature on flexural strength of freshwater ice suggesting that no discernible relationship exists. However, with the implementation of ML models the effects of temperature on flexural strength are clearly evident. All 10 ML models (4 individual and 6 ensemble) indicated some degree of dependence of flexural strength on temperature. Further investigation into this relationship using current and additional ML algorithms is warranted, and could improved on the relationships presented here. With many regions experiencing an increase in average annual temperatures, the potential of flexural strength dependencies on temperature could result in lower expected global ice loads on future structures. While a reduction in flexural strength might be advantageous for structures in ice, it would have the opposite effect for industries reliant on the bearing capacity of ice, such as ice road transportation. It is recommended that further research exploring ML modeling should continue to further develop the potential of this new modelling approach.

6 Sea Ice Analysis

In the following sections an investigation of sea ice flexural strength is presented with a discussion on both traditional and ML methods. A portion of the work in this Chapter has been published in a paper entitled "Estimating Level Sea Ice Loads on Sloping Structures Using Machine Learning-Derived Flexural Strength," and presented at the 27th International Conference on Port and Ocean Engineering under Arctic Conditions (POAC 2023); see Burton et al. (2023). Co-authors Dr. Rocky Taylor and Dr. Renat Yulmetov served in conceptualizing the research, securing funding, and providing guidance and support during data analysis and interpretation as well as reviewing and editing the manuscript. The author took on the primary role in research execution, compiling and analyzing data, leading the organization, synthesis and interpretation of results, as well as preparation and revision of the manuscript.

6.1 Traditional Methods: Empirical Models

Traditionally the flexural strength of sea ice was either assumed to be constant, or was estimated through the use of empirical models. These empirical models generally take the form of a single or double parameter model, both single and multi-parameter models are discussed below.

6.1.1 Single Parameter Regression Models

Three common single parameter models include linear, polynomial, and exponential decay. Generic forms for these models can be found in Equations 6.1, 6.2 and 6.3 for linear, polynomial and exponential models respectively:

$$\sigma_f = c_0 \cdot P + c_1 \tag{6.1}$$

$$\sigma_f = c_0 \cdot P^{c_1} \tag{6.2}$$

$$\sigma_f = c_0 \cdot exp\,(c_1 \cdot P) \tag{6.3}$$

where σ_f is the flexural strength of ice, c_0 and c_1 are constants, and P is a physical property of the ice sample such as temperature or brine volume.

The most common ice properties employed in single parameter models are brine volume and temperature, beam volume is generally only included in multi-parameter models.

6.1.1.1 Brine Volume

As discussed in Section 2.3.3, the relationship between the flexural strength of sea ice (σ_f) and brine volume (v_b) has been documented by a number of researchers (Aly et al. (2019), Ji et al. (2011), Barrette et al. (1999), Blanchet et al. (1997), Timco and O'Brien (1994), Christensen (1986), Schwarz and Weeks (1977), Weeks and Assur (1967), and Butkovich (1959)). A number of researchers have developed flexural strength models following an exponential decay in relation to brine volume, including Karulina et al. (2019) (Equation 6.4), Ji et al. (2011) (Equation 6.5) and Timco and O'Brien (1994) (Equation 6.6).

$$\sigma_f = 0.5266 \cdot \exp\left(-2.804\sqrt{v_b}\right) \tag{6.4}$$

$$\sigma_f = 2.41 \cdot \exp\left(-4.29\sqrt{v_b}\right) \tag{6.5}$$

$$\sigma_f = 1.760 \cdot \exp\left(-5.88\sqrt{v_b}\right) \tag{6.6}$$

Other researchers took a linear approach such as Blanchet et al. (1997) (Equation 6.7) and Schwarz and Weeks (1977) (Equation 6.8).

$$\sigma_f = 1.0 - 1.85\sqrt{v_b} \tag{6.7}$$

$$\sigma_f = 1.03 \cdot \left(1 - \sqrt{\frac{v_b}{0.209}}\right) \tag{6.8}$$

Using the generic exponential decay formulae (Equation 6.3), an empirical model was derived based on the observed data as shown in Equation 6.9. A comparison between the models is provided in Figure 6.1, and upon observation one can determine that the new model appears to operate within the bounds set by the Timco and O'Brien and Ji et al. models. At lower brine volumes the new model approaches the Timco and O'Brien model, while at higher brine volumes the model approaches the Ji et al. model.

$$\sigma_f = 1.70 \cdot \exp\left(-4.21\sqrt{v_b}\right) \tag{6.9}$$

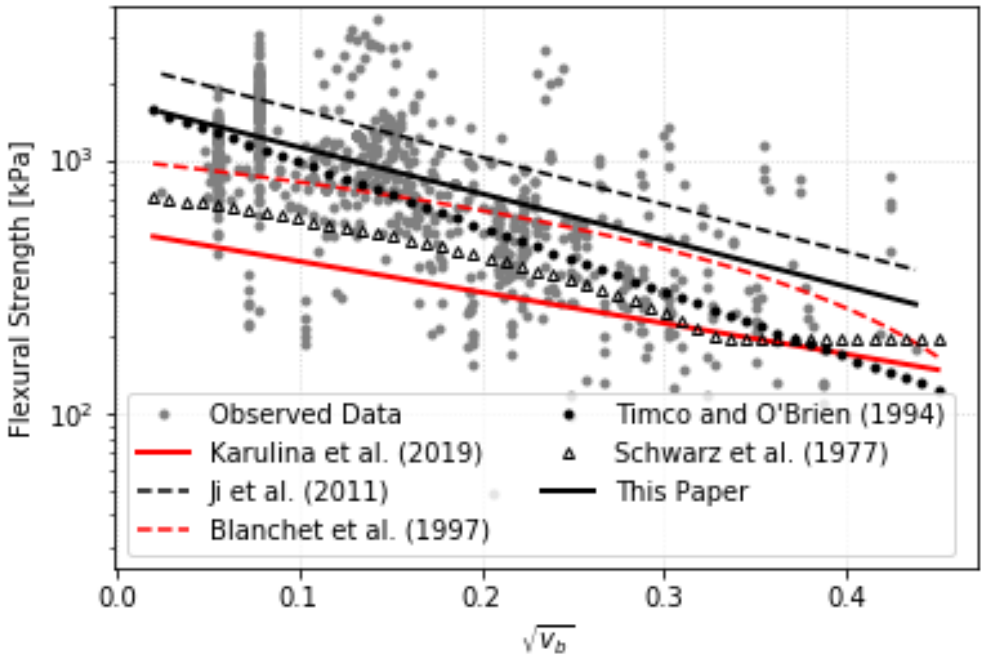

Figure 6.1: Single parameter empirical model : Flexural strength as a function of the square root of brine volume fraction

Brine volume was not documented by every author in the database, and as discussed previously entries without a brine volume were subject to removal from the database. However, if both salinity and temperature are available than brine volume can be approximated using the equation derived by Frankenstein and Garner (1967), see Equation 2.31 reproduced below, thus preserving the entry in the database using a calculated value for brine volume.

$$v_b = S\left(\frac{49.185}{T} + 0.532\right) \qquad \text{(2.31 revisited)}$$

6.1.1.2 Temperature

As discussed in Section 2.3.4, there is a general consensus that flexural strength of sea ice decreases with increasing ice temperatures (e.g. Timco and O'Brien, 1994). The use of temperature alone to model flexural strength seems to be employed less frequently than brine

volume however, linear models for deriving flexural strength based solely on ice temperature were presented by Ji et al. (2011) (see Equation 2.39) and Saeki et al. (1978) (see Equation 2.37).

$$\sigma_f = 0.35 - 0.09 \cdot T \qquad [\text{MPa}] \tag{2.39 revisited}$$

$$\sigma_f = 3.4 - 0.64 \cdot T \qquad [\text{kg/cm}^2] \tag{2.37 revisited}$$

Two additional models were developed based on the observed data, one based on a linear model (Equation 6.10) while the other based on a polynomial model (Equation 6.11).

$$\sigma_f = 0.482 - 0.046 \cdot T \tag{6.10}$$

$$\sigma_f = 0.378\,|T|^{0.424} \tag{6.11}$$

The Ji et al. (2011) and Saeki et al. (1978) models along with the two new models are presented in Figure 6.2 for comparison, overall it appears the polynomial model has a better fit to the data.

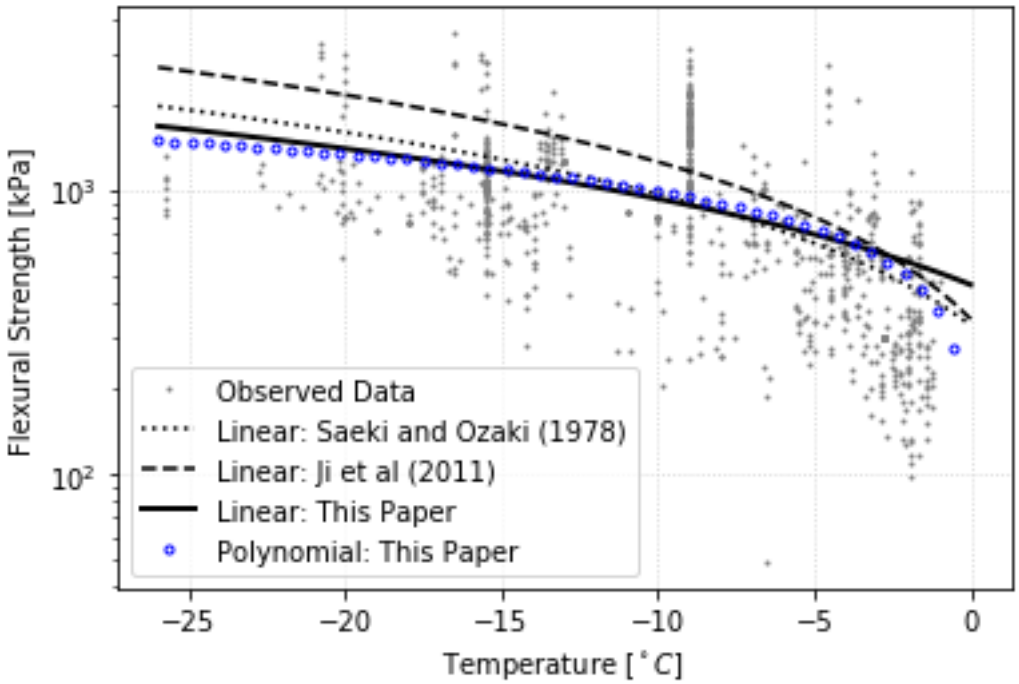

Figure 6.2: Single parameter empirical model : Flexural strength as a function of temperature

6.1.1.3 Beam Volume

As discussed in Section 2.3.2, the relationship between decreasing flexural strength with increasing beam volume has been demonstrated by a number of researchers (e.g. Frederking and Sudom (2013), Lau et al. (2001), Williams and Parsons (1994), Maattanen (1975) and Lavrov (1971)). This relationship is often referred to as a "scale-effect" and while it is accepted by many its significance is still debated among researchers. For example, Blanchet et al. (1997), Timco and O'Brien (1994), Parsons et al. (1992), Parsons and Lal (1991) found no significant evidence of scale-effect as related to the flexural strength of sea ice.

The relationship between the flexural strength of sea ice and beam volume is generally modelled in conjunction with another ice parameters such as brine volume. Flexural strength models based solely on beam volume are not readily available in literature and during this research no published models were found to serve as a benchmark for this ice parameter. A

polynomial regression model was applied to the prediction of flexural strength based solely on beam volume and fit to the current database, the resultant model is presented in Equation 6.12 and Figure 6.3.

$$\sigma_f = 0.392 \cdot V^{-0.155} \tag{6.12}$$

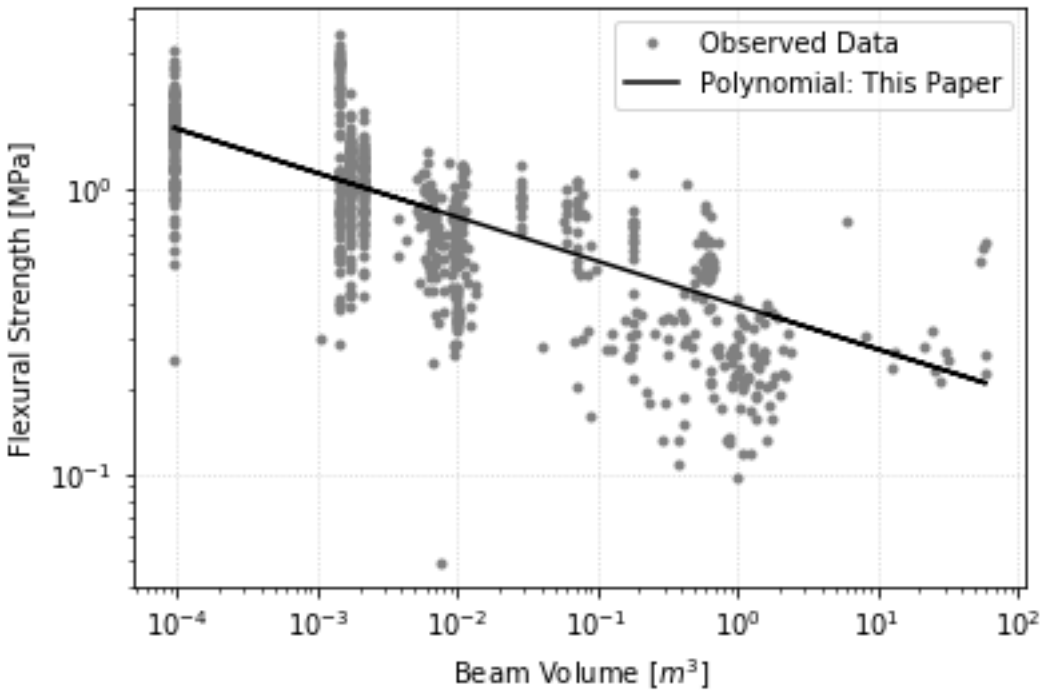

Figure 6.3: Single parameter empirical model : Flexural strength as a function of beam volume

6.1.2 Multi-Parameter Regression

The empirical representation of the relationship between flexural strength and sea ice parameters cannot be fully explained by any single ice property. Furthermore, individual ice properties are not necessarily independent and underlining correlations can and do exist between the various properties. For instance, temperature and brine volume are correlated through salinity as discussed in Section 2.3.4.1. One common multiple parameter regression

model employs features of both polynomial and exponential decay models, and a generic form of this model is provided in Equation 6.13:

$$\sigma_f = c_0 \cdot P_1^{c_1} \cdot e^{c_2 \cdot P_2} \tag{6.13}$$

where σ_f is the flexural strength of ice, c_0, c_1, and c_2 are constants, and P_1 and P_2 are physical properties of the ice sample such as temperature or brine volume.

One of the most common multi-parameter parings is that of beam volume and brine volume, and has been employed by several researchers including Aly et al. (2019) and Williams and Parsons (1994) as shown in Equations 6.14 and 6.15 respectively.

$$\sigma_f = 1760 \cdot \left(\frac{V}{V_1}\right)^{-0.057} e^{-5.395\sqrt{v_b}} \tag{6.14}$$

$$\sigma_f = 1324 \cdot \left(\frac{V}{V_1}\right)^{-0.054} e^{-4.969\sqrt{v_b}} \tag{6.15}$$

where V is beam volume, V_1 is a reference volume and v_b is brine volume. A reference volume of 0.01m^3 was set by Williams and Parsons (1994) and 1.0m^3 by Aly et al. (2019).

Using the same generic formulae a two-parameter model of flexural strength (see Equation 6.16) was developed based on the current database and is presented along with the previously discussed models in Figure 6.4 as a function of beam volume, and in Figure 6.5 as a function of brine volume. The results generated by the Aly et al. and Williams and Parsons models are very similar. The new model is similar to the others but tends to result in higher strength values.

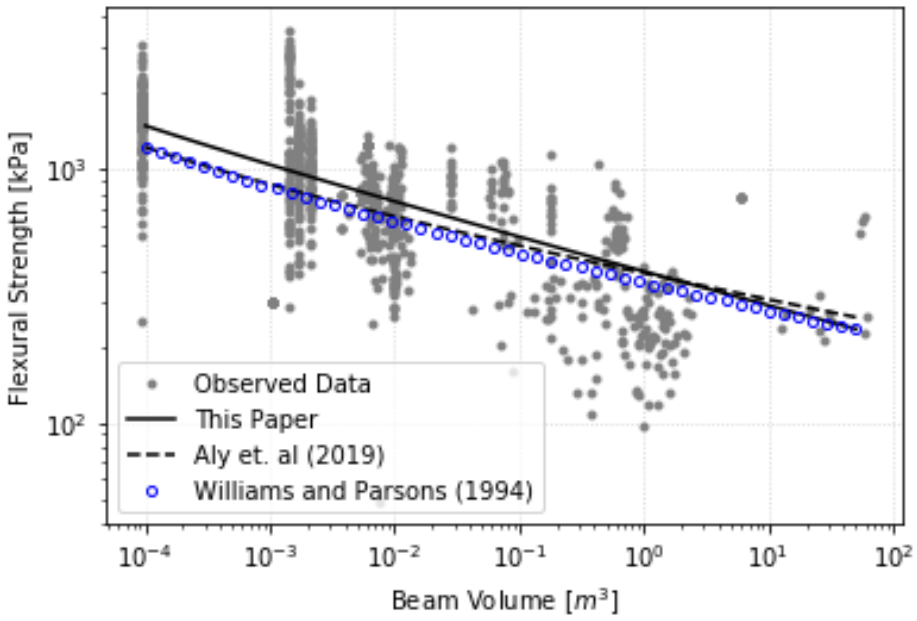

Figure 6.4: Multi-parameter empirical model: Flexural strength as a function of beam volume

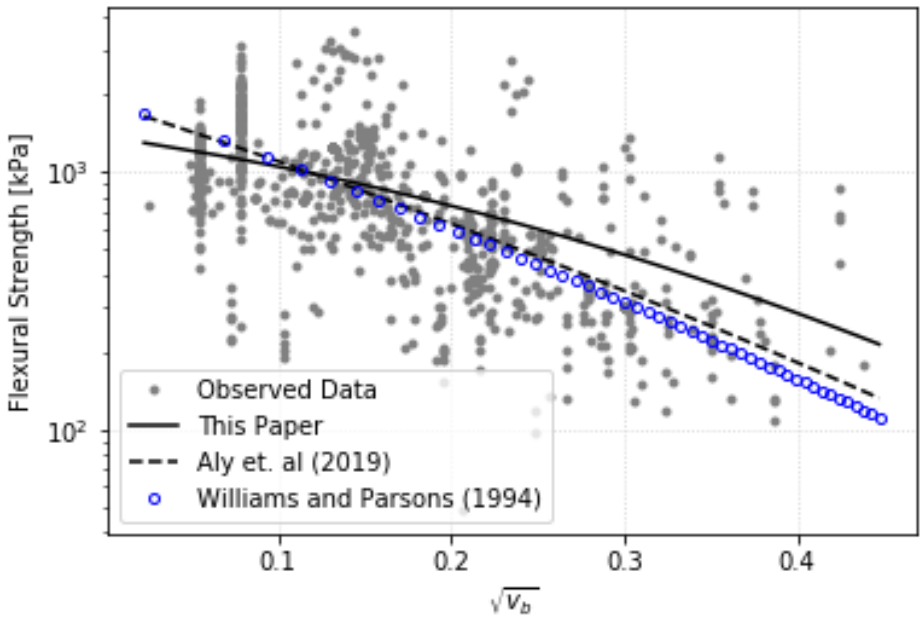

Figure 6.5: Multi-parameter empirical model: Flexural strength as a function of brine volume

$$\sigma_f = 559 \left(\frac{V}{V_1}\right)^{-0.128} e^{-1.358\sqrt{v_b}} \tag{6.16}$$

6.2 Machine Learning

In this work, ML regression algorithms were developed and applied to predict the flexural strength of sea ice. Four machine learning models were developed based on the MLPR, ETR, GBR and KNR algorithms. All models were generated and tuned using a Python machine learning library developed by Scikit-learn (2021). These models were compared and contrasted looking at model bias, accuracy and generalization as well as their ability to extrapolate and predict strengths for values outside of the training data. The application of ensemble modelling was also investigated, in which two or more models were blended, attempting to overcome their individual weaknesses by building upon their combined strengths.

6.2.1 Observed and Simulated Data

There are two primary datasets used during model development, observed data and simulated data. Observed data refers to the data as originally presented within the flexural strength database (see Section 3) and forms the basis for model development. Simulated data refers to data which has been generated based on original observed data, for the purpose of enhancing the visibility of data trends. Details on the simulated dataset are provided in the following section.

6.2.1.1 Simulated Data

As evident from the observed data, the flexural strength of sea ice exhibits a high degree of variability. Models fitted to the observed data tend to mirror this variability making data trends harder to observe. To help reduce this variability the observed data were simplified

into four relationships: brine volume vs beam volume (Figure 6.6a), brine volume vs temperature (Figure 6.6b), beam volume vs brine volume (Figure 6.6c) and temperature vs brine volume (Figure 6.6d).

To improve the visual representation of data trends three simulated databases were developed based from beam volume, brine volume and temperature. The simulated database based on brine volume defines both beam volume (V) and temperature (T) as a function of brine volume (v_b), as shown in Equations 6.17 and 6.18 and presented in Figure 6.6a and 6.6b. For the simulated database based on beam volume, v_b is defined as function of beam volume using Equation 6.19 and presented in Figure 6.6c. Temperature is then estimated based on Equation 6.18 in the same manner as the simulated brine volume database. For the simulated database based on temperature, v_b is defined as a function of temperature as described in Equation 6.20 and presented in Figure 6.6d, V is then defined as a function of v_b as presented in Equation 6.17.

$$V = 0.0384 v_b - 6.203 \tag{6.17}$$

$$T = -18.838 + 3.164 \cdot \ln v_b \tag{6.18}$$

$$v_b = 5.151 \cdot \ln V + 60.896 \tag{6.19}$$

$$v_b = 120.414 \cdot \exp(0.187\, T) \tag{6.20}$$

The ability to decipher a relationship between brine volume and temperature based on observed data is expected based on the correlation between these two properties as discussed

in Section 2.3. However, beam volume has no direct correlation with the other parameters, as this property is selected by the researcher when determining the appropriate size for a given test program, hence the large amount of scatter seen in the observed data of Figures 6.6a and 6.6c. However, to complete the simulated database a reasonable assumption of beam volume was required, either a constant or some relationship with the another parameter would be required. Therefore the linear trends between beam volume and brine volume, as presented above, were selected as they provided a monotonic trend which helped promote trendline presentations.

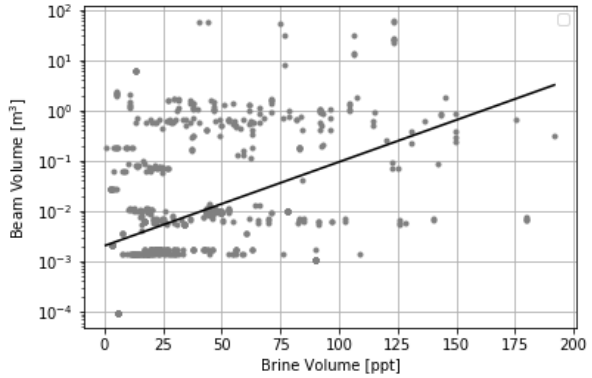

(a) Brine volume vs beam volume

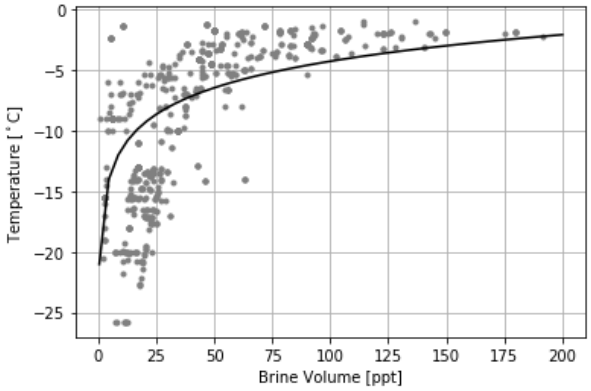

(b) Brine volume vs temperature

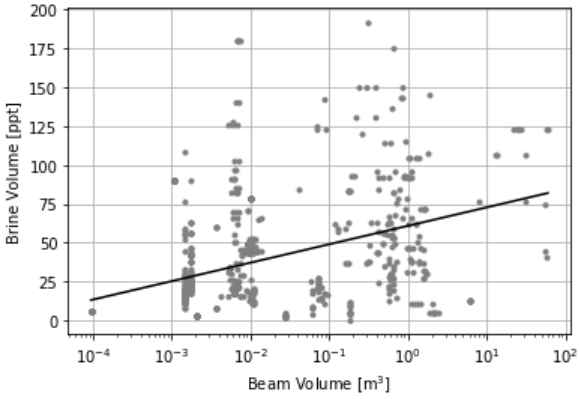

(c) Beam volume vs brine volume

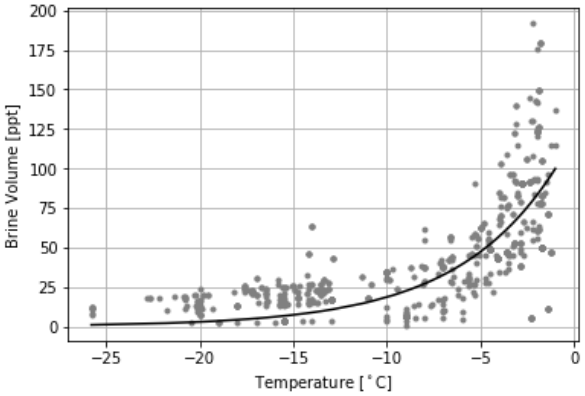

(d) Temperature vs brine volume

Figure 6.6: Trendlines of simulated database based on the observed data

6.2.2 Independent Models

In the following sections the implementation of the four ML algorithms mentioned above will be discussed. The general process for tuning the model to the data began with the default hyperparameters, followed by hyperparameters selected using Scikit-Learn's parameter optimization tool, and finally a manual tuning of the hyperparameters. The parameter optimization tool within scikit-learn performs a cross-validated search across a matrix of user supplied hyperparameters.

When tuning the models careful consideration is given to both the statistical accuracy metrics and the generalization of the model. As noted earlier when plotting model predictions using the observed data a higher degree of variability in the predictions is expected in comparison to the simulated data. However, careful observation of the model predictions using the observed data must be performed to distinguish between variability within the model and the overfitting of the model.

6.2.2.1 Multilayer Perceptron Regressor

As discussed in Section 4.2.1 the the MLPR algorithm has a number of hyperparameters which require tuning to achieve an optimized model. Four of most influential hyperparameters were found to be *alpha* or the strength of the L2 regularization term (default = 0.001), the *size of hidden layer* (default = 100), the *activation function* (default = "relu") and the *solver* (default = "adam") used to optimize the weight of each node to node link.

MLPR output with default hyperparameters is show in Figure 6.7, and presents a very reasonable starting point for the optimization of the model. Using the optimization tool a new set of hyperparameters were established, with the resultant model presented in Figure 6.8. However, upon viewing the output it is obvious that the newly established hyperparameters are overfitting the data and further tuning is required.

The results of the optimizations tool were not satisfactory, requiring further tuning of the hyperparameters. Using the default hyperparameters as the basis, the *alpha* parameter was incrementally increased from the default value (0.001) until an optimum value was determined at 13. The *size of the hidden layer* was subsequently decreased from 100 to 20. During the manual tuning process the overall model accuracy as well as the fit of the model to the observed and simulated datasets were used as indicators when adjusting the hyperparameters. Results for the manual tuning are provided in Figure 6.9 for both the training and test data sets. A summary of the default, optimizer and manually tuned hyperparameters are provided in Table 6.1.

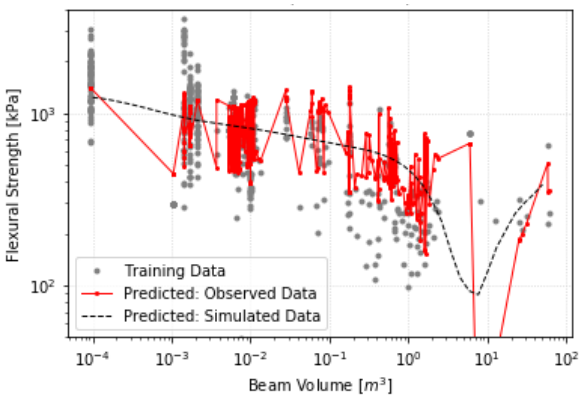

(a) Strength vs beam volume: Training data

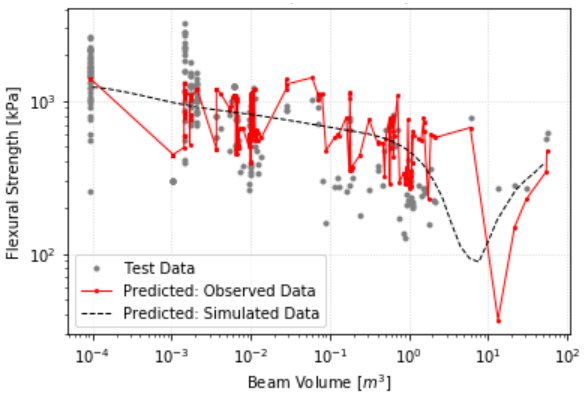

(b) Strength vs beam volume: Test data

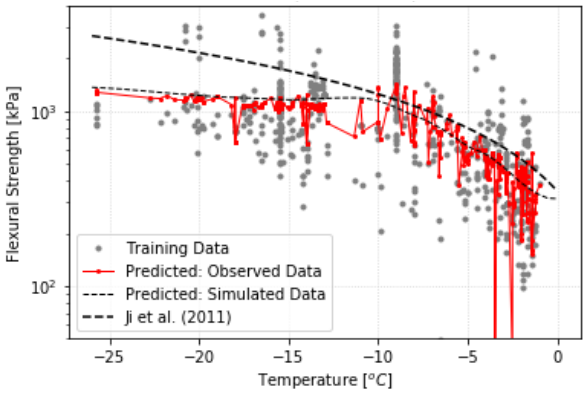

(c) Strength vs temperature: Training data

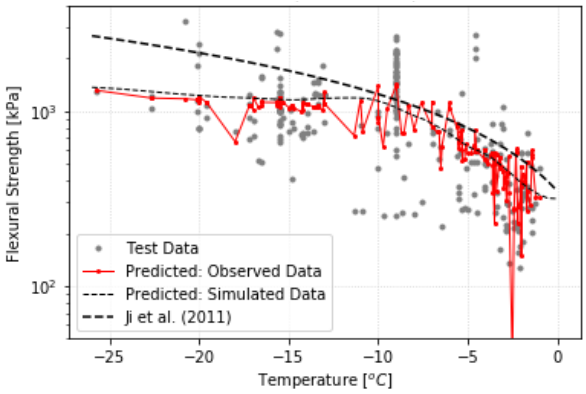

(d) Strength vs temperature: Test data

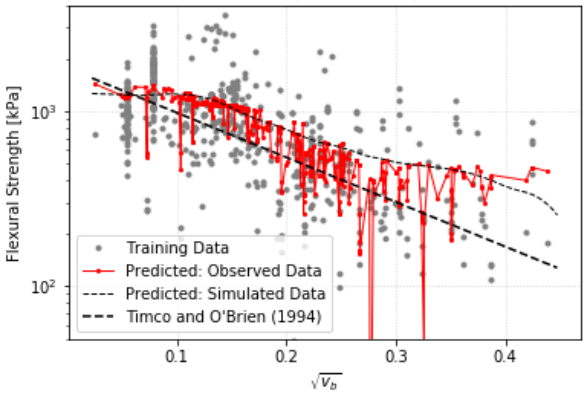

(e) Strength vs brine volume: Training data

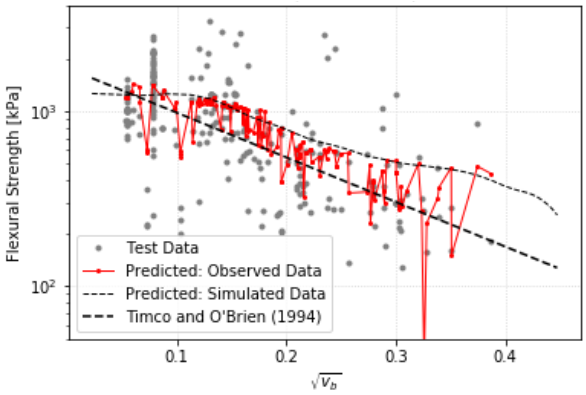

(f) Strength vs brine volume: Test data

Figure 6.7: MLPR: Default parameters

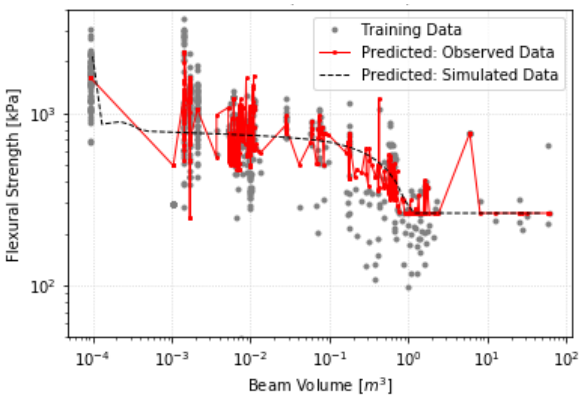

(a) Strength vs beam volume: Training data

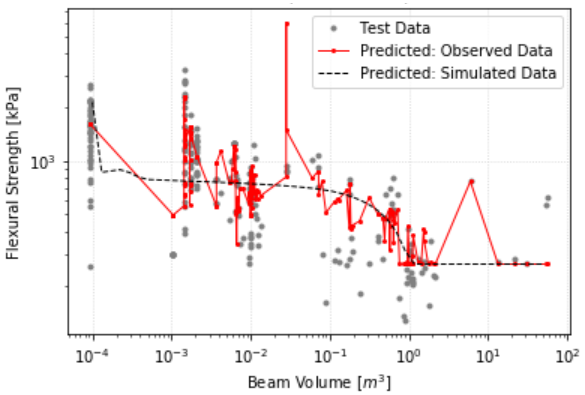

(b) Strength vs beam volume: Test data

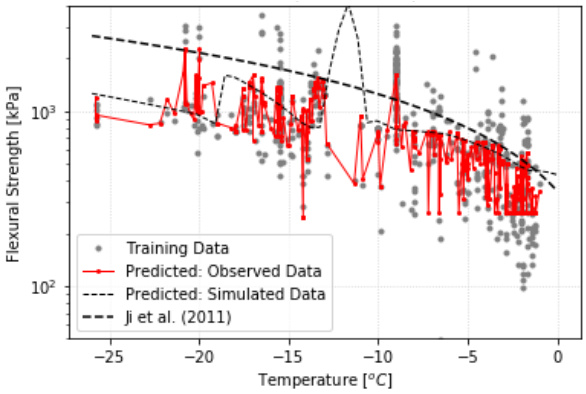

(c) Strength vs temperature: Training data

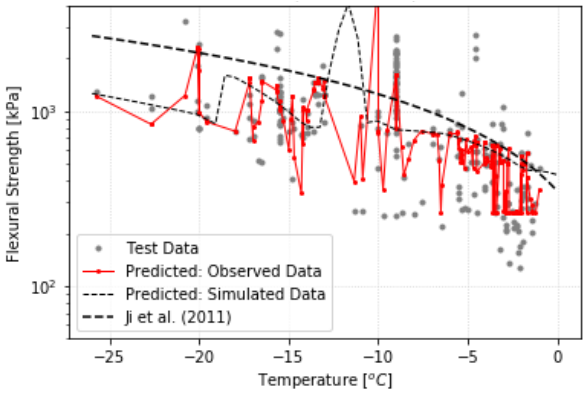

(d) Strength vs temperature: Test data

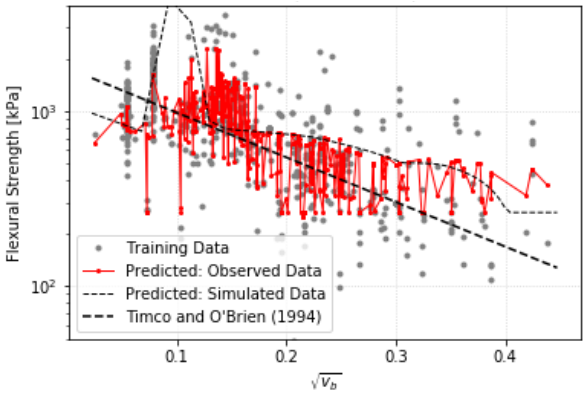

(e) Strength vs brine volume: Training data

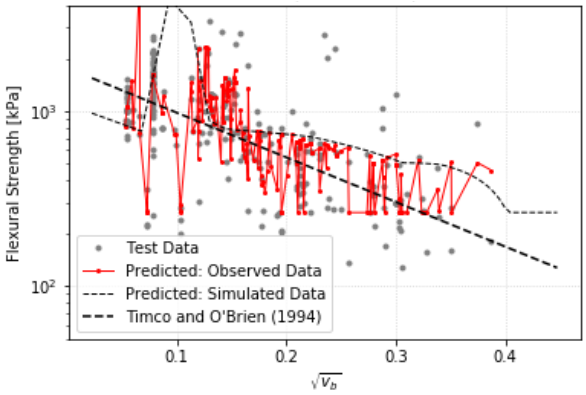

(f) Strength vs brine volume: Test data

Figure 6.8: MLPR: Grid search selected parameters

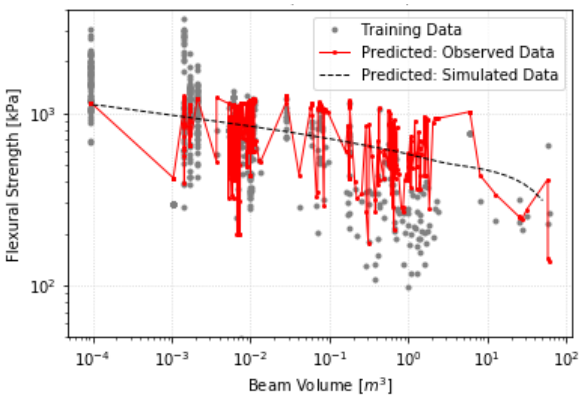

(a) Strength vs beam volume: Training data

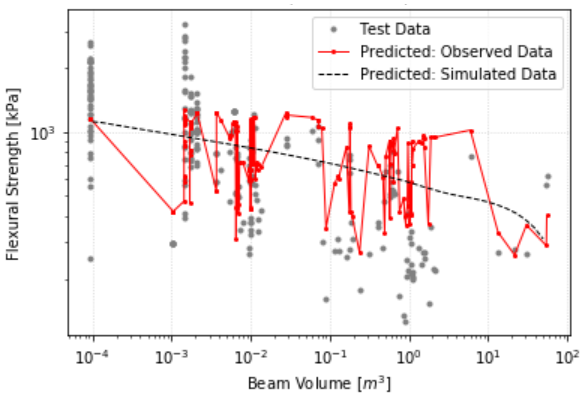

(b) Strength vs beam volume: Test data

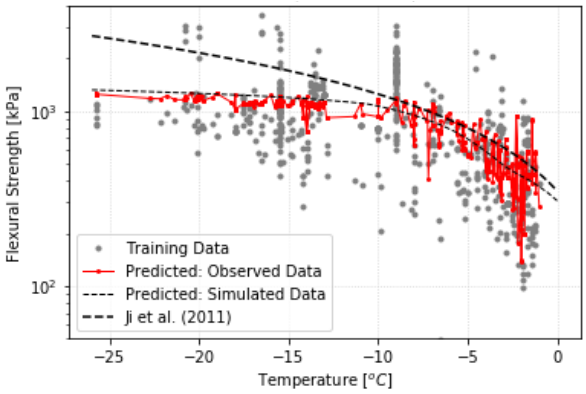

(c) Strength vs temperature: Training data

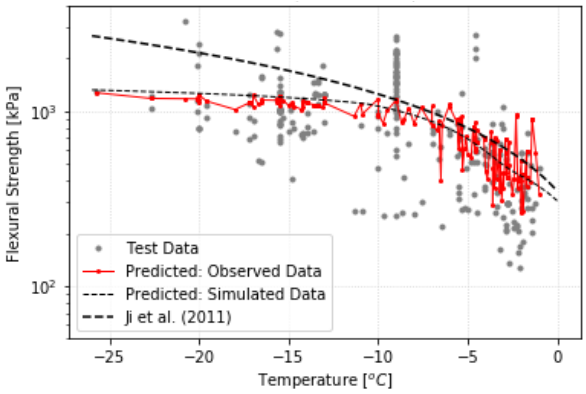

(d) Strength vs temperature: Test data

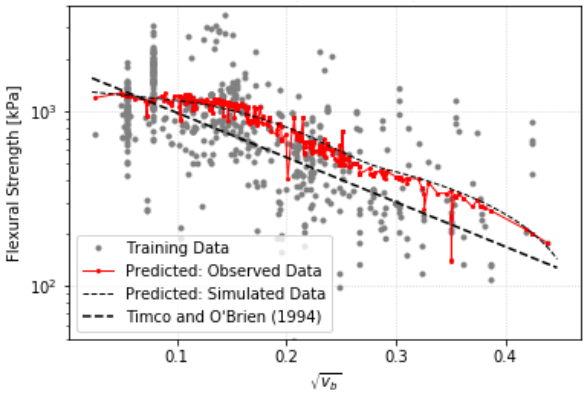

(e) Strength vs brine volume: Training data

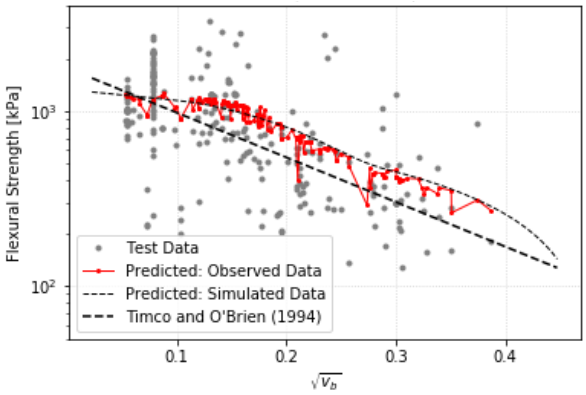

(f) Strength vs brine volume: Test data

Figure 6.9: MLPR: Manually tuned parameters

Table 6.1: MLPR: Hyperparameter summary

Hyperparameter	**Default**	**Grid Search**	**Manual**
Size of hidden layer	100	(7,7)	20
alpha	0.001	0.001	13
Activation function	relu	tanh	relu
Solver	*adam*	*lgfbs*	*lgfbs*

6.2.2.2 Extra Trees

As discussed in Section 4.2.2.1 the ETR algorithm has a number of hyperparameters which require tuning to achieve an optimized model. Three of most influential hyperparameters were found to be the maximum depth (default = "none"), number of estimators (default = 100) and minimum samples per leaf (default = 2).

A ETR has been applied to the data using the Scikit-learn library function within Python. The ETR regressor was run by tuning three input parameters: *max depth*, *number of estimators* and *minimum samples per leaf*.

The first tuning attempt began with the default settings, and the results are presented in Figure 6.10. The general overall trends presented using the default parameters are very good for both the observed and simulated datasets. However, there is evidence of overfitting within the model which is clearly evident when inspecting the observed data. As a result further tuning was considered necessary. Parameter optimization tools were employed and the optimal *number of estimators*, *maximum depth* and *minimum samples per leaf* were determined to be 30, 11 and 1 respectively. The result of the ETR model based on these optimization parameters is shown in Figure 6.11.

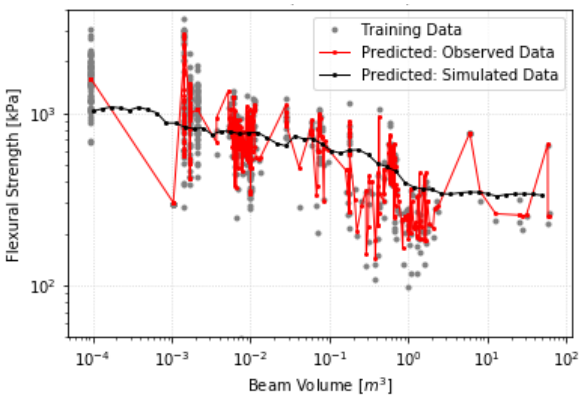

(a) Strength vs beam volume: Training data

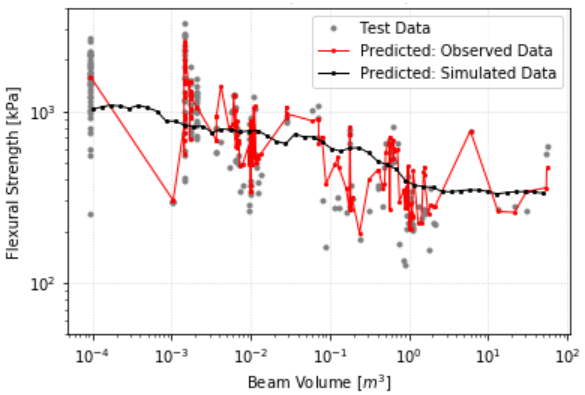

(b) Strength vs beam volume: Test data

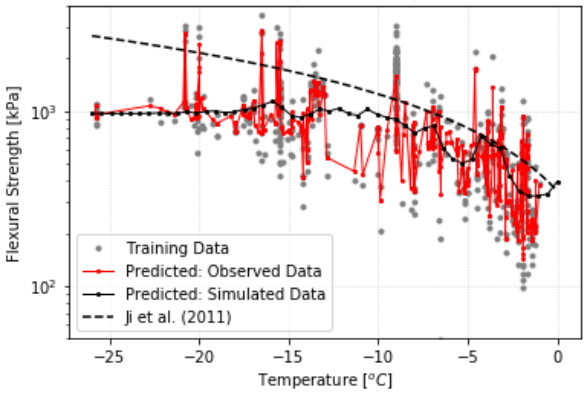

(c) Strength vs temperature: Training data

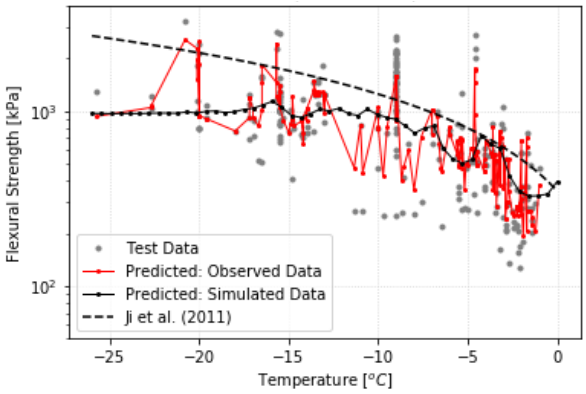

(d) Strength vs temperature: Test data

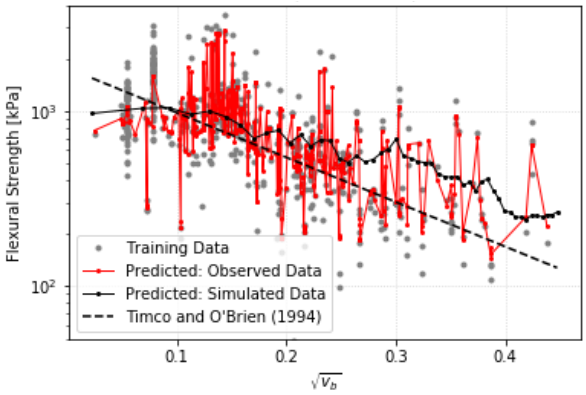

(e) Strength vs brine volume: Training data

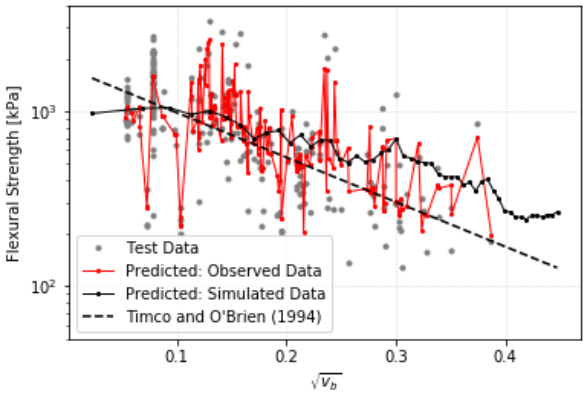

(f) Strength vs brine volume: Training data

Figure 6.10: ETR: Default parameters

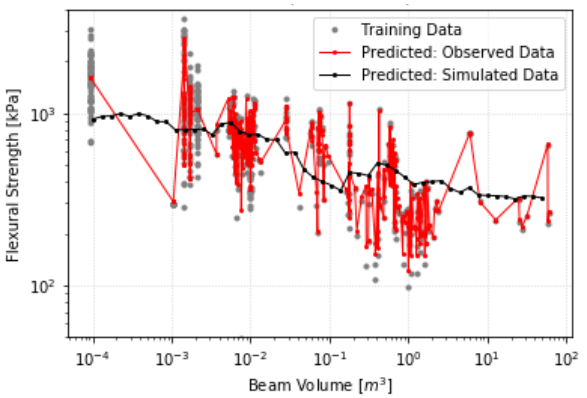

(a) Strength vs beam volume: Training data

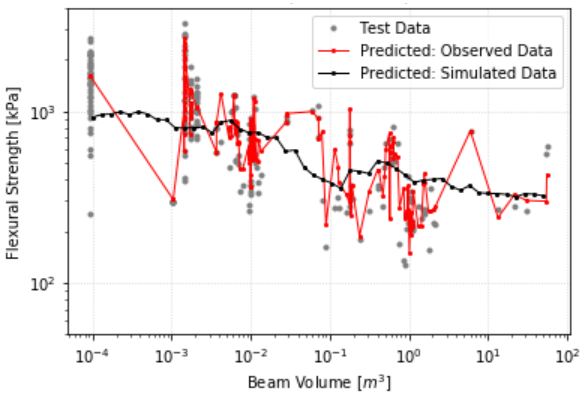

(b) Strength vs beam volume: Test data

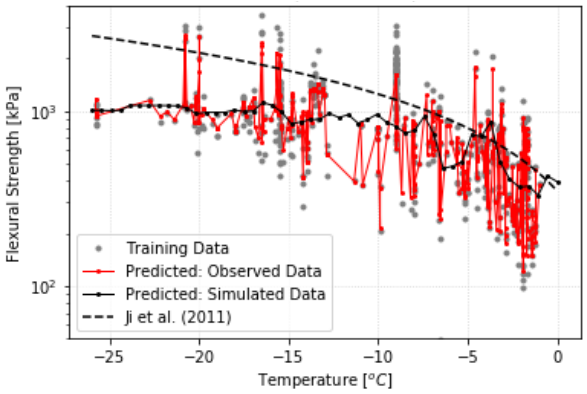

(c) Strength vs temperature: Training data

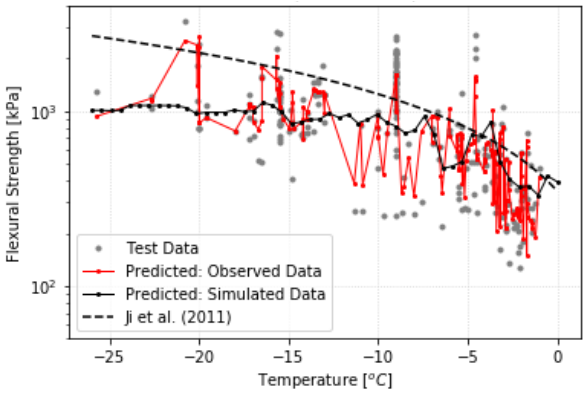

(d) Strength vs temperature: Test data

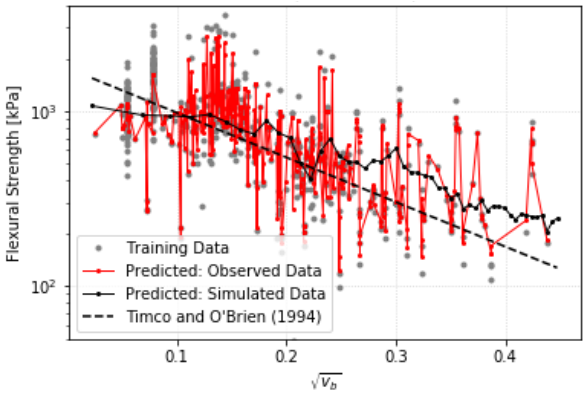

(e) Strength vs brine volume: Training data

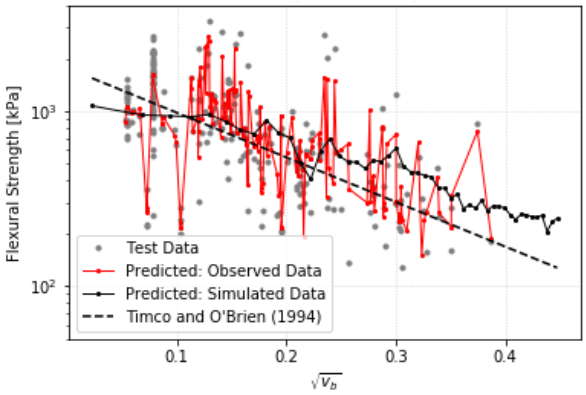

(f) Strength vs brine volume: Test data

Figure 6.11: ETR: Grid search parameters

The parameters defined by the optimization tool helped slightly in reducing the overfitting tendency observed in the default model. However, the model is still showing significant signs of overfitting. Further tuning of the input parameters was considered necessary in an

effort to improve the fit of the model. Various combinations of parameters were tested, the *number of estimators* was increased to 75, *max depth* was decreased to 5 and the *minimum samples per leaf* was kept at 1, the results are shown in Figure 6.12. These modification were successful in improving the overall fit of the data, although some overfitting is still present the overall model was significantly improved. A summary of the default, optimizer and manually tuned hyperparameters are provided in Table 6.2.

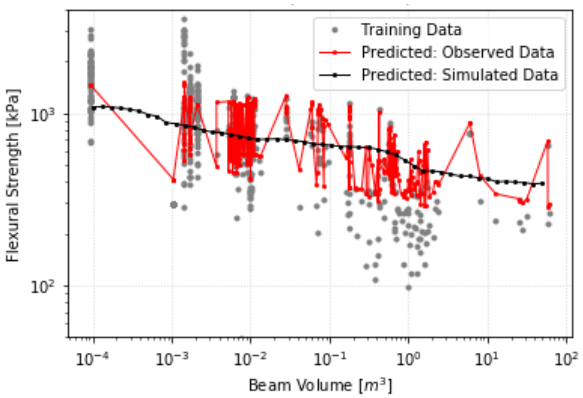

(a) Strength vs beam volume: Training data

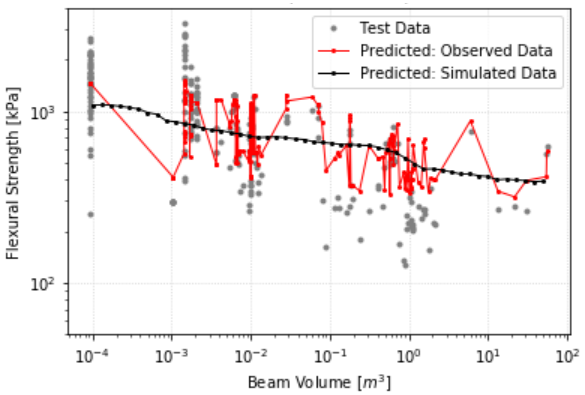

(b) Strength vs beam volume: Test data

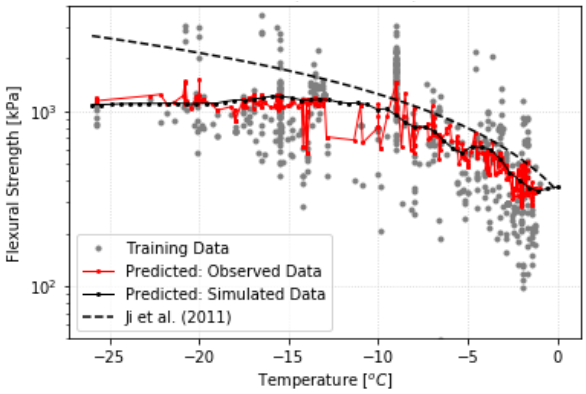

(c) Strength vs temperature: Training data

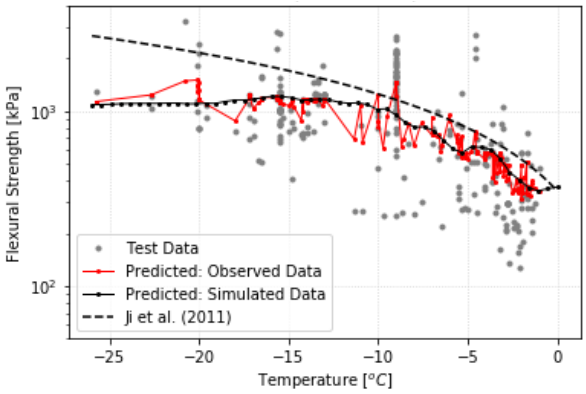

(d) Strength vs temperature: Test data

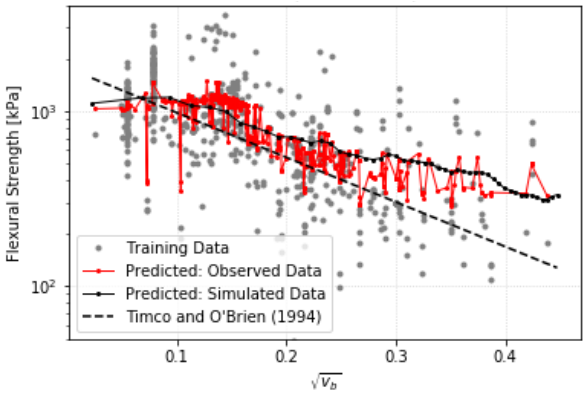

(e) Strength vs brine volume: Training data

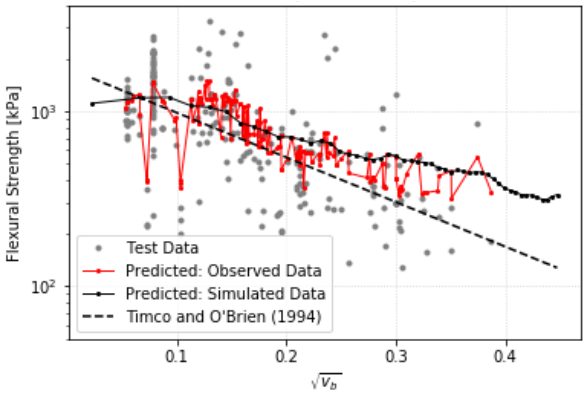

(f) Strength vs brine volume: Test data

Figure 6.12: ETR: Manually tuned parameters

Table 6.2: ETR: Hyperparameter summary

Hyperparameter	**Default**	**Grid Search**	**Manual**
Maximum Depth	"none"	11	5
Number of Estimators	100	30	75
Minimum samples per leaf	2	1	1

6.2.2.3 Gradient Boosted Trees

As discussed in Section 4.2.2.2 the GBR algorithm has a number of hyperparameters which require tuning to achieve an optimized model. Four of the most influential hyperparameters were found to be the *maximum depth* (default = 3), *number of estimators* (default = 100), *minimum samples per leaf* (default = 1) and *learning rate* (default = 0.1).

GBR output with default hyperparameters is show in Figure 6.13 and clearly indicates that the model is overfitting the data. The parameter optimization tools were employed resulting in an optimal hyperparameters settings with the *number of estimators* equal to 500, *learning rate* of 0.2, *minimum samples per leaf* equal to 5 and *max depth* equal to 7. Output using the grid search is shown in Figure 6.14.

The optimization tool did not perform well for the GBR model resulting in an increase in model overfitting. The application of manual tuning of the hyperparameters was performed resulting in the *number of estimators* equal to 500, *learning rate* equal to 0.01, *minimum samples per leaf* of 5 and *max depth* equal to 2. Output using the manual hyperparameters is presented in Figure 6.15 and demonstrates a significant improvement over the previous GBR models. A summary of the default, optimizer and manually tuned hyperparameters are provided in Table 6.3.

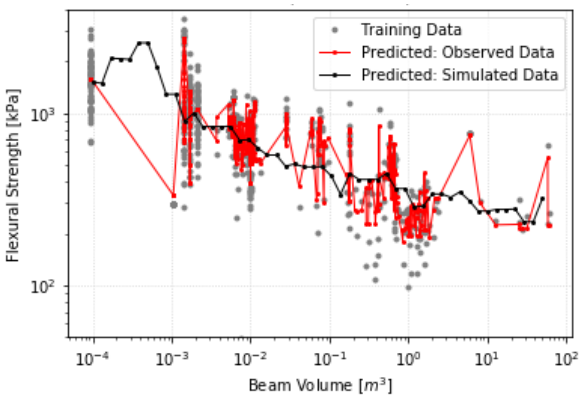

(a) Strength vs beam volume: Training data

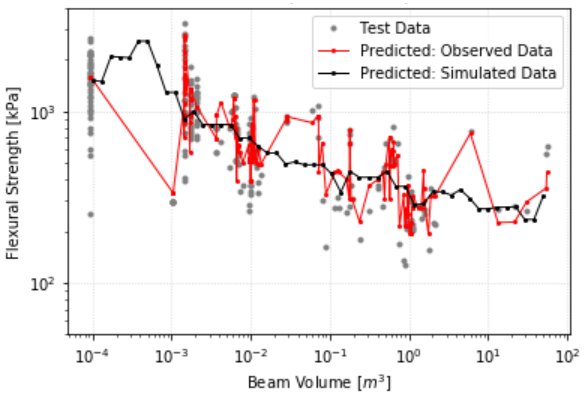

(b) Strength vs beam volume: Test data

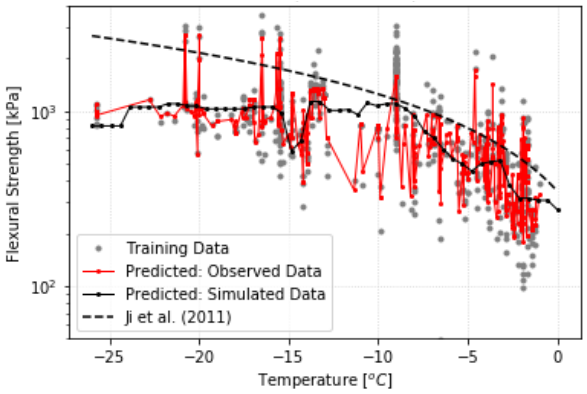

(c) Strength vs temperature: Training data

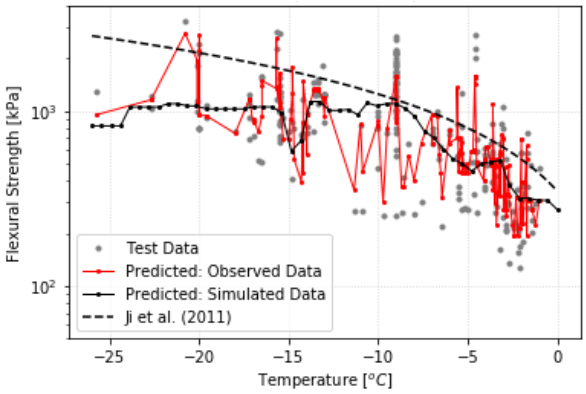

(d) Strength vs temperature: Test data

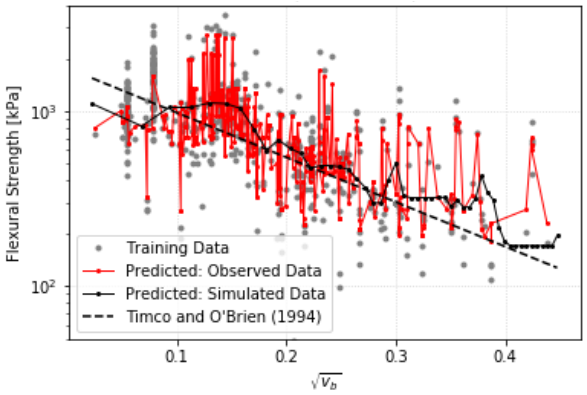

(e) Strength vs brine volume: Training data

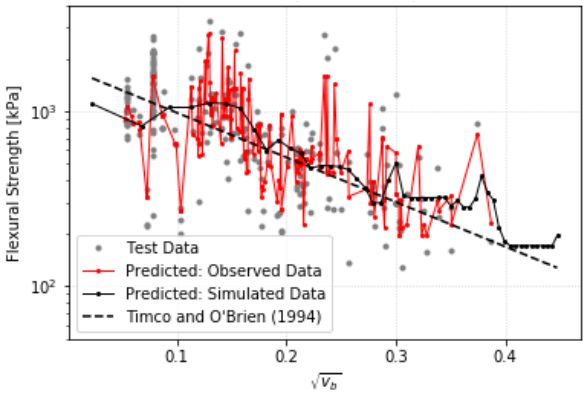

(f) Strength vs brine volume: Test data

Figure 6.13: GBR: Default parameters

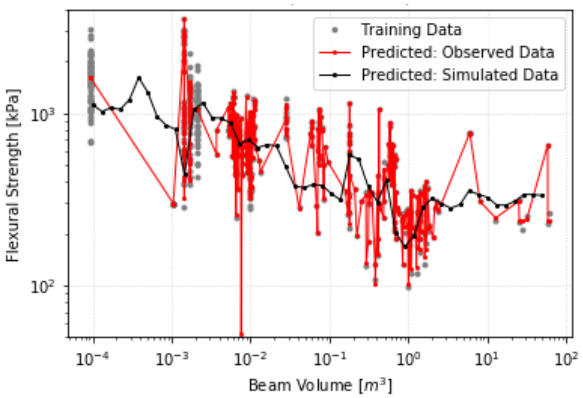

(a) Strength vs beam volume: Training data

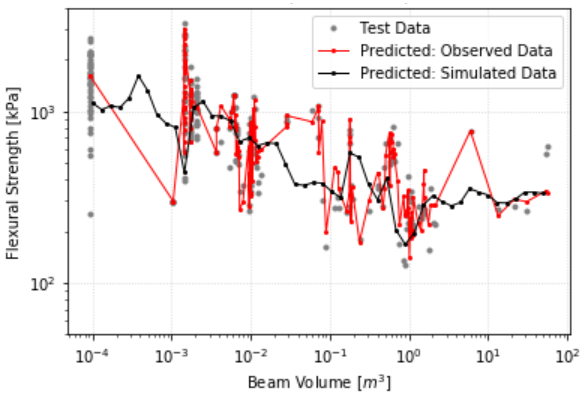

(b) Strength vs beam volume: Test data

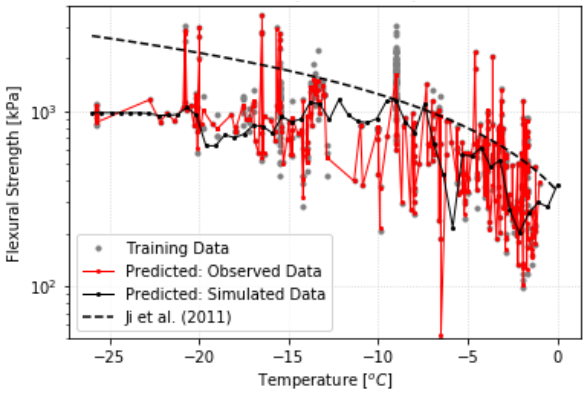

(c) Strength vs temperature: Training data

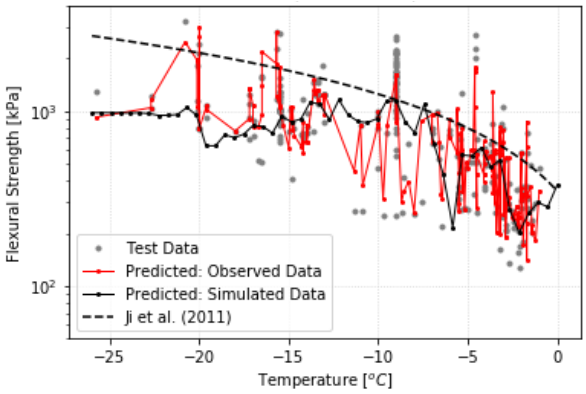

(d) Strength vs temperature: Test data

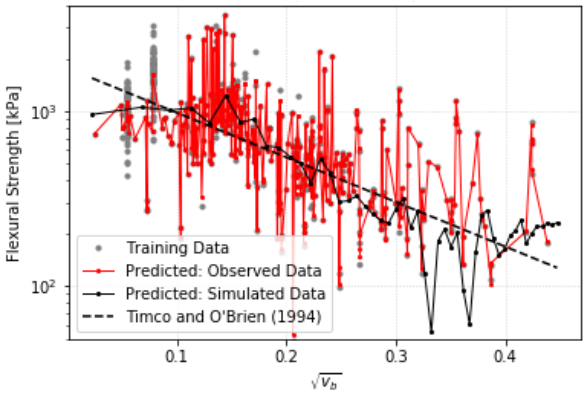

(e) Strength vs brine volume: Training data

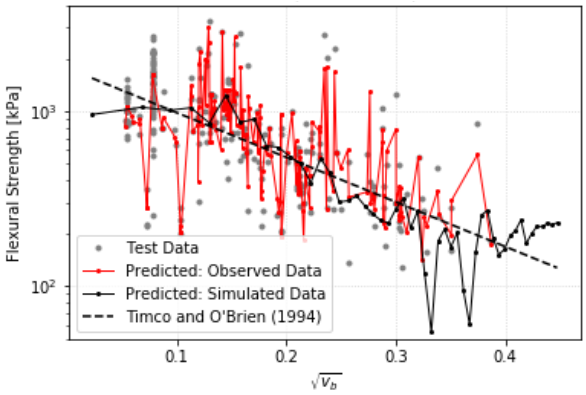

(f) Strength vs brine volume: Test data

Figure 6.14: GBR: Grid search selected parameters

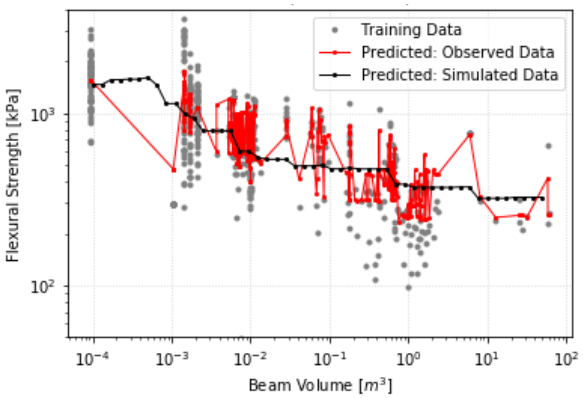

(a) Strength vs beam volume: Training data

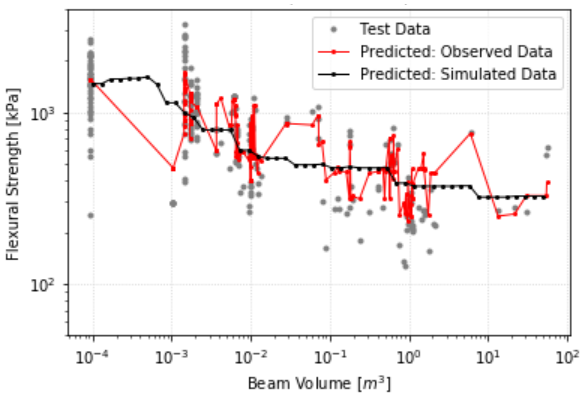

(b) Strength vs beam volume: Test data

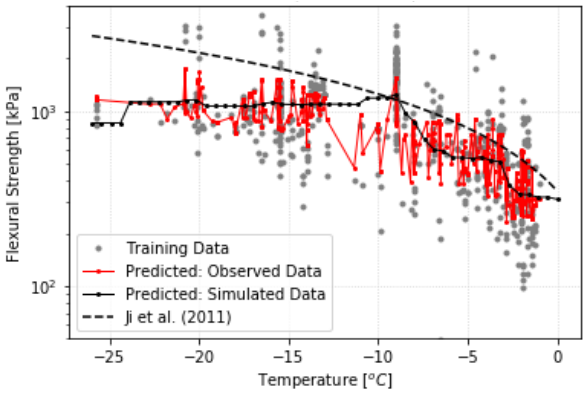

(c) Strength vs temperature: Training data

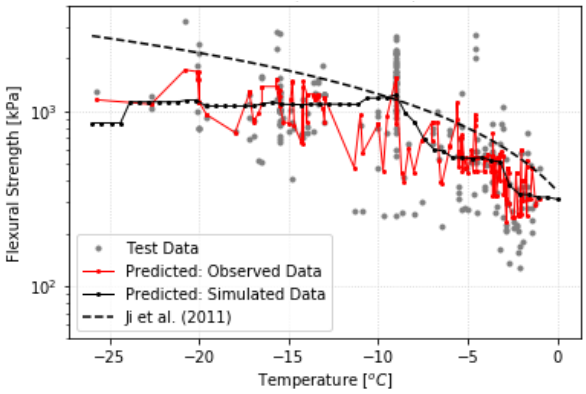

(d) Strength vs temperature: Test data

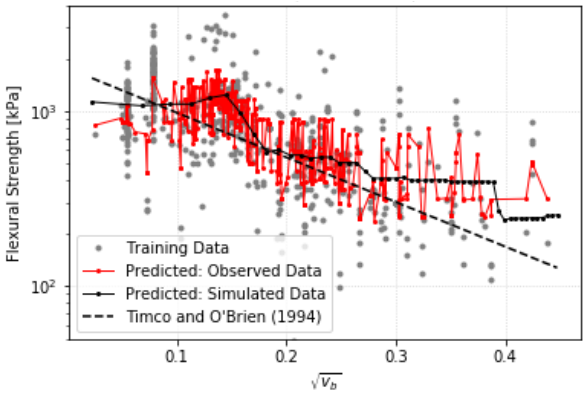

(e) Strength vs brine volume: Training data

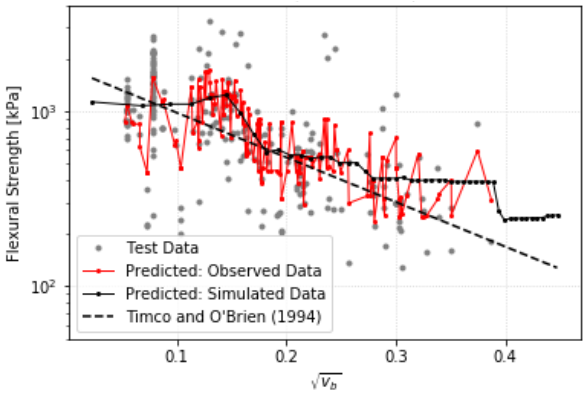

(f) Strength vs brine volume: Test data

Figure 6.15: GBR: Manual search selected parameters

Table 6.3: GBR: Hyperparameter summary

Hyperparameter	**Default**	**Grid Search**	**Manual**
Maximum Depth	3	7	2
Number of Estimators	100	500	500
Minimum samples per leaf	1	3	5
Learning rate	0.01	0.02	0.01

6.2.2.4 k-nearest Neighbours

As discussed in Section 4.2.3, the KNR algorithm is the simplest of the ML algorithms introduced in this work, and has only 3 hyperparameters which require tuning to achieve an optimized model including *number of neighbors* (default = 5), *weighting method* (default = uniform) and the *algorithm* used to compute the nearest neighbor (default = auto).

KNR output with default hyperparameters is shown in Figure 6.16, and presents a model which is overfitting the data. The parameter optimization tools were employed resulting in the *number of neighbors* increasing to 10 and the *weighting method* changing to "distance". The results of these modifications to the hyperparameters are shown in Figure 6.17 and shows an increase in the overfitting of the model.

The effect of the optimization tool on the KNR model was ineffective and overfitting of the data is still prevalent. It was therefore necessary to tune the model manually, and after several rounds of adjustments the final hyperparameters consisted of the model *weighting method* returning to "uniform" and the *number of neighbors* increasing to 50. KNR output with manual hyperparameters is presented in Figure 6.18 and demonstrates a significant reduction in overfitting. Model trend lines are also improved, where the simulated data trends present a significant reduction in the number of local maximum and minimums. There does appear to be a tendency towards a less continuous trend line when observing

strength versus beam volume and brine volume. A summary of the default, optimizer and manually tuned hyperparameters are provided in Table 6.4.

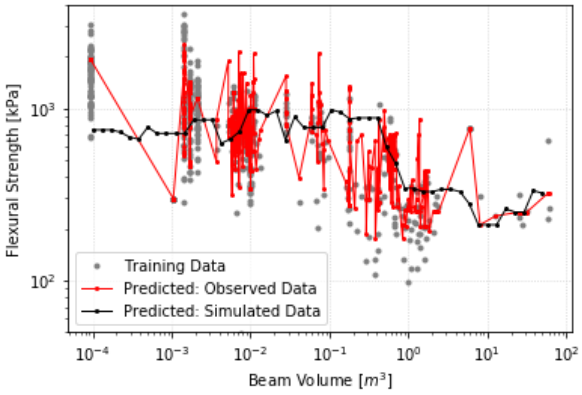

(a) Strength vs beam volume: Training data

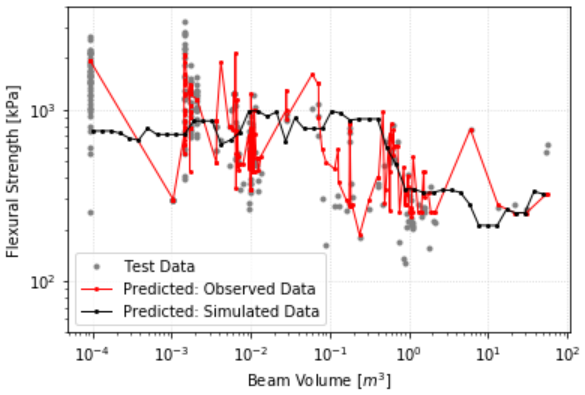

(b) Strength vs beam volume: Test data

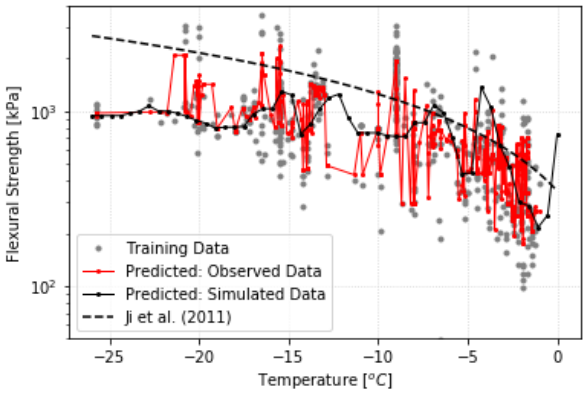

(c) Strength vs temperature: Training data

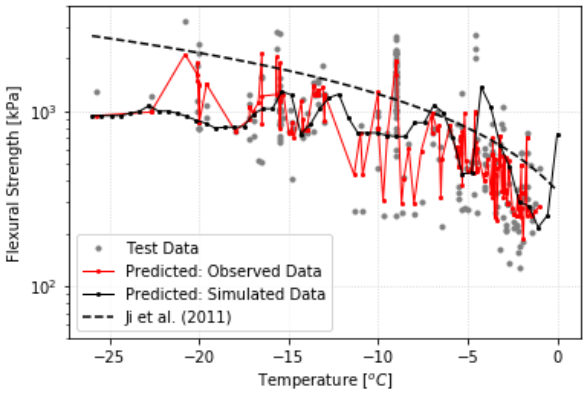

(d) Strength vs temperature: Test data

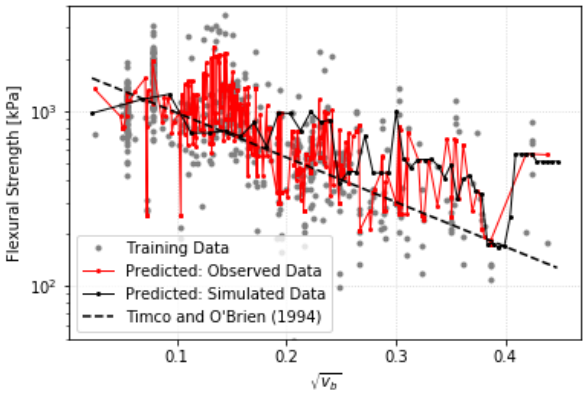

(e) Strength vs brine volume: Training data

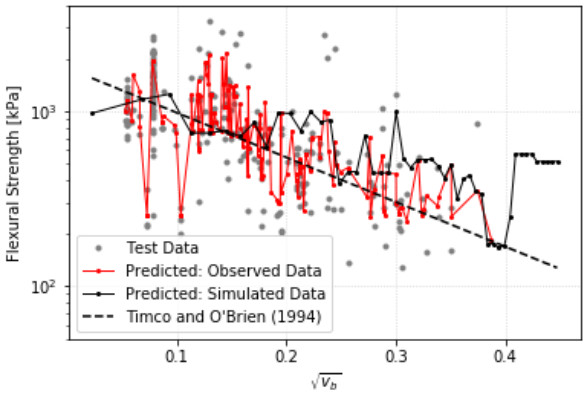

(f) Strength vs brine volume: Test data

Figure 6.16: KNR: Default parameters

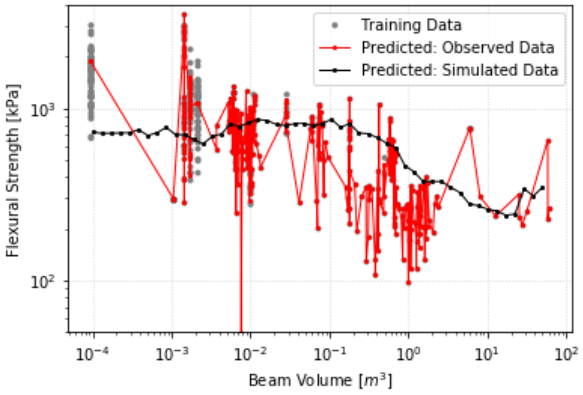

(a) Strength vs beam volume: Training data

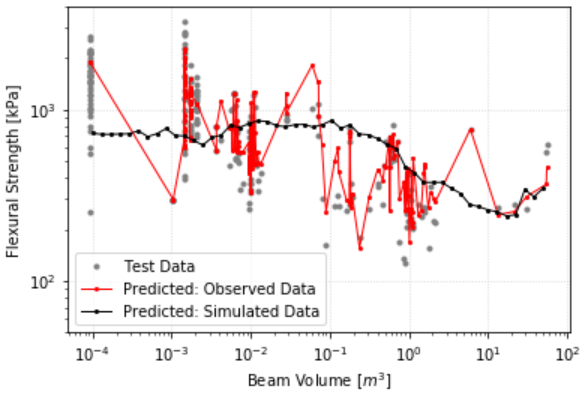

(b) Strength vs beam volume: Test data

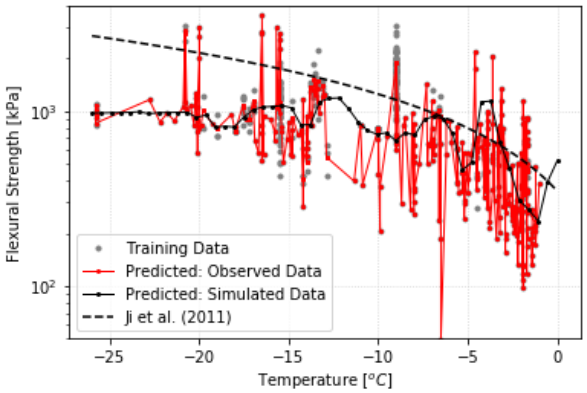

(c) Strength vs temperature: Training data

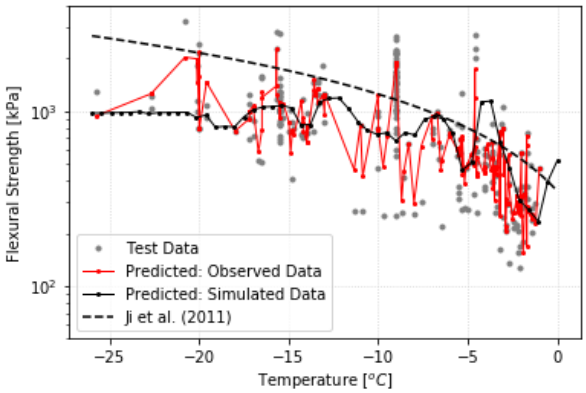

(d) Strength vs temperature: Test data

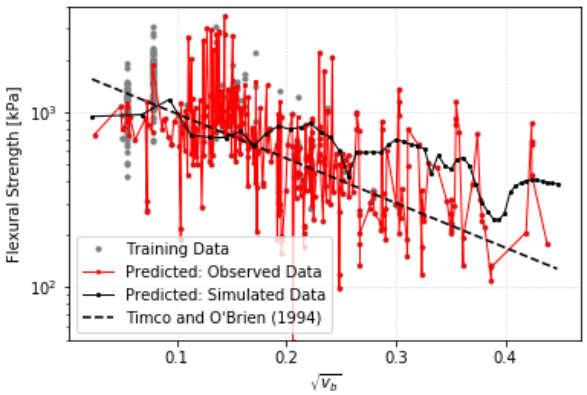

(e) Strength vs brine volume: Training data

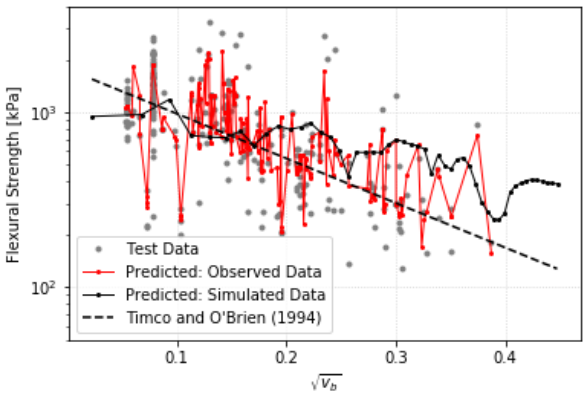

(f) Strength vs brine volume: Test data

Figure 6.17: KNR: Grid search selected parameters

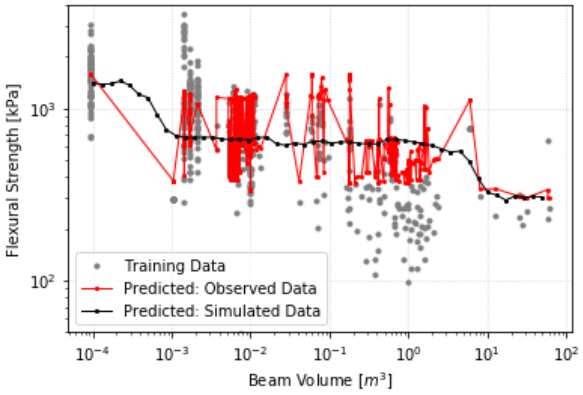

(a) Strength vs beam volume: Training data

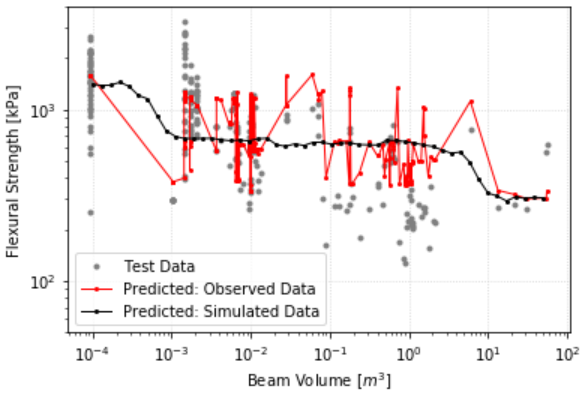

(b) Strength vs beam volume: Test data

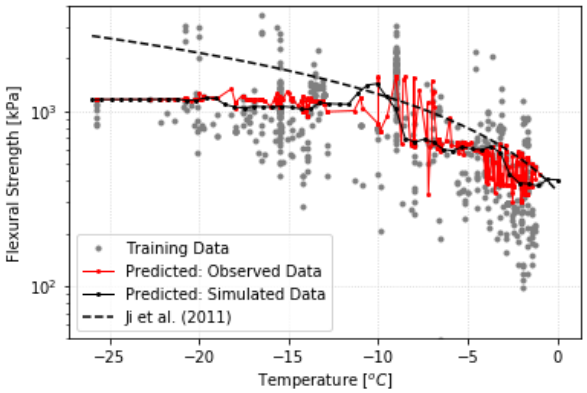

(c) Strength vs temperature: Training data

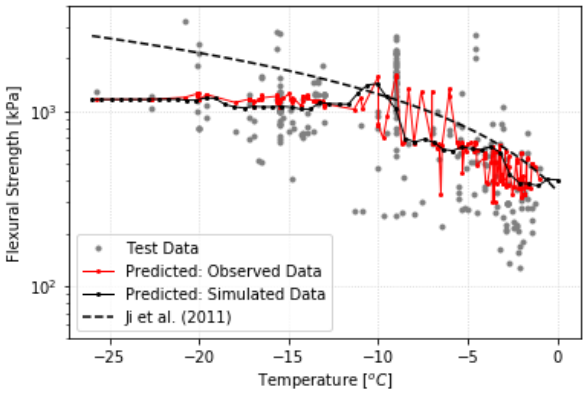

(d) Strength vs temperature: Test data

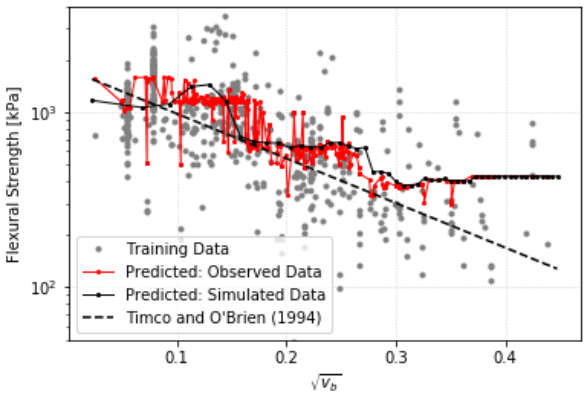

(e) Strength vs brine volume: Training data

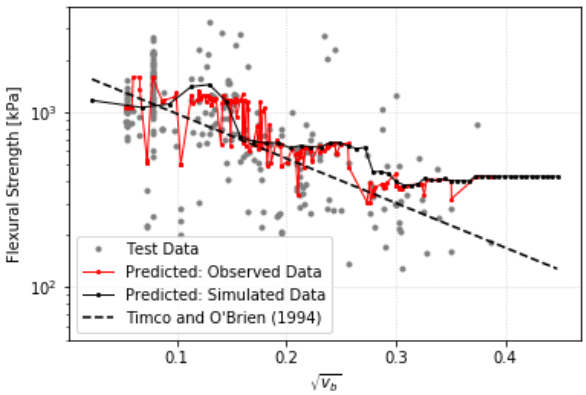

(f) Strength vs brine volume: Test data

Figure 6.18: KNR: Manually tuned parameters

Table 6.4: KNR: Hyperparameter summary

Hyperparameter	**Default**	**Grid Search**	**Manual**
Number of Neighbors	5	10	50
Weighting Method	"uniform"	"distance"	"uniform"
Algorithm	"auto"	"ball tree"	"auto"

6.2.3 Ensemble Models

The use of single algorithm models can result in accurate predictions however, models employing an ensemble approach using multiple algorithms often outperform their single algorithm counterparts. Averaging ensembles help to balance out the individual weaknesses (e.g. variance and bias) of the independent models. In this section the four independent models were combined for form six ensemble models each composed of two individual ML models. The predictions from the ensemble modes are shown in Figures 6.19 through 6.24 and include trendlines based on the observed (training and test data) and simulated datasets.

In Figures 6.19 and 6.20 each of the six ensembles are plotted against the square root of brine volume fraction and compared against the Timco and O'Brien (1994) brine model. Each of the ensemble models tends to overpredict in comparison to the empirical model. In Figures 6.21 and 6.22 the ensemble models are plotted against temperature and compared to the Saeki et al. (1978) temperature model. For temperatures above -10°C the ensemble and empirical models have good agreement, with the ensemble models generally overpredicting at lower temperatures. In Figures 6.23 and 6.24 the ensemble models are plotted against beam volume, however, there is no published empirical model for comparison. The trendlines from all six models indicate the expected trend of decreasing flexural strength with increasing brine volume, temperature and beam volume. In all cases the "MLPR + ETR" ensemble produced the smoothest trendline out of the six ensemble models tested. Further discussion on the ensemble models will be presented in the next section.

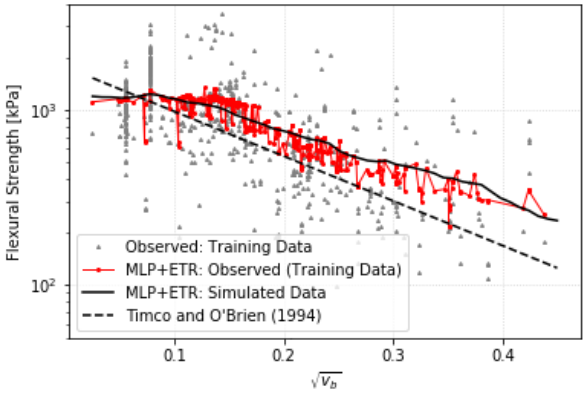

(a) MLPR + ETR

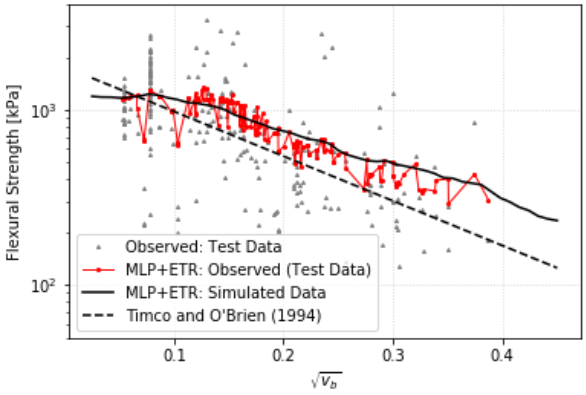

(b) MLPR + ETR

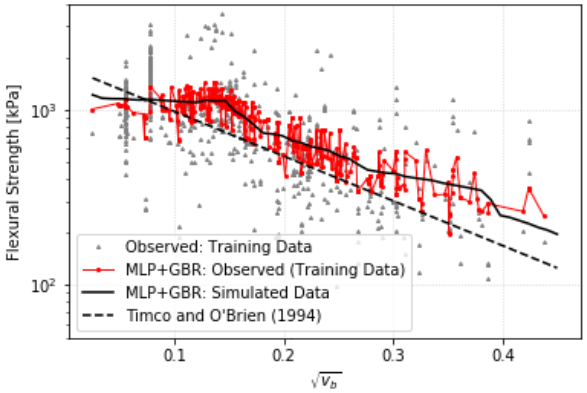

(c) MLPR + GBR

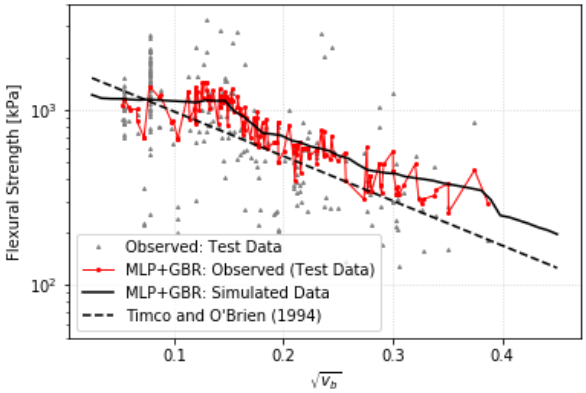

(d) MLPR + GBR

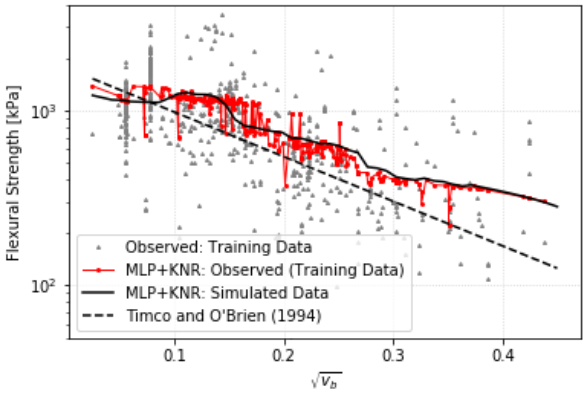

(e) MLPR + KNR

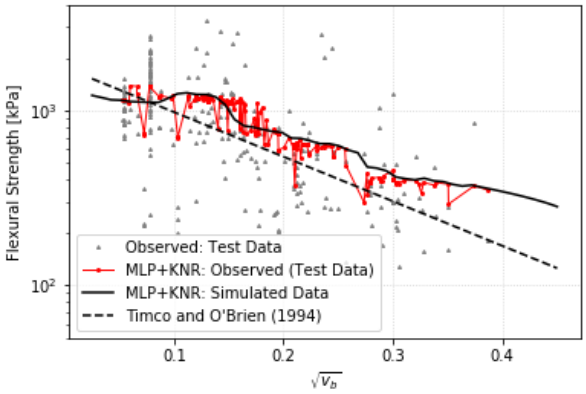

(f) MLPR + KNR

Figure 6.19: Ensemble models: Flexural strength as a function of brine volume (Part 1)

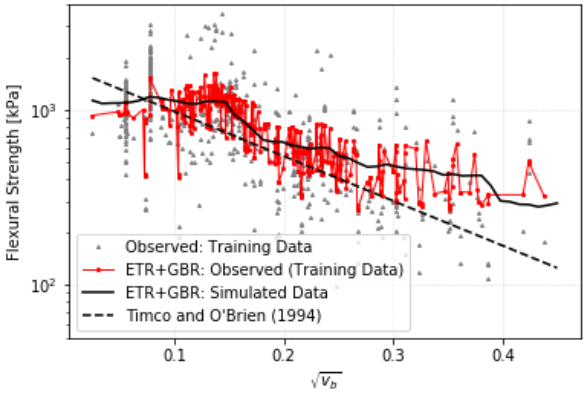

(a) ETR + GBR

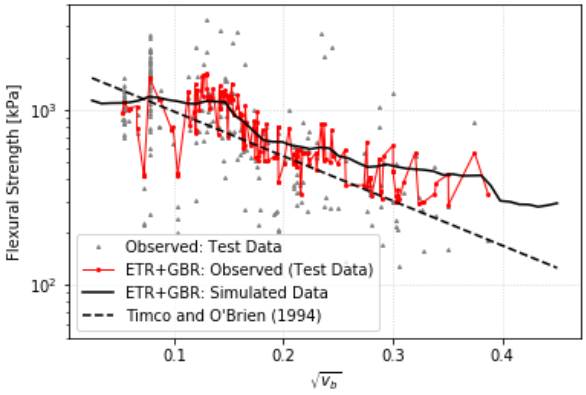

(b) ETR + GBR

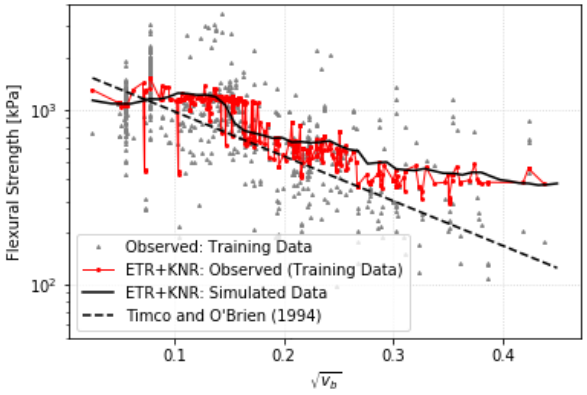

(c) ETR + KNR

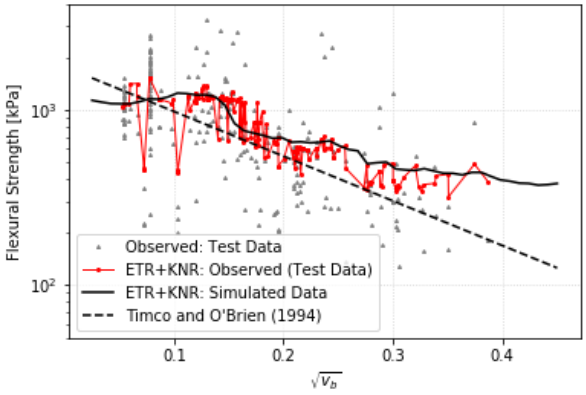

(d) ETR + KNR

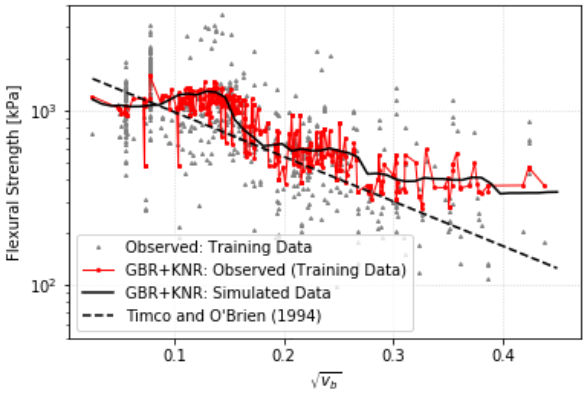

(e) GBR + KNR

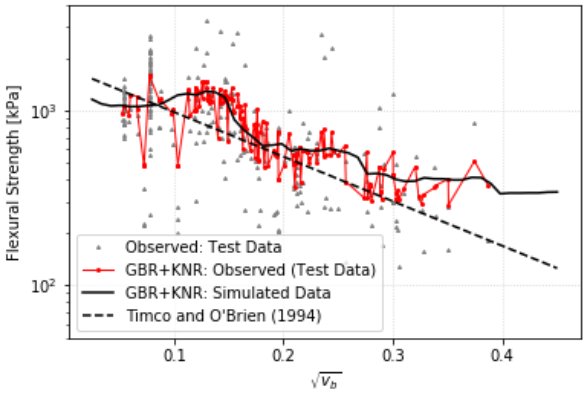

(f) GBR + KNR

Figure 6.20: Ensemble models: Flexural strength as a function of brine volume (Part 2)

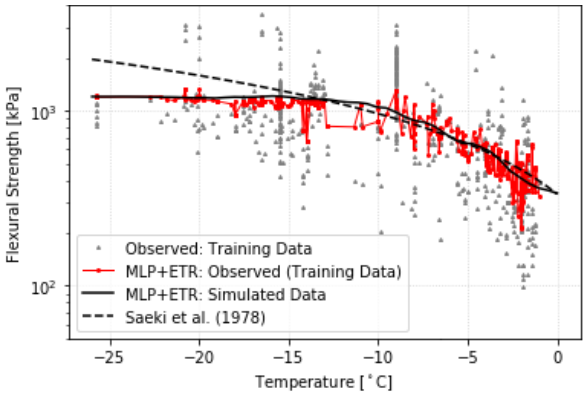

(a) MLPR + ETR

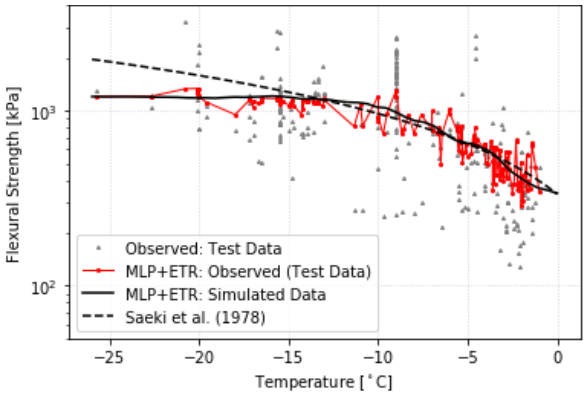

(b) MLPR + ETR

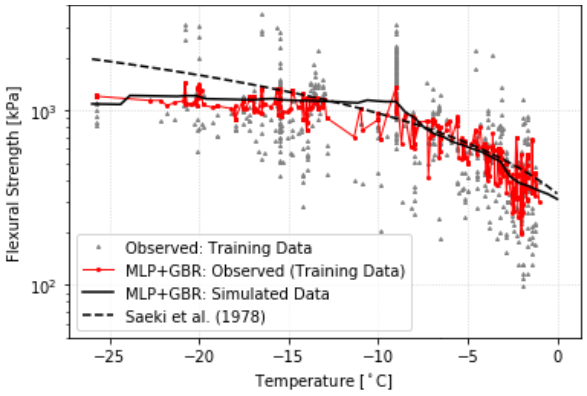

(c) MLPR + GBR

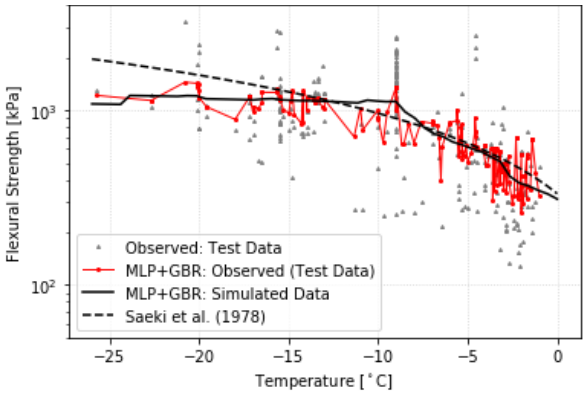

(d) MLPR + GBR

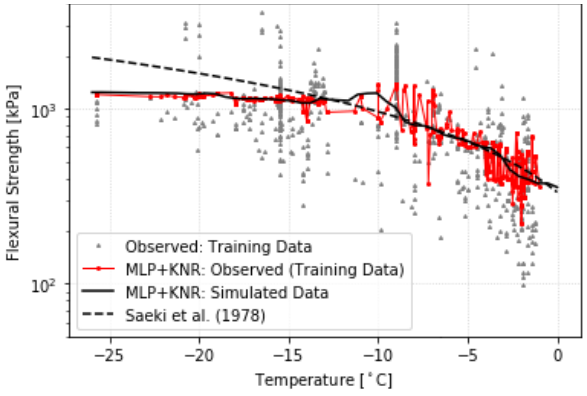

(e) MLPR + KNR

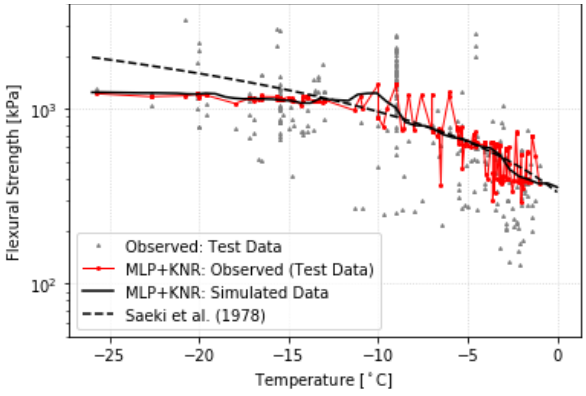

(f) MLPR + KNR

Figure 6.21: Ensemble models: Flexural strength as a function of temperature (Part 1)

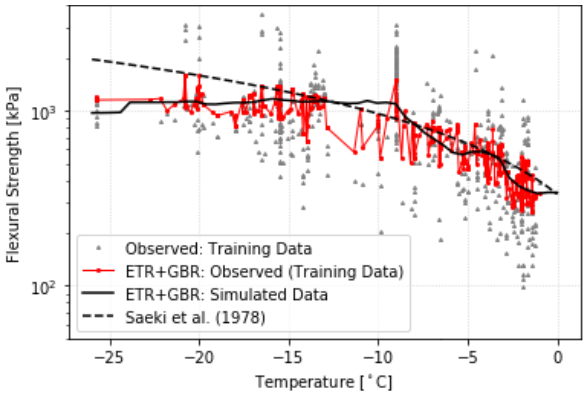

(a) ETR + GBR

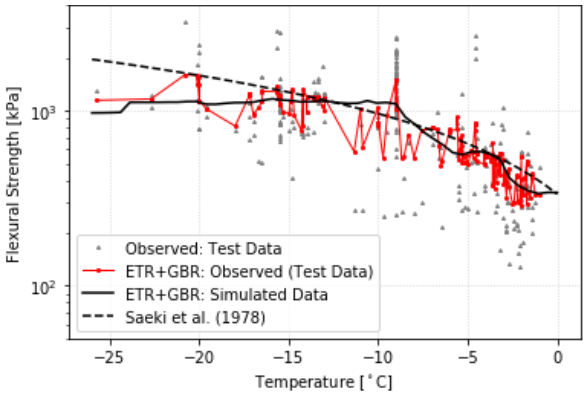

(b) ETR + GBR

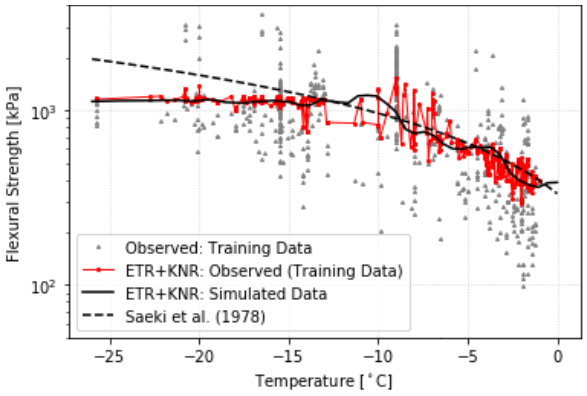

(c) ETR + KNR

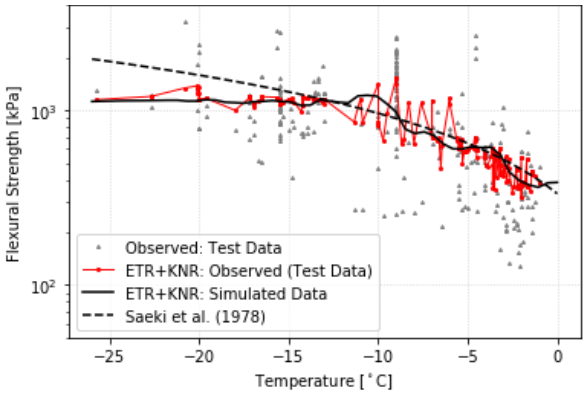

(d) ETR + KNR

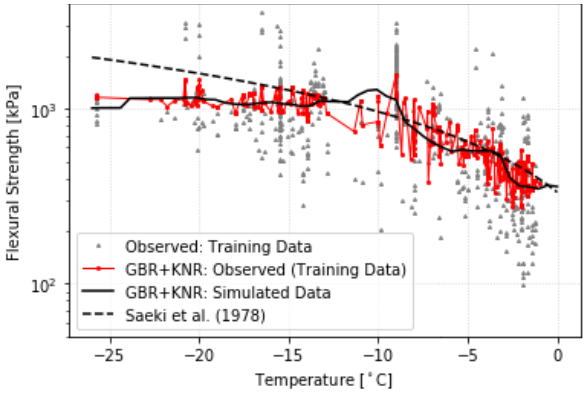

(e) GBR + KNR

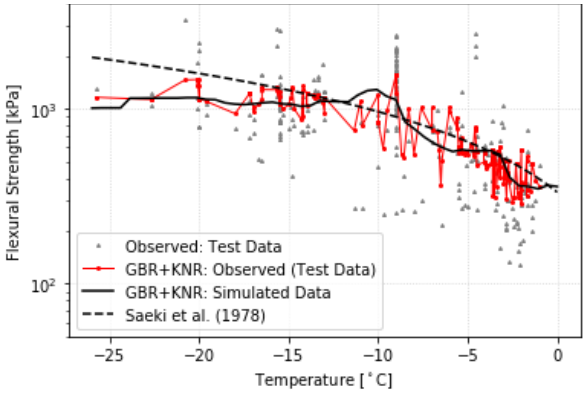

(f) GBR + KNR

Figure 6.22: Ensemble models: Flexural strength as a function of temperature (Part 2)

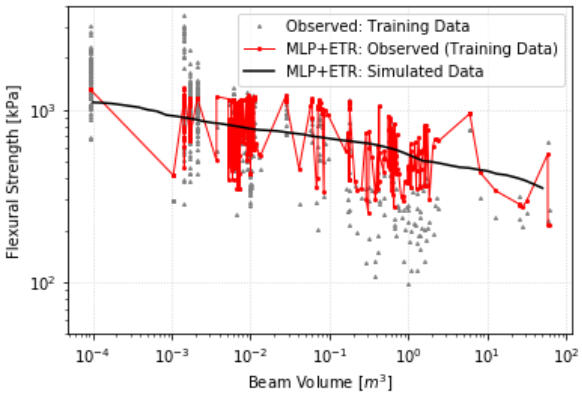

(a) MLPR + ETR

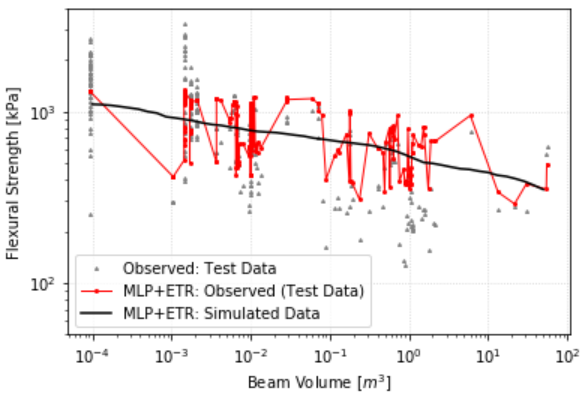

(b) MLPR + ETR

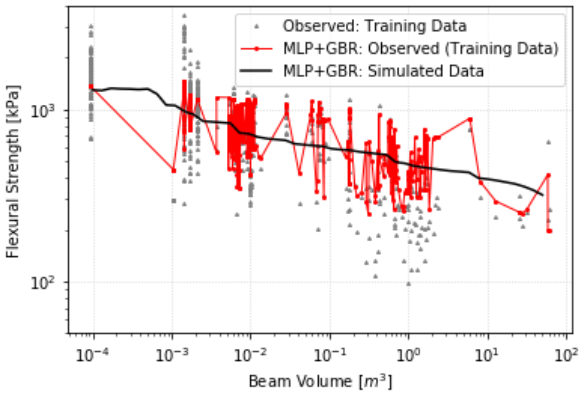

(c) MLPR + GBR

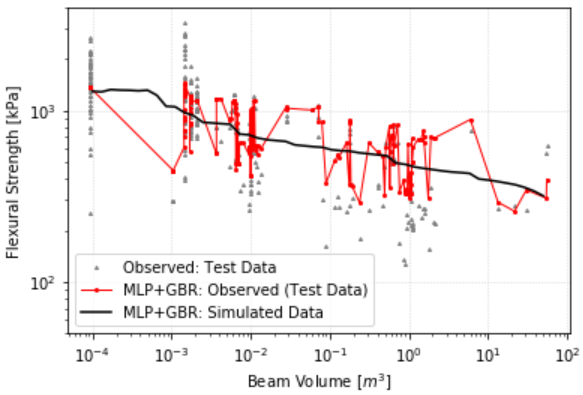

(d) MLPR + GBR

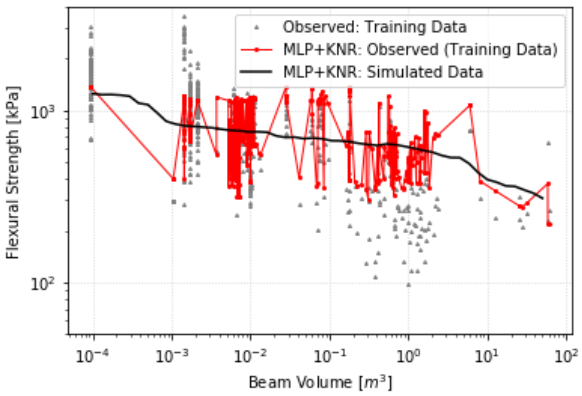

(e) MLPR + KNR

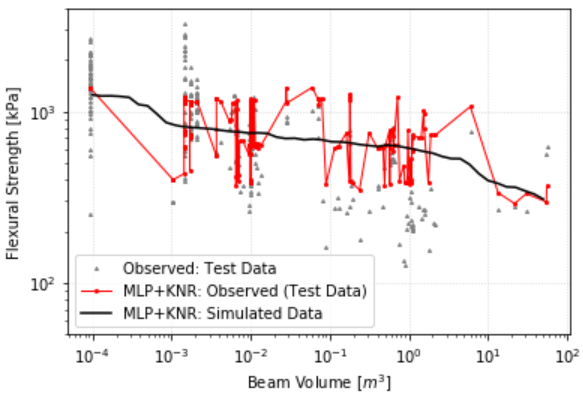

(f) MLPR + KNR

Figure 6.23: Ensemble models: Flexural strength as a function of beam volume (Part 1)

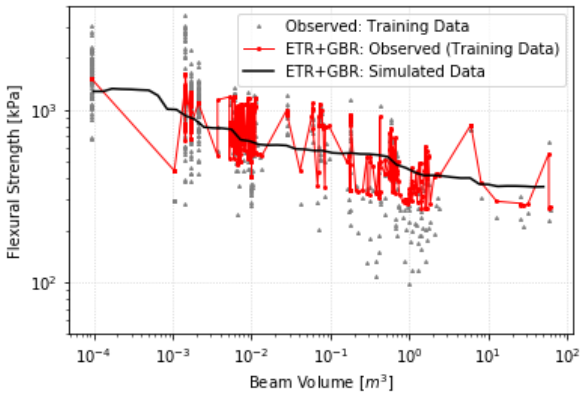

(a) ETR + GBR

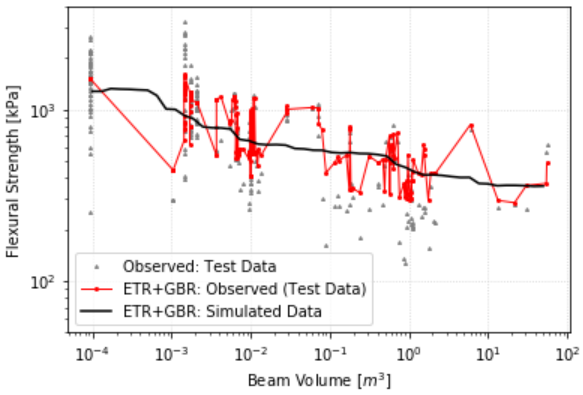

(b) ETR + GBR

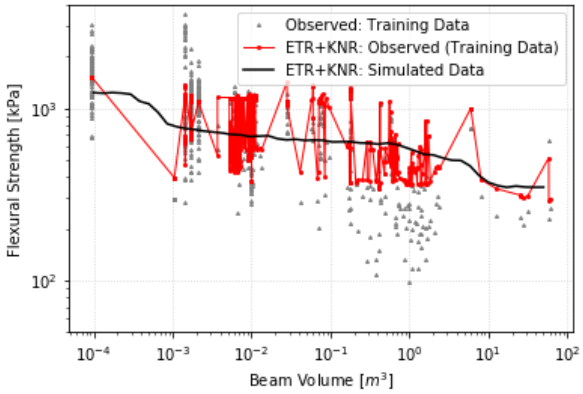

(c) ETR + KNR

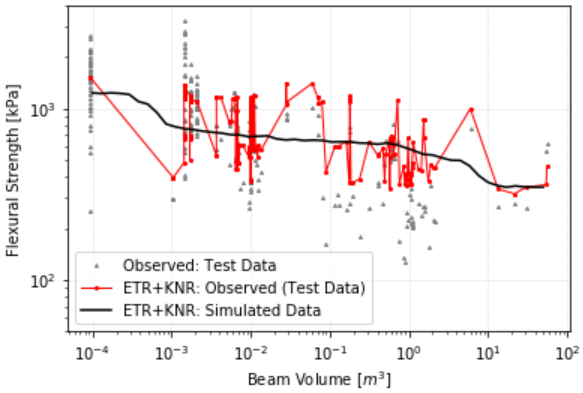

(d) ETR + KNR

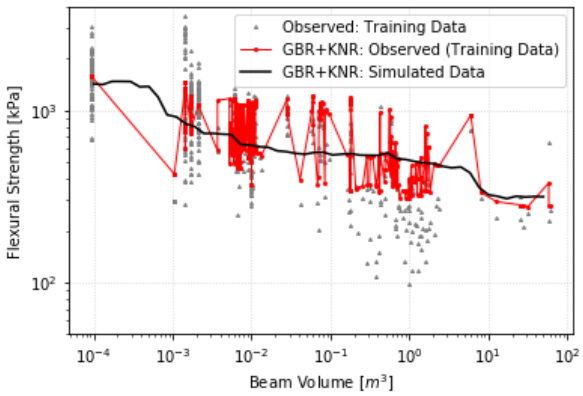

(e) GBR + KNR

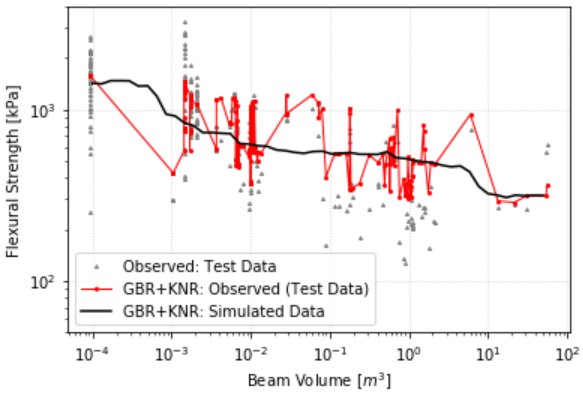

(f) GBR + KNR

Figure 6.24: Ensemble models: Flexural strength as a function of beam volume (Part 2)

6.2.4 Observed vs Predicted

A comparison between observed and predicted values was conducted to further observe the performance of the individual and ensemble ML models, the results are presented in Figures 6.25 and 6.26. A summary of each model (individual and ensemble) was generated by categorizing the data according to the error between predicted and observed values, based on Equation 5.5 reproduced below. Errors greater than +10% were categorized as overpredicted, errors less than -10% are under-predicted while the remainder are considered approximately equivalent. A summary of all ten models showing the percentage of predicted data in each category is provided in Table 6.5.

$$err = \frac{Predicted - Observed}{Observed} \qquad \text{(5.5 revisited)}$$

Table 6.5: Percent error: Observed vs predicted (test data)

Model	**Over**	**Under**	**Approx**
MLPR	57	29	14
ETR	55	24	21
GBR	42	27	31
KNR	52	27	21
MLPR + ETR	55	26	19
MLPR + GBR	54	24	22
MLPR + KNR	57	27	16
ETR + GBR	49	23	28
ETR + KNR	52	23	25
GBR + KNR	49	23	28

Comparing the observed vs predicted plots and summary table, the difference between the ML models is not significant. The scatter present in each of the plots is to be expected when compared to the variability present in the observed data. In general the ML models tend towards an overprediction of flexural strength. The scatter within the individual models is similar with the exception of the KNR model, which appears to discretize the data into

distinct bands. This descretization of data is less prevalent in the ensemble models where the KNR model is employed.

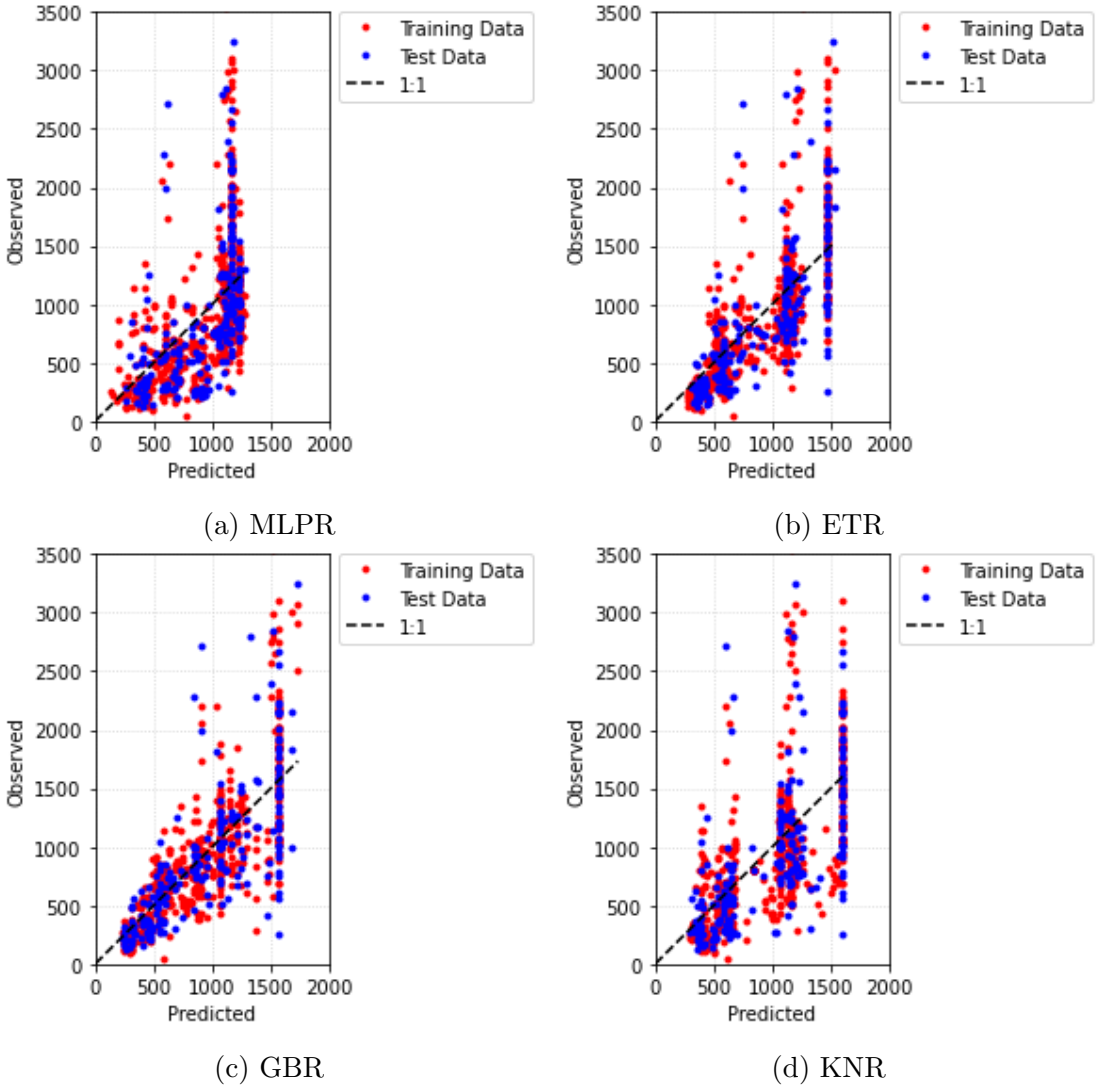

(a) MLPR

(b) ETR

(c) GBR

(d) KNR

Figure 6.25: ML: Observed vs predicted (individual)

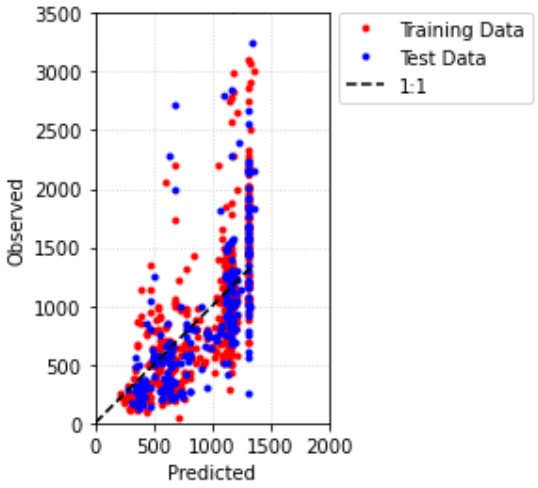

(a) MLPR + ETR

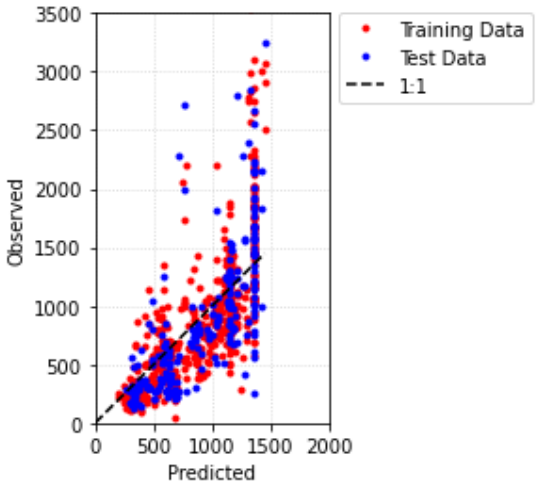

(b) MLPR + GBR

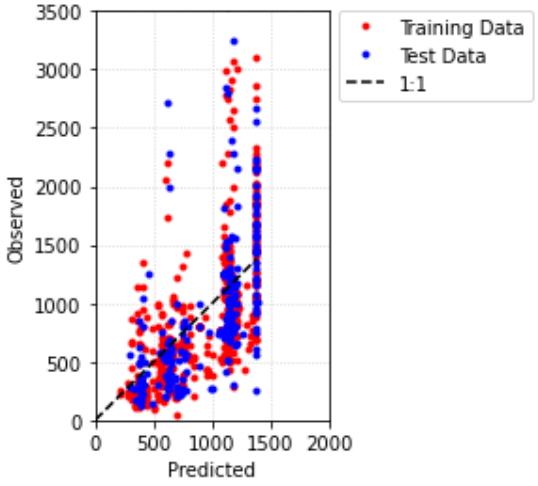

(c) MLPR + KNR

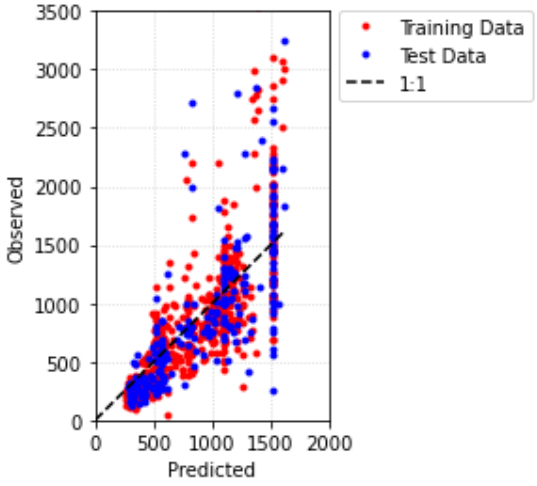

(d) ETR + GBR

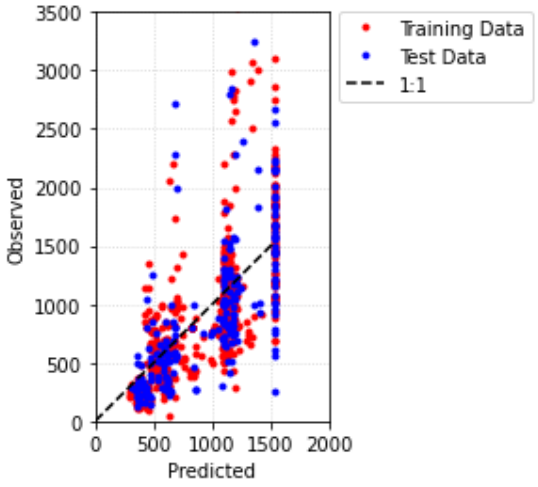

(e) ETR + KNR

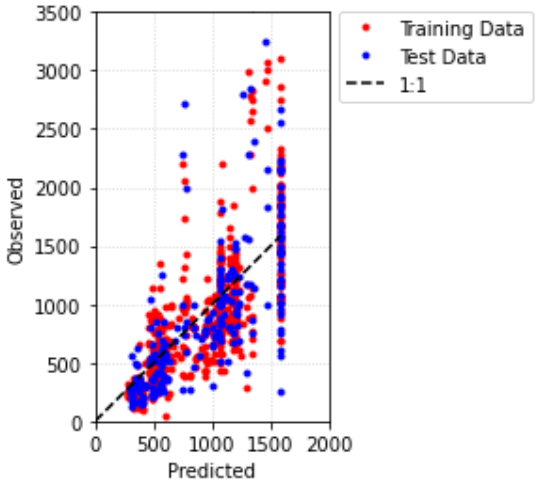

(f) GBR + KNR

Figure 6.26: ML: Observed vs predicted (ensemble)

6.2.5 Model Comparison

Each of the four ML models resulted in overall trendlines which are in agreement with the expected relationship trends discussed in Section 2.3. Employing the simulated datasets these relationship trends are presented in Figure 6.27 for flexural strength as a function of beam volume, brine volume and temperature. The statistical accuracy metrics of R^2 and RMSE for each of the four models are presented in Table 6.6 below. The GBR model has the lowest error values and highest R^2 of the four models presented however, this accuracy comes at a cost as it also experiences the highest degree of variability across all three model features. The MLPR on the other hand has the least desirable accuracy metrics yet produces the smoothest trendlines out of the four models presented.

Table 6.6: Comparisons of independent models

Model	R^2 **Train**	R^2 **Test**	**RMSE Train**	**RMSE Test**
MLPR	0.357	0.318	0.465	0.502
ETR	0.562	0.518	0.384	0.422
GBR	0.636	0.580	0.350	0.394
KNR	0.436	0.417	0.435	0.464

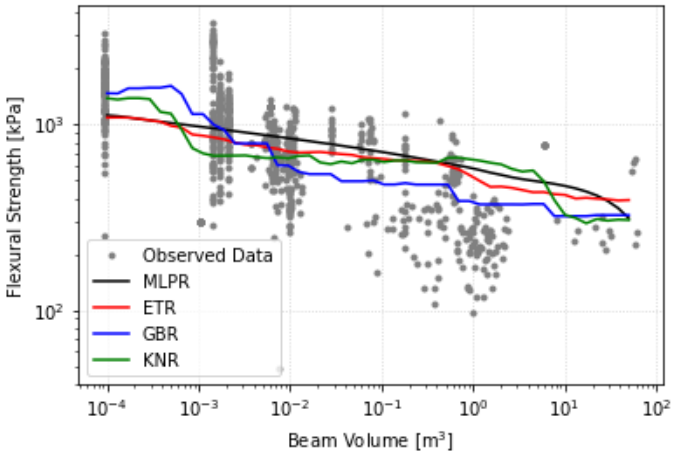

(a) Flexural strength as a function of beam volume

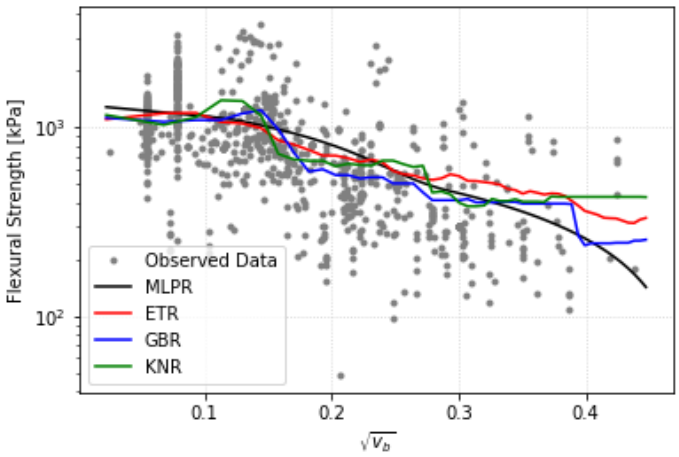

(b) Flexural strength as a function of the square root of the brine volume fraction

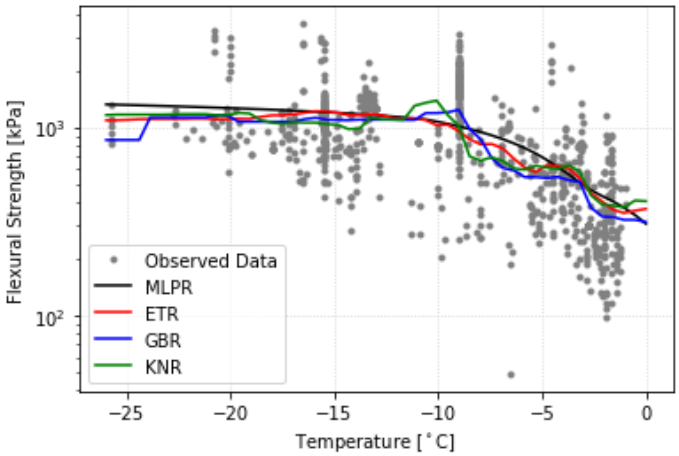

(c) Flexural strength as a function of temperature

Figure 6.27: Comparisons of independent models

All six ensemble models produced trendlines which were in agreement with the expected relationship trends as discussed in Section 2.3, these trends are presented in Figure 6.28 employing the simulated datasets. The statistical accuracy metrics for the ensemble models are provided in Table 6.7.

Ensemble models employing the GBR have the most favourable accuracy metrics however, like the individual models these models also demonstrated higher variability across the three model features. Also in similar fashion to the individual models, the ensemble models with the least favourable accuracy metrics ("MLPR + ETR" and "MLPR + KNR") have the smoothest trendlines.

The ability of an ensemble model to handle data extrapolation in an effective and expected manner is important in model selection. As discussed in Chapter 4.2, the internal processes of the ETR, GBR and KNR algorithms result in less than favorable extrapolated results. In short, when extrapolating these three algorithms tend to base their predictions on the same estimators resulting in constant predictions for extrapolation. The MLPR algorithm is more adaptable to extrapolation than the other three making it the ideal companion when exploring ensemble modelling. Reviewing the model statistics, observed trendlines and extrapolation characteristics, the most favourable model is the "MLPR + ETR" ensemble.

Table 6.7: Comparisons of ensemble models

Model	R^2 **Train**	R^2 **Test**	**RMSE Train**	**RMSE Test**
MLPR + ETR	0.479	0.441	0.418	0.454
MLPR + GBR	0.542	0.498	0.393	0.431
MLPR + KNR	0.428	0.401	0.439	0.470
ETR + GBR	0.611	0.561	0.362	0.403
ETR + KNR	0.512	0.478	0.405	0.439
GBR + KNR	0.567	0.525	0.382	0.419

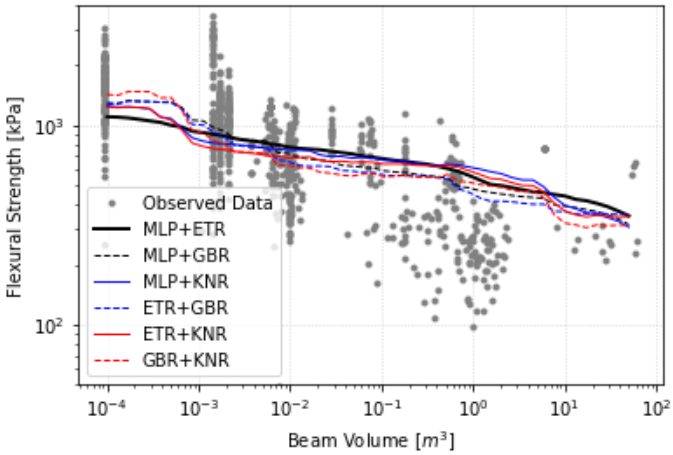

(a) Flexural strength as a function of beam volume

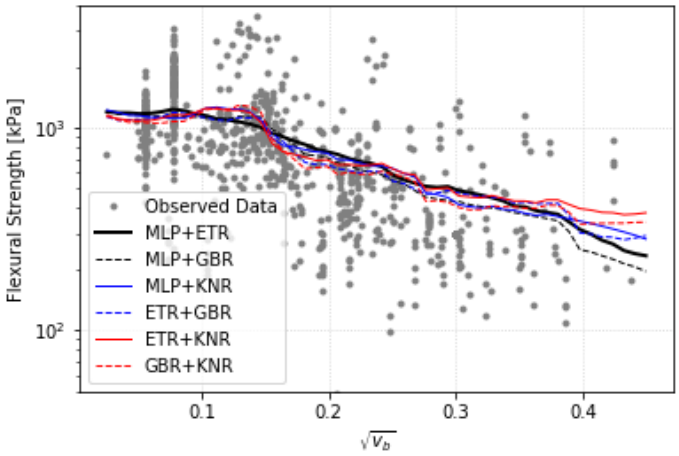

(b) Flexural strength as a function of the square root of the brine volume fraction

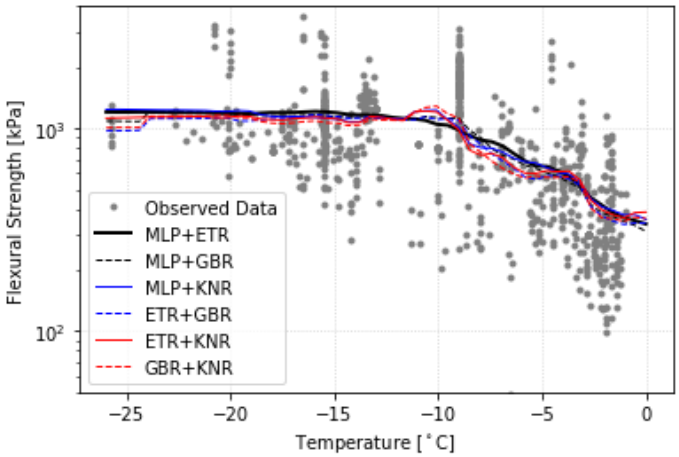

(c) Flexural strength as a function of temperature

Figure 6.28: Comparisons of ensemble models

6.3 Level Ice Loads

A comparison study was conducted to determine how the modelling of flexural strength could impact the level ice loads on a structure, and how the variability in the ice parameters can impact these loads. A single pier from the Confederation Bridge was chosen as the reference structure for the study, and the relevant geometry are provide in Figure 6.29. These bridge piers have a conical ice shield conical near the waterline with an approximate diameter (D) of 13.9m at the mean sea level (MSL).

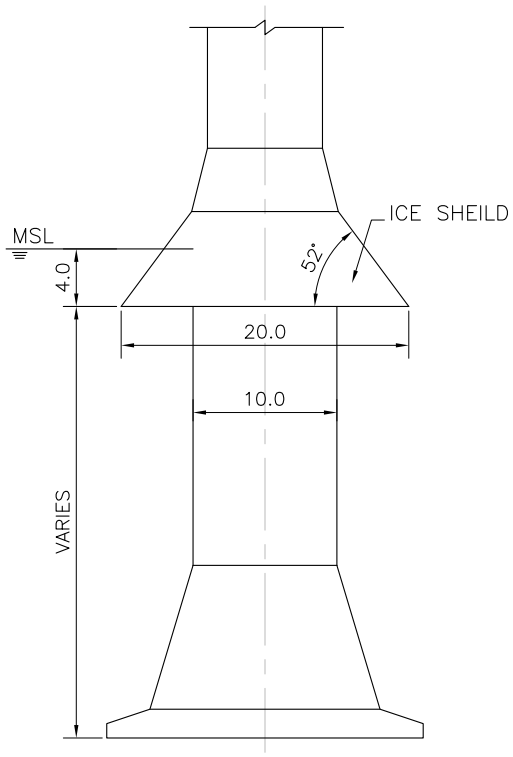

Figure 6.29: Confederation bridge pier geometry

The force required to initiate the flexural failure of an ice sheet impacting the bridge pier is based on the method discussed in Brown et al. (2001) and presented in Equation 6.21:

$$F_{sheet} = \Bigg\{ \underbrace{0.68\zeta\sigma_f D \left[\frac{\rho_w g h_{ice}^5}{E}\right]^{0.25}}_{\text{Flexural Failure Force}} + \underbrace{\left[\zeta(\sin\alpha + \mu\cos\alpha)) + \frac{\sin\alpha + \mu\cos\alpha)}{tan\alpha}\right] h_f h_{ice} \rho_i g D}_{\text{Ride-up Force}} \Bigg\} \underbrace{\left(1 + \frac{\pi^2 l_c}{4D}\right)}_{\text{Correction Factor}} \tag{6.21}$$

where ζ is defined in Equation 6.22, σ_f is the flexural strength of the ice, ρ_w is the density of surrounding water, g is gravity, h is the ice thickness, E is the Young's moduls of ice, α is the cone angle, μ is the ice-cone coefficient of friction, h_f is the ride-up height, ρ_i is the density of ice, l_c is the elastic critical length defined in Equation 6.23, and v is poissons ratio. There are three primary components in Equation 6.21 including the forces to cause flexural failure of the ice sheet, the forces required to push broken ice blocks up the sloped surface and a correction factor as discussed in Croasdale et al. (1994) to account for a under-prediction of loads when l_c is not sufficiently small compared to diameter of the structure. The ride-up force is independent of the flexural strength of the ice sheet and is an unnecessary term in a comparative study such as being discussed here. As a result the flexural load calculation can be simplified as shown in Equation 6.24

$$\zeta = \frac{\sin\alpha + \mu\cos\alpha)}{\cos\alpha - \mu\sin\alpha} \tag{6.22}$$

$$l_c = \left(\frac{E h^3}{12\rho_w g\,(1 - v^2)}\right)^{1/4} \tag{6.23}$$

$$F_{Flex} = 0.68\,\sigma_f D \left[\frac{\sin\alpha + \mu\cos\alpha}{\cos\alpha - \mu\sin\alpha}\right] \left[\frac{\rho_w g h^5}{E}\right]^{0.25} \left[1 + \frac{\pi^2 l_c}{4D}\right] \tag{6.24}$$

Deterministic design loads were calculated using the flexural strength outputs from the "MLPR + ETR" ensemble model using simulated ice parameters. For comparison these simulated ice parameters were also feed into select empirical models.

The first comparison study examines the impact of temperature on the level ice loads as shown in Figure 6.30. In this study three databases are generated with constant temperatures of -1, -5 and -10°C, each having a constant brine volume of 35 ppt and beam volume was estimated at $7h^3$ based upon recommendations by Schwarz et al. (1981). The empirical benchmark for this comparison employed the temperature model developed by Saeki et al. (1978) (see Equation 2.37). The ML and empirical predictions are very similar at warmer temperatures (-1°C), however as temperatures decrease the separation between Saeki et al. and the ML model rapidly increases, with the ML predictions being approximately 750 kPa lower at -10°C.

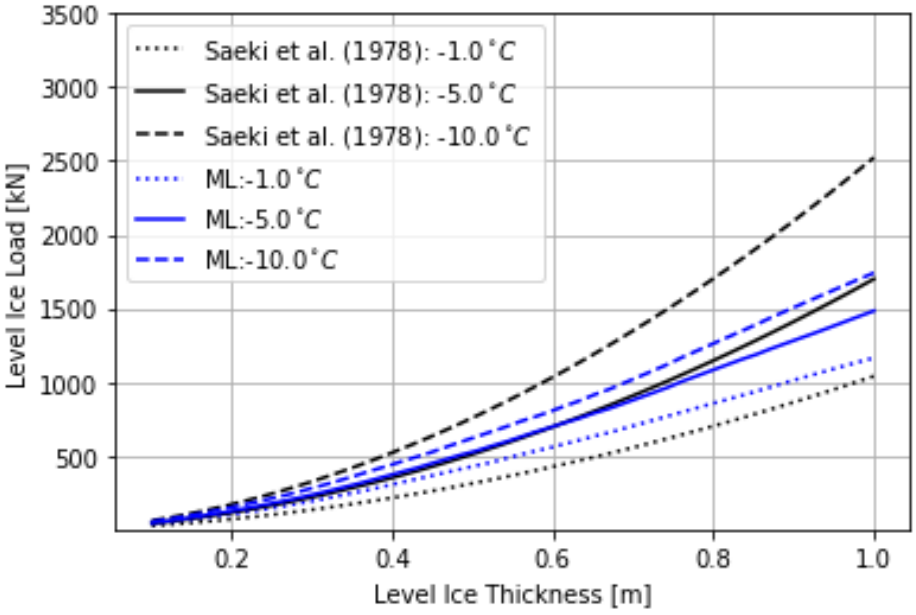

Figure 6.30: Level ice loads: As a function of temperature and beam volume

The second comparison study examines the impact of brine volume and temperature on the level ice loads as shown in Figure 6.31. In this study temperature was varied from -1 to

-20°C, beam volume was held constant at approximately 0.45m^3 (estimated based on a level ice thickness of 0.4m), and brine volume was estimated based on temperature using Equation 6.20. In this comparison, the ML model is compared against the empirical models of Saeki et al. (1978), Timco and O'Brien (1994), Ji et al. (2011) and Aly et al. (2019). In general as the temperatures decrease the separation between the empirical models increases. Overall the empirical models by Timco and O'Brien (1994) and Aly et al. (2019) are reasonable close, in particular for temperatures above -10°C. For temperatures greater than -12°C the Saeki et al. and ML models have nearly identical trends. The ML model predictions are about halfway between Aly et al. and Ji et al. from -1 to -12°C, however for temperatures below -12°C the ML is relatively constant.

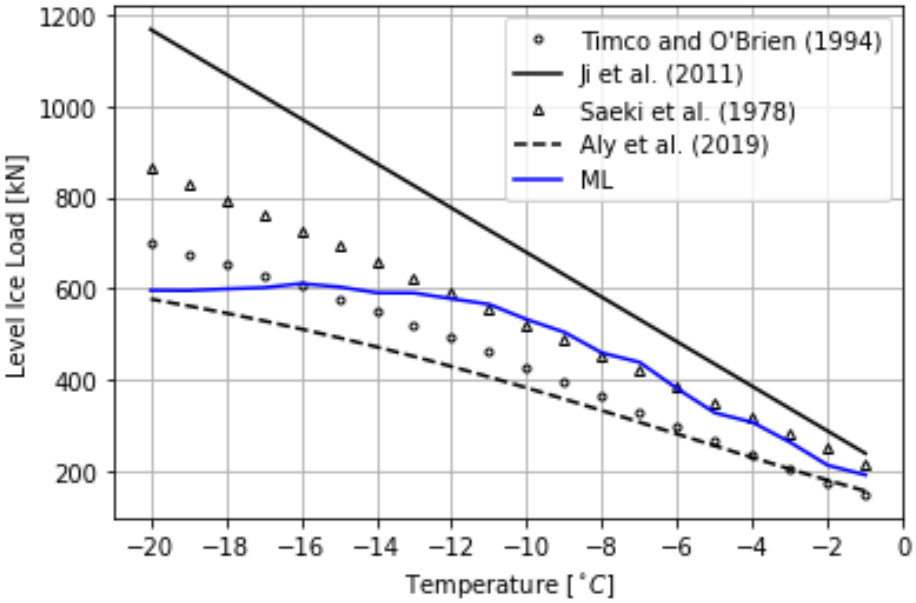

Figure 6.31: Level ice loads: As a function of temperature and brine volume

6.4 Summary

The influence of beam volume, brine volume and ice temperature on the flexural strength of sea ice was investigated using ML algorithms, and compared with traditional empirical

models. A total of ten ML models (four individual models and six ensemble models) were developed and tested, and have shown great promise in demonstrating the presence of scale effects trends as well as temperature and brine volume dependencies.

Summary plots of the flexural strength as a function of beam volume, brine volume and temperature are provided in Figure 6.32. These comparison plots present the MLPR and "MLPR + ETR" ensemble models, the newly developed empirical models and select published empirical models depending on the ice parameters under comparison. When comparing models as a function of beam volume the empirical models presented are those published by Williams and Parsons (1994) and Aly et al. (2019), which employ both beam volume and brine volume. When comparing models as a function of brine volume the empirical models also include the brine model published by Timco and O'Brien (1994). The linear model presented by Ji et al. (2011) was used when comparing temperature models. To aid in the presentation of smoother trend lines, the simulated databases were used with the ML models.

As demonstrated in Figure 6.32 the empirical and ML models display similar overall trends. For beam volume and brine volume the ML models generally result in slightly higher flexural strengths. When comparing temperature dependencies, the ML models are generally slightly lower than the empirical.

The flexural strength of sea ice was found to have dependence on beam volume, brine volume and ice temperature, these relationships have been demonstrated here through the application of both traditional models and ML models as demonstrated in Figure 6.32. All ten ML models investigated showed a degree of dependence of flexural strength on beam volume, brine volume and temperature.

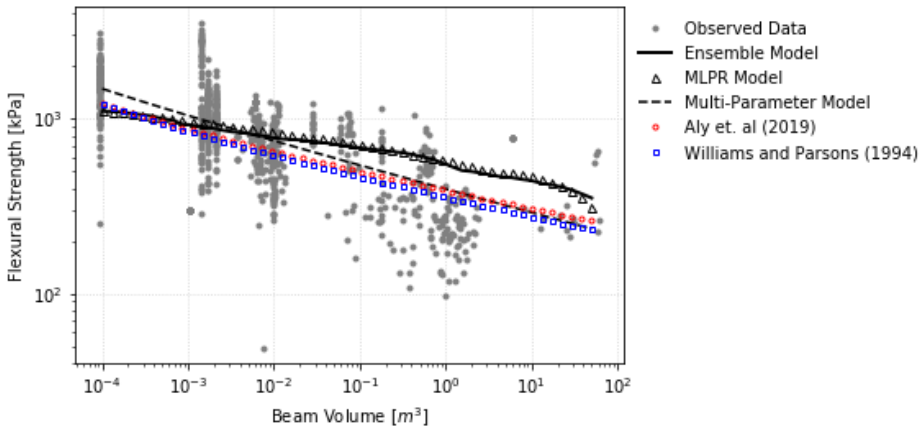

(a) Flexural strength as a function of beam volume

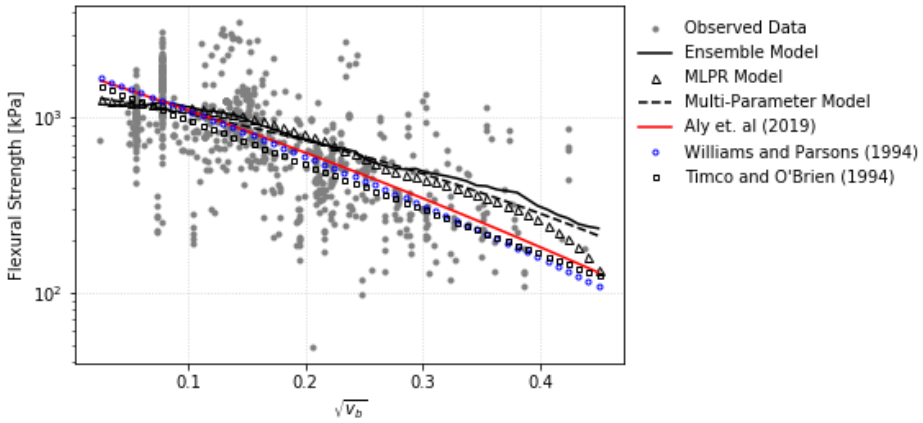

(b) Flexural strength as a function of the square root of the brine volume fraction

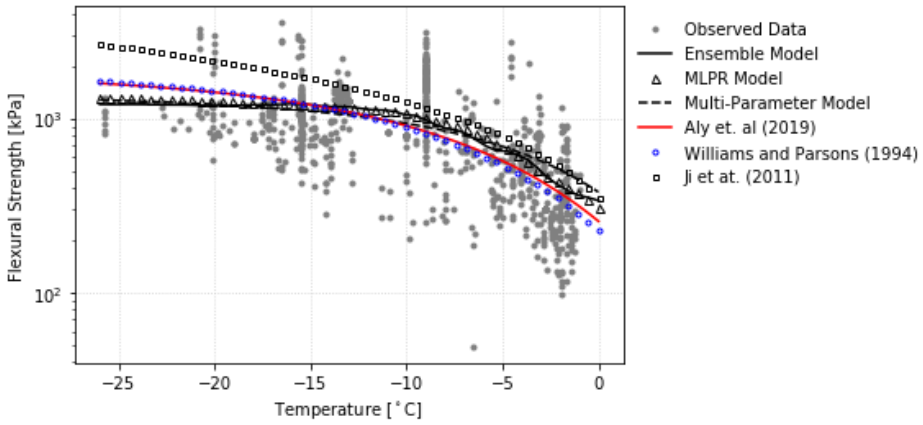

(c) Flexural strength as a function of temperature

Figure 6.32: Summary of ML and select empirical models

The relationship between flexural strength and brine volume has been well documented by multiple researchers, as discussed in Section 2.3.3. The inclusion of beam volume in the formulation of flexural strength is generally coupled with brine volume (see Section 2.3.2). The effect of temperature is often ignored completely, however two empirical models based on temperature (Saeki et al. (1978) and Ji et al. (2011)) were included in this work.

An analysis of level ice loads using the ML and empirical models mirrored the trends observed in flexural strength with higher temperatures, brine volumes and beam volumes resulted in lower ice loads. The ML ensemble model was on average 15% higher than the Timco and O'Brien (1994), 26% higher than Aly et al. (2019) models, and about 28% lower than the Ji et al. (2011) model. Overall, the use of ML has shown promissing results in modelling the dependicies of flexural strength on temperature, brine volume and beam volume. The continuation of research in this area is recommended.

7 Conclusions and Recommendations

The goal of this work was to explore the potential application of ML algorithms to the prediction of sea ice and freshwater ice flexural strength. ML can be a very useful tool and has been used with much success in many fields, however it is not necessarily the solution to every data problem. In this work ML predictions were compared against those from more traditional empirical methods, as well as the expected physical trends based on ice properties as a means to determine the applicability of ML to ice mechanics issues such as the estimation of flexural strength.

7.1 Discussions and Conclusions

The development of any ML model requires a large quantity of quality data. The majority of data used in this work were extracted from an extensive database compiled by Aly et al. (2019), containing flexural strength measurements for both freshwater and sea ice test programs. ML models were developed for predicting the flexural strength of freshwater ice and sea ice based on beam volume, temperature and brine volume. The database was filtered to ensure data was present for each of these three parameters with additional filtering limiting the database to only naturally occurring ice samples. The resultant database had approximately 640 and 800 freshwater and sea ice entries respectively. The performance of each model was evaluated against three key metrics: statistical accuracy, prediction of expected physical behaviours, and the ability of the model to generalize to new unseen data.

A total of ten ML models were developed, four based on individual algorithms plus six ensemble models. The four individual regression algorithms were multilayer perceptron, extra trees, gradient boosted trees and k-nearest neighbour, the six ensemble models were composed of pairs of these four individual models.

To evaluate the ability of each model to predict the underlining expected physical behaviours, these behaviours had to be defined. An investigation was performed to determine the theoretical and observational influence of beam volume, brine volume and temperature on the flexural strength of ice. A brief summary of the relationship between these three ice properties and the flexural strength of ice are discussed below.

Brine Volume: The influence of brine volume on ice strength has been investigated by a number of researchers and it is generally well accepted that ice strength is inversely proportional to brine volume (e.g. Weeks and Assur (1967), Dykins (1968), Weeks and Assur (1972), Tozawa and Taguchi (1986), Timco and O'Brien (1994) and Frederking and Sudom (2013)). The ML models aligned well with the expected trends, showing clear trends of lower flexural strength with increasing brine volume.

Scale Effect: The presence, or at least the significance, of scale effect trends in both sea ice and freshwater ice has been debated in the literature. The existence of scale effect trends have been deemed inconclusive by several researchers (e.g. Gow and Ueda (1989) and Parsons and Lal (1991))). Conversely, researchers have also found that the presence of scale effects trends in ice are of significance (e.g. Tozawa and Taguchi (1986), Williams and Parsons (1994) and Lau et al. (2001)) and should be considered when modelling flexural strength. The ML models clearly demonstrate the presence of scale effect trends in both freshwater and saline ice, aligning well with work of researchers such as Williams and Parsons (1994).

Temperature: Like beam volume, the effects of temperature are debated in the literature, and have varying results depending on whether the discussion is on freshwater ice or sea

ice. Weeks and Assur (1972) noted a dependency between strength and temperature in both freshwater and sea ice. Maattanen (1975) noted a reduction in flexural strength with temperature in brackish and low salinity ice, while Gow (1977) and Gow et al., 1978 noted a dependence between strength and temperature in freshwater beams. Several authors (e.g. Lainey and Tinawi (1984) and Gow and Ueda (1989)) noted that a link between flexural strength and temperature exists within freshwater ice, however the link is not significant. Brine volume is highly correlated to temperature, or at least to the temperature history of an ice sample, therefore it can be difficult to determine the influence of these individuals parameters. In general, the flexural strength is expected to decrease with increasing temperatures. The ML models were able to demonstrate trend of decreasing flexural strength with increasing ice temperature.

This investigation into the expected physical behaviour determined that any flexural strength model should present trends of decreasing flexural strength as beam volume, brine volume and/or temperature increases.

The application of ML algorithms for the estimation of ice flexural strength (saline and freshwater) has shown great promise. In freshwater ice, the ML models were able to demonstrate the presence of scale effect trends as well as temperature dependencies. The impact of temperature on the flexural strength of freshwater ice is generally considered insignificant by many researchers and is likewise omitted from flexural strength models. Through the application of ML as discussed here, the influence of temperature on the flexural strength of freshwater ice is clearly evident. When investigating 50-year design loads on a representative structure the ML experienced an approximate 18% decrease in load when temperatures were increased from -20 to -1 °C.

When considering sea ice, the ML models demonstrated flexural strength dependencies on brine volume, beam volume and temperature. Previously published models of sea ice flexural

strength are generally limited to single or double parameters where temperature is often ignored. The implementation of ML models marks the first time a three parameter model has been used to estimate sea ice flexural strength. In general there was good agreement between the ML and traditional models, although ML predictions were on average about 16% higher.

7.2 Recommendations for future research

There are a number of recommendations which could improve upon the current work:

1. Further development of the current models and investigation into the use of additional algorithms is recommended. In the present work a good deal of effort was employed in training and tuning the algorithms presented. However, there is always room for improvement and potential exists for the progression of the models through further tuning of these algorithms. Similarly, the work here was also limited to four supervised learning regression algorithms, exploring additional algorithms may highlight algorithms which offer improvements over the current selection.

2. The addition of new data is recommended as it becomes available. ML models are sensitive to the quality and quantity of the input data. ML algorithms perform better on large datasets, therefore updating the model should be considered as new data becomes available.

3. An investigation into the impact of skewed and clustered dataset on ML models versus more "traditional" models is recommended. The nature of flexural strength testing often results in a database that is highly skewed or subjected to data clustering. Testing programs often involve a multitude of tests, where a large number of ice samples could be extracted from the same ice sheet resulting in nearly identical conditions such as temperature and brine volume. Beam volume is often restricted by the limitations

of the testing equipment and can likewise contribute to a clustered dataset. Within the sea ice database, over 85% of data are for beam volumes less than $0.6m^3$, more than 50% of data have brine volumes of 25‰ or less, while approximately 30% of the data are for tests between −15° to −16°C and −8° to −9°C. Therefore, further work to investigate the influence of data skewing and clustering on the ML models compared with the more "traditional" models is recommended.

4. Further investigation into the expected minimum strength of an ice beam is recommended. During the discussion of Weibull weakest link modelling, it was stated that the lower limit of ice beam strength is often assumed to be zero, this is a common assumption as it allows for a simplification of the model. While zero would be an acceptable "theoretical" minimum, the actual expected minimum would not be zero.

5. The current models (freshwater and sea ice) would benefit from the addition of new flexural strength tests, in particular field testing of large scale beams would be of benefit. The majority of each database is composed of relatively small scale beam tests, therefore the addition of large scale test would help offset the skewness of the current databases.

6. There are a few improvements which could be made to the collection and or reporting of flexural strength test results which would benefit all researchers.

    - *Additional test parameters and ice properties*: The inclusion of additional model features in the form of physical ice properties (e.g. grain size or grain structure) or testing parameters (e.g. loading direction and rate) would be beneficial. In the current work, physical parameters such as grain size, grain structure, ice density and total porosity were not included in the development of the ML models. The reason for their exclusion is the inconsistency in which they are recorded or presented in technical publications. The ML algorithms used in the current work

do not accept null values, therefore the inclusion of such parameters would reduce the number of entries in the model feature database decreasing the performance of the models. Therefore should the recording of additional model features become more prevalent in future publications, their inclusion should be considered in the models.

- *Total porosity, weight and density*: The inclusion of total porosity in the model development would be an improvement over brine volume alone. The effect of the total ice porosity on the flexural strength of ice was discussed briefly in Section 2.3.3. In order to determine the total porosity of an ice sample, careful measurements of beam volume and weight are required along with the density of the solid ice forming the sample. The total porosity (or the necessary information upon which to calculate total porosity) are rarely provided in technical publications however their inclusion would be beneficial.

- *A standard loading rate*: The use of a standard loading rate would allow for a better more direct comparison between test programs. As the loading rate and other test parameters are not generally provided, it is reasonable to assume that some degree of the variability within the flexural strength database could be attributed to the loading rate or other missing parameters. A standard loading rate could also help eliminate the impact of beam mass and the hydrodynamic effect.

- *A standard testing method*: The use of a standard testing method, in a similar manner as a standard loading rate, would remove one variable from the equation when looking at the variability between results from different test programs. Four-point bending tests should be the favoured testing method as they offer measurements accuracy improvements over both cantilever and three-point bend-

ing. However, it is well understood that each method has its own merits and method selection is based on the needs of the test program. That being said, where possible four-point bending tests should be the method of choice.

The application of ML to the field of ice mechanics, specifically the estimation of flexural strength, has shown great promise. The expansion of the flexural strength databases, further tuning of the current algorithms, and the addition of new ML algorithms are key components moving forward. With further research and development the ML model predictions are expected to improve and become more robust. The continuation of research in the area of ML and ice mechanics has the potential to add real value to the field.

References

Aly, M., Taylor, R., Bailey Dudley, E., & Turnbull, I. (2019). Scale effect in ice flexural strength. *Journal of Offshore Mechanics and Arctic Engineering*, *141*(5).

Barrette, P., Phillips, R., Clark, J., Crocker, G., & Jones, S. (1999). Flexural behavior of model sea ice in a centrifuge. *Journal of cold regions engineering*, *13*(3), 122–138.

Belyadi, H., & Haghighat, A. (2021). *Machine learning guide for oil and gas using python: A step-by-step breakdown with data, algorithms, codes, and applications*. Gulf Professional Publishing.

Blanchet, D., Abdelnour, R., & Comfort, G. (1997). Mechanical properties of first-year sea ice at tarsiut island. *Journal of cold regions engineering*, *11*(1), 59–83.

Brown, T., Jordaan, I., & Croasdale, K. (2001). A probabilistic approach to analysis of ice loads for the confederation bridge. *Canadian Journal of Civil Engineering*, *28*(4), 562–573.

Buil, P., Kellner, L., Ehlers, S., & von Bock und Polach, F. (2022). Analyzing flexural strength data of ice: How useful is explainable machine learning? *International Conference on Offshore Mechanics and Arctic Engineering*, *85918*, V006T07A012.

Burton, R., Yulmetov, R., & Taylor, R. (2022). Estimating freshwater level ice loads on sloping structures using machine learning-derived flexural strength. *Proceedings of the 26th IAHR International Symposium on Ice, Montreal, Canada*.

Burton, R., Yulmetov, R., & Taylor, R. (2023). Estimating level sea ice loads on sloping structures using machine learning-derived flexural strength. *27th International Conference on Port and Ocean Engineering under Arctic Conditions, Glasgow, United Kingdom*.

Butkovich, T. R. (1956). *Strength studies of sea ice* (Vol. 20). Snow Ice; Permafrost Research Establishment, Corps of Engineers, US Army.

Butkovich, T. R. (1959). *On the mechanical properties of sea ice, thule, greenland, 1957* (Vol. 54). US Army Snow Ice; Permafrost Research Establishment, Corps of Engineers.

Christensen, F. (1986). Sea ice strength measurements from the inner danish waters in early 1985. *Ice technology*, 247–253.

Cox, G. F., & Weeks, W. F. (1988). Profile properties of undeformed first-year sea ice.

Croasdale, K., Thijssen, J., & Allyn, N. (2019). Ice load signatures for ridge actions on wind turbines with conical collars. *Proceedings of the International Conference on Port and Ocean Engineering Under Arctic Conditions*.

Croasdale, K., Cammaert, A., & Metge, M. (1994). A method for the calculation of sheet ice loads on sloping structures. *Proc. 12th Int. Symposium on Ice, The Norwegian Institute of Technology, Trondheim, Norway, August*, 23–26.

Daly, S. F. (2016). Characterization of the lake erie ice cover.

Dykins, J. (1968). Tensile and flexural properties of saline ice. *Physics of Ice. Plenum Press, New York, NY*, 251–270.

Dykins, J. (1971). *Ice engineering–material properties of saline ice for a limited range of conditions.* (tech. rep.). NAVAL CIVIL ENGINEERING LAB PORT HUENEME CALIF.

Frankenstein, G. (1959). Strength data on lake ice.

Frankenstein, G., & Garner, R. (1967). Equations for determining the brine volume of sea ice from -0.5° to -22.9°c. *Journal of Glaciology*, *6*(48), 943–944.

Frankenstein, G., & Garner, R. (1970). *Dynamic young's modulus and flexural strength of sea ice* (Vol. 222). Corps of Engineers, US Army, Cold Regions Research; Engineering Laboratory.

Frederking, R., & Sudom, D. (2013). Review of flexural strength of multi-year ice. *The Twenty-third International Offshore and Polar Engineering Conference*.

Frederking, R., & Timco, G. (1983). On measuring flexural properties of ice using cantilever beams. *Annals of glaciology*, *4*, 58–65.

Gow, A. J. (1977). Flexural strength of ice on temperate lakes. *Journal of Glaciology*, *19*(81), 247–256.

Gow, A. J., & Langston, D. (1975). *Flexural strength of lake ice in relation to its growth structure and thermal history.* (tech. rep.). Cold Regions Research and Engineering Lab Hanover NH.

Gow, A. J., & Ueda, H. T. (1989). Structure and temperature dependence of the flexural properties of laboratory freshwater ice sheets. *Cold Regions Science and Technology*, *16*(3), 249–270.

Gow, A. J., Ueda, H. T., Govoni, J. W., & Kalafut, J. (1988). *Temperature and structure dependence of the flexural strength and modulus of freshwater model ice* (tech. rep.). Cold Regions Research and Engineering Lab Hanover NH.

Gow, A. J., Ueda, H. T., & Ricard, J. A. (1978). *Flexural strength of ice on temperate lakes: Comparative tests of large cantilever and simply supported beams* (tech. rep.). Cold Regions Research and Engineering Lab Hanover NH.

Ji, S.-y., Wang, A.-l., Su, J., & Yue, Q.-j. (2011). Experimental studies on elastic modulus and flexural strength of sea ice in the bohai sea. *Journal of Cold Regions Engineering*, *25*(4), 182–195.

Jordaan, I. (2005). *Decisions under uncertainty: Probabilistic analysis for engineering decisions*. Cambridge University Press.

Karulina, M., Marchenko, A., Karulin, E., Sodhi, D., Sakharov, A., & Chistyakov, P. (2019). Full-scale flexural strength of sea ice and freshwater ice in spitsbergen fjords and north-west barents sea. *Applied Ocean Research*, *90*, 101853.

Kujala, P., Riska, K., Varsta, P., Koskivaara, R., & Nyman, T. (1990). Results from in situ four point bending tests with baltic sea ice. *Proceedings of the IAHR Symposium on Ice Problems, Helsinki, Finland*, 19–23.

Lainey, L., & Tinawi, R. (1981). Parametric studies of sea ice beams under short and long term loadings. *IAHR International Symposium on Ice, Québec 1981. Proceedings*, 607–619.

Lainey, L., & Tinawi, R. (1984). The mechanical properties of sea ice—a compilation of available data. *Canadian Journal of Civil Engineering*, *11*(4), 884–923.

Lau, M., Phillips, R., McKenna, R., & Jones, S. (2001). Size effect on the flexural strength of ice in model testing. *16th International Conference on Port and Ocean Engineering Under Arctic Conditions, Ottawa, ON, Canada*, 12–17.

Lavrov, V. V. (1971). *Deformation and strength of ice* (tech. rep.).

Maattanen, M. (1975). On the flexural strength of brackish water ice by in situ test. *Proceedings of the International Conference on Port and Ocean Engineering under Arctic Conditions*.

Palmer, A., Goodman, D., Ashby, M., Evans, A., Hutchinson, J., & Ponter, A. (1983). Fracture and its role in determining ice forces on offshore structures. *Annals of glaciology*, *4*, 216–221.

Parsons, B., Lal, M., Williams, F., Dempsey, J., Snellen, J., Everard, J., Slade, T., & Williams, J. (1992). The influence of beam size on the flexural strength of sea ice, freshwater ice and iceberg ice. *Philosophical Magazine A*, *66*(6), 1017–1036.

Parsons, B., & Lal, M. (1991). Distribution parameters for flexural strength of ice. *Cold regions science and technology*, *19*(3), 285–293.

Saeki, H., Nomura, T., & Ozaki, A. (1978). Experimental study on the testing methods of strength and mechanical properties for sea ice. *Proc. of 4th IAHR Symposium on Ice, part, 1*.

Saeki, H., Ozaki, A., & Kubo, Y. (1981). Experimental study on flexural strength and elastic modulus of sea ice. *Proceedings of Port and Ocean Engineering under Arctic Conditions, POAC*, *81*, 536–547.

Samuel, A. L. (1959). Some studies in machine learning using the game of checkers. *IBM Journal of research and development*, *3*(3), 206–226.

Sanderson, T. J. (1988). Ice mechanics and risks to offshore structures.

Schwarz, J. (1975). On the flexural strength and elasticity of saline ice. *Proc. IAHR 3rd Int. Symp. on Ice Problems, Hanover, NH*, 373–386.

Schwarz, J., Frederking, R., Gavrillo, V., Petrov, I., Hirayama, K.-I., Mellor, M., Tryde, P., & Vaudrey, K. (1981). Standardized testing methods for measuring mechanical properties of ice. *Cold Regions Science and Technology*, *4*(3), 245–253.

Schwarz, J., & Weeks, W. (1977). Engineering properties of sea ice. *Journal of Glaciology*, *19*(81), 499–531.

Scikit-learn. (2021). *Userguide*. Retrieved September 30, 2021, from https://scikit-learn.org/stable/user_guide.html

Timco, G. (1985). Flexural strength and fracture toughness of urea model ice.

Timco, G., & Weeks, W. (2010). A review of the engineering properties of sea ice. *Cold regions science and technology*, *60*(2), 107–129.

Timco, G., & Frederking, R. (1990). Compressive strength of sea ice sheets. *Cold Regions Science and Technology*, *17*(3), 227–240.

Timco, G., & O'Brien, S. (1994). Flexural strength equation for sea ice. *Cold Regions Science and Technology*, *22*, 285–298.

Tozawa, S., & Taguchi, Y. (1986). A preliminary study of scale effect on structural strength of ice specimen. *International offshore mechanics and arctic engineering. Symposium.* *5*, 336–340.

Vaudrey, K. (1977). *Ice engineering-study of related properties of floating sea-ice sheets and summary of elastic and viscoelastic analyses* (tech. rep.). CIVIL ENGINEERING LAB (NAVY) PORT HUENEME CA.

Wang, J., Brown, J., & Frederking, R. (2020). Full-scale/model-scale comparison of podded icebreaker's performance in ice with flexural strength measurement study. *SNAME Maritime Convention*, D023S007R001.

Weeks, W., & Ackley, S. F. (1986). *The growth, structure, and properties of sea ice*. Springer.

Weeks, W., & Assur, A. (1967). *The mechanical properties of sea ice* (Vol. 2). US Army Materiel Command Cold Regions Research & Engineering Laboratory.

Weeks, W., & Assur, A. (1972). Fracture of lake and sea ice. In *Fracture of nonmetals and composites* (pp. 879–978). Elsevier.

Weeks, W., & Gow, A. (1980). Crystal alignments in the fast ice of arctic alaska. *Journal of Geophysical Research: Oceans*, *85*(C2), 1137–1146.

Weibull, W. (1951). A statistical distribution function of wide applicability. *Journal of applied mechanics*.

Williams, F., Crocker, G., & Butt, S. (1993). Northumberland strait ice properties measurements. *National Research Council, Institute for Marine Dynamic, St. John's, NL, Canada, Technical Report No. TR-1993-06*.

Williams, F., Everard, J., & Butt, S. (1992). *Ice and snow measurements in support of the operational evaluation of the nathaniel b. palmer in the antarctic winter environment*. Institute for Marine Dynamics.

Williams, F., Kirby, C., & Slade, T. (1993). Strength and fracture toughness of first-year arctic sea ice. *Institute for Marine Dynamics TR-1993-12, St. John's, NF, Canada*.

Williams, F., & Parsons, B. (1994). Size effect in the flexural strength of ice.

Williams, F., Spencer, D., Parsons, B., Hackett, P., Gagnon, R., Everard, J., & Butt, S. (1991). Full-scale ice breaker trials ccgs sir john franklin indian arm/little burnt bay 1991. *National Research Council Canada, St. John's, NL, Canada, Technical Report No. TR-1991-03*.

Zhou, Z.-H. (2021). *Machine learning*. Springer Nature.